Reactivity of Metal (Co, Ni, Cu) Bound Peptides with Organometallic Fragments and Small Molecules

by

Arnab Dutta

A Dissertation Presented in Partial Fulfillment
of the Requirements for the Degree
Doctor of Philosophy

Approved September 2012 by the
Graduate Supervisory Committee:

Anne Jones, Chair
Willem Vermaas
Ana Moore

ARIZONA STATE UNIVERSITY

December 2012

ABSTRACT

Understanding the mechanisms of metalloproteins at the level necessary to engineer new functionalities is complicated by the need to parse the complex overlapping functions played by each amino acid without negatively impacting the host organism. Artificial or designed metallopeptides offer a convenient and simpler platform to explore metal-ligand interactions in an aqueous, biologically relevant coordination context. In this dissertation, the peptide SODA (ACDLPCG), a synthetic derivative of the nickel-binding pocket of nickel superoxide dismutase, is used as a scaffold to construct a variety of novel metallopeptides and explore their reactivity. In Chapter 2, I show that SODA binds Co(II) and the resulting peptide, CoSODA, reacts with oxygen in an unexpected two step process that models the biosynthesis of Co nitrile hydratase. First, the thiolate sulfur is oxidized and then the metallocenter is oxidized to Co(III). In Chapter 3, I show that both CoSODA and CuSODA form CN- adducts. Spectroscopic investigations of these metallopeptides are compared with data from NiSODA and Ni(CN)SODA to show the remarkable geometric versatility of SODA with respect to interactions with metallocenters. In Chapter 4, exploiting the propensity of sulfur ligands to form bridging structures, NiSODA is used as a metallosynthon to direct synthesis of hetero bi- and tri-metallic peptides as models for [NiFe]-hydrogenases and the A cluster of acetyl-CoA synthase carbon monoxide dehydrogenase. Building on this synthetic strategy, in Chapter 5, I demonstrate synthesis of NiRu complexes including a Ru(bipyridine)$_2$ moiety and characterize their photochemistry.

DEDICATION

First, I would like to dedicate this work to my parents; without their support I would not be able to arrive at this juncture of my life. They have sacrificed their own happiness, in all means, to provide their unequivocal support throughout my career and my mere expression of thanks does not suffice to acknowledge their effort. Even though I stayed at a half a world's distance from them for the last five years, they always remained in my heart at every single moment.

Secondly I would like to thank all my chemistry teachers form my school and college days, especially Mr. Tilak Mukherjee, Mr. Manimohan Dutta, Prof. Snigdha Gangopadhyay and Dr. Chandan Saha. Their tremendous efforts in initiating and sustaining my curiosity about chemistry will never be forgotten. I would also like to mention the influence and impact of Prof. Goutam Lahiri from Department of Chemistry, IIT Bombay, on my academic and personal life. I am extremely grateful for his good advice and encouragement that ignited the desire in me to pursue research in future.

Finally, I would like to thank all my friends including Dinesh, Souvik, Manas, Basab, Anindya, Sumit, Rakesh, Suman and Manikandadas for providing me a pseudo-family here at Tempe. All the magical moments we experienced together will be cherished as an invaluable asset for the rest of my life.

ACKNOWLEDGMENTS

Funding: I would like to acknowledge Center for Bio-Inspired Solar Fuel Production, an energy frontier research center funded by the U.S. Department of Energy, Office of Science, Office of Basic Energy Sciences under the award number DE-SC0001016, Science Foundation of Arizona (SFAz) for a graduate student fellowship, and the Department of Chemistry and Biochemistry at Arizona State University for the financial, academic and technical support provided for the research described in this thesis.

Collaborations: I am thankful to Dr. Jason Shearer and his student Jennifer Schmitt, from University of Nevada, Reno, for their enormous support in X-ray absorbance spectroscopy (XAS) experiments, which were instrumental for the cobalt and copper metallopeptide studies. I would also like to acknowledge Dr. Hilairy Hartnett and her graduate student Alex Hamilton for helping me out with ESI-MS. I am grateful to Dr. Marco Flores for introducing me to world of EPR. Despite being encountered with a novice like me, Dr. Flores meticulously and encouragingly guided me to comprehend the subtle changes in metallopeptides at the molecular level. I am also thankful to Dr. Thomas Groy for spending hours to solve molecular structures from the complicated XRD pattern of Ni-Ru systems. I must acknowledge Dr. Gerdenis Kodis, who navigated me during the ultrafast spectroscopic experiments and helped simulating the data to interpret the complex excited state molecular dynamics. I would also like to thank Dr. Gwyneth Gordon in the W.M. Keck Foundation Laboratory, Dr. Ulrich Haussermann, Dr. Sara Vaiana and her student Stephanie Cope in the Department of Physics, ASU, and

Dr. Tim Katcher in the Leroy Eyring Center for Solid State Science for assisting me with ICP-MS, FTIR, fluorescence, and XPS studies, respectively.

Support: I strongly believe my journey from an inexperienced student to a competent researcher in the past five years may not have been possible without the guidance of my advisor Prof. Anne Katherine Jones. She has been a constantly inspiring influence, teaching me not only the proper use of ethical science, but also advising me on the development of communication skills. I would also like to acknowledge my graduate committee members Prof. Ana Moore and Prof. Wim Vermass for their continuous support and assistance throughout my Ph.D. career. I am also grateful to my temporary committee members Dr. Don Seo and Dr. Ian Gould for their critical suggestions that improved my research. Finally, I would like to acknowledge all my present and past coworkers in the lab, including Dr. Chelsea McIntosh, Nicholas Teodori, Nataline Meinhardt, Souvik Roy, Patrick Kwan, Dr. Lu Gan, Dr. Idan Ashur, Dr. Angelo Cereda and all the undergraduates including Daniel, Julian, Rob and Sarah. I would like to thank Chelsea, Nick and Natie for welcoming this shy Indian boy with open arms and helping to familiarize him to a new environment. Souvik, I am grateful to you for patiently listening to my incipient chemical ideas and correcting them appropriately. Dr. Gan, thanks for your invaluable and insightful suggestions about research and life. Patrick, I really appreciate your thoroughly reviewing my first drafts and organizing them for further corrections. Dr. Ashur, thanks for teaching me the first lesson of electrochemistry. All your contributions towards my development as a researcher and a human being will be remembered.

TABLE OF CONTENTS

CHAPTER Page

LIST OF TABLES

LIST OF FIGURES

Figure Page

Figure Page

LIST OF SCHEMES

LIST OF ABBREVIATIONS

Abbreviation	Extended version
CD	Circular dichroism
CT	Charge transfer
CODH-ACS	Carbon monoxide dehydrogenase-Acetyl-Coenzyme A synthase
DAS	Decay associated spectra
DCM	Dichloromethane
DMF	N, N′–di-methyl formamide
EDT	Ethane dithiol
EPR	Electron Paramagentic Resonance
ESI-MS	Electron spray ionization mass spectrometry
EXAFS	Extended X-ray absorbance fine structure
Fmoc	9-fluorenylmethoxycarbonyl
FTIR	Fourier transformed Infra-red
HBTU	o-benzotriazole-N,N,N',N'-tetramethyluronium hexafluorophosphate
HPLC	High performance liquid chromatography
IC	Internal conversion
IRF	Instrument response function
ISC	Inter-system crossing
LMCT	Ligand to metal charge transfer
MALDI-MS	Matrix assisted laser desorption/ ionization mass spectrometry
MC	Metal centered

Abbreviation	Extended version
MLCT	Metal to ligand charge transfer
NEM	N-ethyl morpholine
NHase	Nitrile hydratase
NiSOD	Nickel superoxide dismutase
NMR	Nuclear paramagnetic resonance
SOD	Superoxide dismutase
SODA	Superoxide dismutase (alanine modified) (sequence: ACDLPCG)
TCSPC	Time correlated single photon counting
TFA	Trifluoroacetic acid
TIPS	Triisopropylsilane
UV-vis	Ultraviolet- visible
VR	Vibrational relaxation
XANES	X-ray absorbance near edge spectroscopy
XAS	X-ray absorbance spectroscopy
XPS	X-ray photoelectron specroscopy
XRD	X-ray diffraction
ZFS	Zero-field splitting

Chapter 1

Introduction: Scope and prospects of artificial metallopeptides as models for N_2S_2 coordinated metalloproteins

1.1. ***Metals in biology*****:** More than ten transition metals as well as several alkaline (Na, K) and alkaline earth metals (Mg, Ca, Sr, Ba) play crucial roles in the evolutionary development of various biomolecules and approximately one–third of characterized proteins contain one or more metal ions essential for function.[1–4] Metalloproteins mediate a variety of biophysical processes including electron transfer, signal transduction, small molecule activation, substrate transport, gene regulation, and regio- and stereo-selective transformation of metabolites.[1,5] Metals are also key components in the skeletal structures found throughout biology.[1,6] Metalloenzymes and metallocofactors are also critical components in biogeochemical cycles (carbon, oxygen, nitrogen, sulfur etc.), connecting the abiotic and biotic worlds.[1,7,8]

1.2. ***Industrial applications of native enzymes*****:** Metalloenzymes have found widespread use in such industries as polymer, detergent, textile, fuel-alcohol, and organic chemical production.[9] The cobalt containing metalloenzyme Co-nitrile hydratase (NHase) is extensively used in chemical industry.[10,11] It hydrolyzes aliphatic or aromatic nitriles to the corresponding amides; this catalytic activity is extensively employed in the polymer industry to produce more than 50,000 tons of acrylamide per year.[11–13] Some variants of Co-NHase have also been used in bioremediation since they can degrade various toxic nitrile compounds that arise

from anthropogenic activities.[14,15] The zinc bound enzyme hydantoinase is another example of a metalloenzyme extensively employed in industry; its stereo-selective hydrolytic activity is used in production of optically pure amino acids and synthesis of organic molecules such as antibiotics and pesticides.[16,17] Recent demand for carbon neutral fuels has spurred interest in H_2 as a possible fuel, and hydrogenases, the enzymes that reversibly convert H_2 to protons, have been widely explored for use in fuel cells.[18–22] Despite these notable successes, the majority of industrial catalysis is not performed by enzymes. The activity of enzymes is ordinarily limited to a narrow range of physiologically relevant conditions of pH, temperature and solvent.[23] In addition, small molecules such as O_2 or CO can modulate or inhibit the natural reactivity. Finally, transformations of unnatural substrates may be difficult or impossible to achieve using these naturally occurring metalloenzymes.

1.3. ***Inorganic catalysis in industry:*** The growing significance of organometallic catalysis is reflected by the three Nobel prizes in chemistry that have been awarded for discoveries in this research field within the last decade: asymmetric hydrogenation and oxidation (Noyori, Sharpless, Knowles; 2001), olefin metathesis (Schrock, Grubbs, Chauvin; 2005), and palladium catalyzed cross-coupling reactions (Suzuki, Heck, Negishi; 2010). Inorganic and organometallic catalysts are crucial in the energy, medical and food industries. They are employed in large scale synthesis of such compounds as acetic acid (Monsanto), methanol (BASF), adiponitrile (DuPont), and polymers of ethylene (Shell).[24–27] A recent combination of novel high throughput synthetic approaches

and enhanced mechanistic understanding has made this explosion of organometallic catalysis possible and is leading to previously unimaginable applications even in commodity industries.[28,29] Nonetheless, the large scale utility of organometallic catalysis is often limited by a reliance on expensive metals and toxic organic solvents. Furthermore, achieving selectivity and stereo-specificity during these transformations still remains difficult.[30] Thus developing efficient and selective catalysts based on abundant materials is a crucial challenge in chemical research.

1.4. ***Bio-inspired artificial metalloproteins*****:** Whereas organometallic complexes can exploit a wider range of metals to catalyze a catalog of reactions and create unnatural products, enzymatic processes are efficient and stereo-selective under benign reaction conditions. Artificial metalloproteins are envisioned as an approach intermediate to these two in which advantages of each of these methods can be combined.[31] One of the most significant goals of utilizing bio-inspired catalytic complexes is to use readily available and sustainable materials to develop catalytic processes relevant to chemical industry.[32] A second use of bio-inspired artificial metalloproteins has been to study physiologically important catalysis in an abiotic context. In general, artificial metalloproteins seek to introduce outer coordination sphere interactions into the catalytic system that modulate active site properties. Although this is achieved via a protein matrix in natural systems, artificial metalloproteins have been based on such supramolecular platforms as calixarenes, bipolar micelles, native protein scaffolds, *de novo* designed peptides, and nucleic acids.[33–41] Peptides, like proteins, utilize

the same multifunctional amino acids as building blocks and thus can create similar coordination environments. However, the relatively simple structures of designed peptide scaffolds offer the opportunity to precisely tune metal/peptide interactions without concomitant loss of biologically essential functionality.

1.5. ***The N_2S_2 metal binding motif in biology*****:** As shown in **Figure 1.1**, a broad range of functional and structural units occurring in biology are based on a simple N_2S_2 metal coordination site. The coordinating sulfurs are provided by cysteines (or methionine, in some cases) with nitrogens originating from a multitude of amines, histidines, and amides. An N_2S_2 coordinated nickel can be found in both superoxide dismutase (SOD) and cluster A of carbon monoxide dehydrogenase-acetyl Co-enzymeA synthase (CODH-ACS).[42–44] However, the reactivities of these two metalloenzymes are dramatically different. Analogous N_2S_2 binding environments are also known for cobalt and copper binding in hydrolytic Co-NHase and the electron transporting Type-I Cu proteins.[45–51]

1.6. ***Scope of this dissertation*****:** In this dissertation, I utilize the seven amino acid peptide SODA (ACDLPCG) to explore the range of reactive metallocenters that can be constructed in a single, small peptide ligand. This peptide, derived from the naturally occurring enzyme nickel superoxide dismutase (NiSOD), is known to bind Ni(II) in a square planar geometry.[52,53] I demonstrate that Co(II) and Cu(II)can also be coordinated by SODA, producing metallopeptides that react with both cyanide (CN^-) and molecular oxygen (O_2) (**Chapter 2**). In the case of Co(II)-SODA, I show that oxidation occurs in two steps with thiolate oxidation preceding metal oxidation (**Chapter 1**). This result is relevant to understanding

the biosynthesis of Co-NHase, an enzyme featuring modified cysteine ligands in three different oxidation states.[54,55] In the second part of the thesis, I describe the use of Ni-SODA as a metallosynthon for the creation of more complicated metallopeptides containing multiple, distinct metals (**Chapter 3, 4**). The cysteinyl sulfurs are reactive sites which I have exploited to develop a general synthetic method. Synthesis of a number of metallopeptides related to the active site of [NiFe]-hydrogenases is described as well as a route to novel photochemically active, sulfur bridged [NiRu] complexes. This work lays the foundation for development of other catalytic metallopeptides and highlights the potential of peptide based ligands in organometallic catalysis.

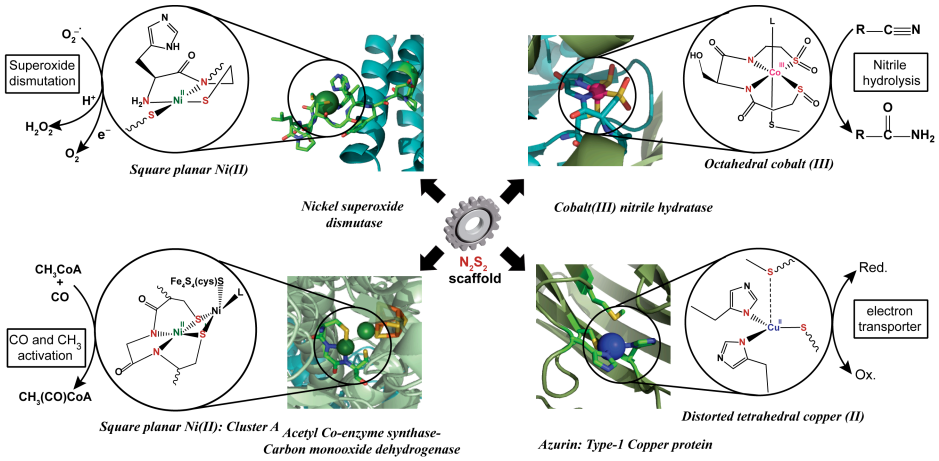

Figure 1.1. Diversity of N_2S_2 coordinated metallocenters in biology. The protein structures were drawn using Pymol [The PyMOL Molecular Graphics System, Version 0.99rc6, Schrödinger, LLC]. PDB codes are as follows: NiSOD: 1T6U; Co-NHase: 1UGP; ACS-CODH: 3I01; and Azurin: 1NWO.

1.7. References

1. Bertini, I., Gray, H. B., Stiefel, E. I. & Valentine, J. S. *Biological Inorganic Chemistry: Structure and Reactivity*. (University Science Books: 2007).

2. Gray, H. B. Biological inorganic chemistry at the beginning of the 21st century. *Proc. Natl. Acad. Sci. U.S.A.* **100**, 3563–3568 (2003).

3. Waldron, K. J., Rutherford, J. C., Ford, D. & Robinson, N. J. Metalloproteins and metal sensing. *Nature* **460**, 823–830 (2009).

4. Guengerich, F. P. Thematic Minireview Series: Metals in Biology 2012. *J. Biol. Chem.* **287**, 13508–13509 (2012).

5. Lippard, S. J. & Berg, J. M. *Principles of Bioinorganic Chemistry*. (University Science Books: 1994).

6. Douchiche, O., Driouich, A. & Morvan, C. Spatial regulation of cell-wall structure in response to heavy metal stress: cadmium-induced alteration of the methyl-esterification pattern of homogalacturonans. *Ann Bot* **105**, 481–491 (2010).

7. *Metal Ions in Biological Systems, Volume 43 - Biogeochemical Cycles of Elements*. (CRC Press: 2005).

8. Morel, F. M. M. & Price, N. M. The Biogeochemical Cycles of Trace Metals in the Oceans. *Science* **300**, 944–947 (2003).

9. Kirk, O., Borchert, T. V. & Fuglsang, C. C. Industrial enzyme applications. *Curr. Opin. Biotechnol.* **13**, 345–351 (2002).

10. Kobayashi, M., Nagasawa, T. & Yamada, H. Enzymatic synthesis of acrylamide: a success story not yet over. *Trends Biotechnol.***10**, 402–408 (1992).

11. Yamada, H. & Kobayashi, M. Nitrile Hydratase and Its Application to Industrial Production of Acrylamide. *Biosci. Biotechnol. Biochem.* **60**, 1391–1400 (1996).

12. Zheng, R.-C., Zheng, Y.-G., Shen, Y.-C. & Flickinger, M. C. Acrylamide, Microbial Production by Nitrile Hydratase. *Encyclopedia of Industrial Biotechnology* (2009).

13. Schulze, B. & Wubbolts, M. G. Biocatalysis for industrial production of fine chemicals. *Curr. Opin. Biotechnol.* **10**, 609–615 (1999).

14. Kobayashi, M. & Shimizu, S. Metalloenzyme nitrile hydratase: Structure, regulation, and application to biotechnology. *Nat. Biotechnol.* **16**, 733–736 (1998).

15. Banerjee, Sharma & Banerjee The nitrile-degrading enzymes: current status and future prospects. *Appl. Microbiol. Biotechnol.* **60**, 33–44 (2002).

16. Altenbuchner, J., Siemann-Herzberg, M. & Syldatk, C. Hydantoinases and related enzymes as biocatalysts for the synthesis of unnatural chiral amino acids. *Curr. Opin. Biotechnol.* **12**, 559–563 (2001).

17. Huang, C.-Y., Chao, Y.-P. & Yang, Y.-S. Purification of industrial hydantoinase in one chromatographic step without affinity tag. *Protein Expression Purif.* **30**, 134–139 (2003).

18. Cammack, R., Frey, M. & Robson, R. *Hydrogen as Fuel*. (CRC: 2002).

19. Jacobson, M. Z., Colella, W. G. & Golden, D. M. Cleaning the Air and Improving Health with Hydrogen Fuel-Cell Vehicles. *Science* **308**, 1901–1905 (2005).

20. Vincent, K. A. *et al.* Electrocatalytic hydrogen oxidation by an enzyme at high carbon monoxide or oxygen levels. *Proc. Natl. Acad. Sci. U.S.A.* **102**, 16951–16954 (2005).

21. Willner, I., Yan, Y.-M., Willner, B. & Tel-Vered, R. Integrated Enzyme-Based Biofuel Cells–A Review. *Fuel Cells* **9**, 7–24 (2009).

22. Hambourger, M. *et al.* [FeFe]-Hydrogenase-Catalyzed H2 Production in a Photoelectrochemical Biofuel Cell. *J. Am. Chem. Soc.* **130**, 2015–2022 (2008).

23. Fontecave, M. & Artero, V. Bioinspired catalysis at the crossroads between biology and chemistry: A remarkable example of an electrocatalytic material mimicking hydrogenases. *C. R. Chim.* **14**, 362–371 (2011).

24. *Applied Homogeneous Catalysis with Organometallic Compounds: A Comprehensive Handbook in Three Volumes*. (Wiley-VCH: 2002).

25. Hagen, J. *Industrial Catalysis: A Practical Approach*. (John Wiley & Sons: 2006).

26. *Asymmetric Catalysis on Industrial Scale: Challenges, Approaches and Solutions*. (Wiley-VCH: 2010).

27. Hintermair, U., Franciò, G. & Leitner, W. Continuous flow organometallic catalysis: new wind in old sails. *Chem. Commun.* **47**, 3691–3701 (2011).

28. Geiger, W. E. Reflections on Future Directions in Organometallic Electrochemistry†. *Organometallics* **30**, 28–31 (2011).

29. Hillard, E. A. & Jaouen, G. Bioorganometallics: Future Trends in Drug Discovery, Analytical Chemistry, and Catalysis. *Organometallics* **30**, 20–27 (2011).

30. *Catalytic Methods in Asymmetric Synthesis: Advanced Materials, Techniques, and Applications*. (2011)

31. Crow, J., Mitchell The perfect host. *Chemistry World* **4**, 50–53 (2007).

32. Deuss, P. J., den Heeten, R., Laan, W. & Kamer, P. C. J. Bioinspired Catalyst Design and Artificial Metalloenzymes. *Chem. Eur. J.* **17**, 4680–4698 (2011).

33. Schühle, D. T., Peters, J. A. & Schatz, J. Metal binding calixarenes with potential biomimetic and biomedical applications. *Coord. Chem. Rev.* **255**, 2727–2745 (2011).

34. Zhang, J., Meng, X.-G., Zeng, X.-C. & Yu, X.-Q. Metallomicellar supramolecular systems and their applications in catalytic reactions. *Coord. Chem. Rev.* **253**, 2166–2177 (2009).

35. Lu, Y., Yeung, N., Sieracki, N. & Marshall, N. M. Design of functional metalloproteins. *Nature* **460**, 855–862 (2009).

36. Goodman, C. M., Choi, S., Shandler, S. & DeGrado, W. F. Foldamers as versatile frameworks for the design and evolution of function. *Nat. Chem. Biol.* **3**, 252–262 (2007).

37. Moore, D. T., Berger, B. W. & DeGrado, W. F. Protein-Protein Interactions in the Membrane: Sequence, Structural, and Biological Motifs. *Structure* **16**, 991–1001 (2008).

38. Gibney, B. R. & Dutton, P. L. De novo design and synthesis of heme proteins. *Adv. Inorg. Chem., Vol 51* **51**, 409–455 (2001).

39. Kennedy, M. L. & Gibney, B. R. Metalloprotein and redox protein design. *Curr. Opin. Struct. Biol.* **11**, 485–490 (2001).

40. Roelfes, G. DNA and RNA induced enantioselectivity in chemical synthesis. *Mol. BioSyst.* **3**, 126–135 (2007).

41. Rosati, F. & Roelfes, G. Artificial Metalloenzymes. *ChemCatChem* **2**, 916–927 (2010).

42. Choudhury, S. B.; Lee, J.-W.; Davidson, G.; Yim, Y.-I.; Bose, K.; Sharma, M. L.; Kang, S.-O.; Cabelli, D. E.; Maroney, M. J. Examination of the Nickel Site Structure and Reaction Mechanism in Streptomyces seoulensis Superoxide Dismutase. *Biochem.* **38**, 3744–3752 (1999).

43. Wuerges, J. Crystal structure of nickel-containing superoxide dismutase reveals another type of active site. *Proc. Natl. Acad. Sci. U.S.A.* **101**, 8569–8574 (2004).

44. Barondeau, D. P., Kassmann, C. J., Bruns, C. K., Tainer, J. A. & Getzoff, E. D. Nickel Superoxide Dismutase Structure and Mechanism. *Biochem.* **43**, 8038–8047 (2004).

45. Nagashima, S.; Nakasako, M.; Dohmae, N.; Tsujimura, M.; Takio, K.; Odaka, M.; Yohda, M.; Kamiya, N.; Endo, I. Novel non-heme iron center of nitrile hydratase with a claw setting of oxygen atoms. *Nat. Struct. Mol. Biol.* **5**, 347–351 (1998).

46. Huang, W.; Jia, J.; Cummings, J.; Nelson, M.; Schneider, G.; Lindqvist, Y. Crystal structure of nitrile hydratase reveals a novel iron centre in a novel fold. *Structure* **5**, 691–699 (1997).

47. Miyanaga, A., Fushinobu, S., Ito, K. & Wakagi, T. Crystal Structure of Cobalt-Containing Nitrile Hydratase. *Biochem. Biophys. Res. Commun.* **288**, 1169–1174 (2001).

48. Nakasako, M.; Odaka, M.; Yohda, M.; Dohmae, N.; Takio, K.; Kamiya, N.; Endo, I. Tertiary and Quaternary Structures of Photoreactive Fe-Type Nitrile Hydratase from Rhodococcus sp. N-771: Roles of Hydration Water Molecules in Stabilizing the Structures and the Structural Origin of the Substrate Specificity of the Enzyme. *Biochem.* **38**, 9887–9898 (1999).

49. Song, L.; Wang, M.; Shi, J.; Xue, Z.; Wang, M.-X.; Qian, S. High resolution X-ray molecular structure of the nitrile hydratase from Rhodococcus erythropolis AJ270 reveals posttranslational oxidation of two cysteines into sulfinic acids and a novel biocatalytic nitrile hydration mechanism. *Biochem. Biophys. Res. Commun.* **362**, 319–324 (2007).

50. Karlsson, B. G., Aasa, R., Malmström, B. G. & Lundberg, L. G. Rack-induced bonding in blue copper proteins: Spectroscopic properties and

reduction potential of the azurin mutant Met-121 → Leu. *FEBS Lett.* **253**, 99–102 (1989).

51. Solomon, E. I.; Penfield, K. W.; Gewirth, A. A.; Lowery, M. D.; Shadle, S. E.; Guckert, J. A.; LaCroix, L. B. Electronic structure of the oxidized and reduced blue copper sites: contributions to the electron transfer pathway, reduction potential, and geometry. *Inorg. Chim. Acta* **243**, 67–78 (1996).

52. Neupane, K. P., Gearty, K., Francis, A. & Shearer, J. Probing Variable Axial Ligation in Nickel Superoxide Dismutase Utilizing Metallopeptide-Based Models: Insight into the Superoxide Disproportionation Mechanism. *J. Am. Chem. Soc.* **129**, 14605–14618 (2007).

53. Neupane, K. P. & Shearer, J. The Influence of Amine/Amide versus Bisamide Coordination in Nickel Superoxide Dismutase. *Inorg. Chem.* **45**, 10552–10566 (2006).

54. Zhou, Z., Hashimoto, Y., Shiraki, K. & Kobayashi, M. Discovery of Posttranslational Maturation by Self-Subunit Swapping. *Proc. Natl. Acad. Sci. U.S.A.***105**, 14849–14854 (2008).

55. Zhou, Z., Hashimoto, Y. & Kobayashi, M. Self-Subunit Swapping Chaperone Needed for the Maturation of Multimeric Metalloenzyme Nitrile Hydratase by a Subunit Exchange Mechanism Also Carries Out the Oxidation of the Metal Ligand Cysteine Residues and Insertion of Cobalt. *J. Biol. Chem.* **284**, 14930–14938 (2009).

Chapter 2

Sequential oxidations of thiolates and cobalt metallocenter in a synthetic metallopeptide: Implications for the biosynthesis of nitrile hydratase

*Arnab Dutta[†§], Marco Flores[†], Souvik Roy[†§], Jennifer C. Schmitt[‡], Alexander G. Hamilton[†], Hilairy E. Hartnett[†∞], Jason Shearer[‡], Anne K. Jones[†§]**

[†]Department of Chemistry and Biochemistry, [§]Center for Bio-Inspired Solar Fuel Production, [∞] School of Earth and Space Exploration; Arizona State University, Tempe, AZ 85287

[‡]Department of Chemistry, University of Nevada, Reno, Nevada 89557

2.0. Abstract

Cobalt nitrile hydratases (Co-NHase) contain a catalytic cobalt (III) ion coordinated in an N_2S_3 first coordination sphere comprised of two amidate nitrogens and three cysteine-derived sulfur donors: a thiolate (-SR), a sulfenate ($-S(R)O^-$), and a sulfinate ($-S(R)O_2^-$). The sequence of biosynthetic reactions that leads to the post-translational oxidations of the metal and the sulfur ligands is unknown, but the process is believed to be initiated directly by oxygen. Herein we utilize cobalt bound in an N_2S_2 first coordination sphere to a seven amino acid peptide known as SODA (ACDLPCG) to model this oxidation process. Upon exposure to oxygen, Co-SODA is oxidized in two steps. In the first fast step (seconds), magnetic susceptibility measurements demonstrated that the metallocenter remains paramagnetic, i.e. Co^{2+}, and sulfur K-edge X-ray absorption spectroscopy (XAS) is used to show that one of the thiolates is oxidized to sulfinate. In a second process on a longer timescale (hours), magnetic susceptibility measurements and Co K-edge XAS show that the metal is oxidized to Co^{3+}. The reactivity of this peptide is intermediate between all previously described models which either quickly convert to final product or are stable in air, and it offers a first glimpse into a possible oxidation pathway for nitrile hydratase biosynthesis.

2.1. Introduction

Post-translational modification of cysteinyl thiolates (RS^-) to such products as disulfide bonds (RS-SR'), sulfenates (RSO^-) or sulfinates (RSO_2^-) is relatively common in biology and has been found to play roles in signal transduction, protein structure, and enzyme functionality.[1–3] Cysteine residues are also commonly used in metalloenzymes to ligate metals or metalloclusters, although, the hydrolytic enzymes nitrile hydratase (NHase) and thiocyanate hydrolase (SCNase) are the only known examples of the rare class of metalloenzymes requiring sulfenate and sulfinate ligands for activity.[4–12] The active site of NHase consists of a low spin Fe(III) or Co(III) ion in an N_2S_3 coordination environment provided by two amide nitrogens from the protein backbone and three cysteines found in a highly conserved $\underline{C}XX\underline{C}(SO_2H)S\underline{C}(SOH)$ motif (**Figure 2.1**). It is interesting to note that each of the three coordinating cysteines is present in a different oxidation state: one thiolate, one sulfenate and one sulfinate. The oxidized cysteines are found in equatorial coordination sites along with the amides, and the thiolate ligand occupies an axial position *trans-* to the presumed substrate-binding site. A number of roles have been proposed for the oxidized cysteines including modulating the Lewis acidity of the metal site, serving as a base during the catalytic cycle, and modifying substrate/product binding affinity.[13]

Conversion of nitriles to amides is an industrially important reaction.[14,15] To help elucidate the mechanistic details of the enzymatic catalysis of these transformations, a number of small-molecule mimics of NHase have been synthesized.[16–22] However, few of these have even modest nitrile hydrolysis activity, and most of those that utilize oxidized sulfur contain bis-sulfinate ligands since controlling the extent of oxidation of the thiolates has proven difficult.[23] This has been especially true for reactions of thiolates with oxygen, as opposed to O-atom transfer reagents, which tend to yield sulfinato complexes.[18,23–34] Nonetheless, oxygen is believed to be the oxidant *in vivo* for modification of the sulfur atoms of NHase.[5,12,35–37] Biosynthetic studies have shown that apo-NHase, *i.e.*, the metal-free protein with cysteine thiolates, can be activated by incubation with Co^{2+} and appropriate activation mediating proteins via a novel mechanism that has been referred to as "self-subunit swapping".[35–37] First, the cobalt binding α-subunit is post-translationally modified and loaded with cobalt while the protein is part of a trimeric αe_2 complex with NhlE, a maturation mediator. Then, the holo-α-subunit is exchanged with an apo-α-subunit from the tetrameric apo-$\alpha_2\beta_2$ NHase to form the functional enzyme. Surprisingly, cobalt cannot be directly incorporated into apo-$\alpha_2\beta_2$ NHase, and this swapping of apo- and holo- proteins is an obligatory part of the maturation. However, although this symphony of protein subunits is now well documented, the chemical steps allowing for specific cysteine modification, cobalt incorporation and oxidation, and exchange of the two forms of the α-subunit are unknown.

Recently, Shearer and coworkers demonstrated the first functional metallopeptide mimic of Co-NHase.[22] The peptide coordinates Co in an N_2S_3 coordination sphere, and, as for the enzyme, two of the cysteines must be oxidized to observe modest activity with acrylonitrile. In this work, we utilize a related seven amino acid peptide known as SODA (A*C*DLP*C*G) to coordinate Co(II) in a less sulfur-rich N_2S_2 environment. We show that, upon exposure of the Co(II)-metallopeptide to air, the first oxidation occurs at the ligands without a change in the oxidation state of the metal. (**Scheme 2.1**). This ligand-oxidized, sulfur bound Co(II) system is then further oxidized to Co(III) to produce a fully oxidized species (**Scheme 2.1**). We propose that these differentially oxidized states are relevant to understanding the biosynthesis of Co-NHase, and possible mechanisms for metal incorporation into the enzyme and the roles of the distinctively oxidized thiolates present in the first coordination sphere during this process are discussed (**Scheme 2.2**).

2.2. Experimental Section

All inorganic syntheses were performed under a nitrogen atmosphere using a double-manifold Schlenk vacuum line. Unless otherwise specified, all the chemicals and solvents, of highest available grades, were obtained from Sigma-

Aldrich (Milwaukee, WI) and were used as received. Aqueous solutions were prepared using purified water (resistivity = 18.2 MΩ□cm).

Physical Measurements

Optical, FTIR, and CD spectroscopy. UV-visible measurements were executed on a Hewlett-Packard 8453 spectrophotometer using quartz cuvettes with a 1 cm pathlength. NMR spectra were recorded at 400 MHz (^{1}H) using Varian Liquid-State NMR instruments in D_2O (99.9%, Cambridge Isotopes Laboratories Inc.). FTIR (Fourier-transform infrared) spectra of the samples were recorded on a Thermo Nicolet Avatar-360 spectrometer in KBr pellets. A KBr pellet without sample was used as a reference for the background. For the samples, each spectrum is an average of 512 scans at 1 cm^{-1} resolution. The KBr pellets for the reduced samples were prepared in an anaerobic glove box. Circular dichroism (CD) spectroscopy was performed on a Jasco-815 spectropolarimeter using a rectangular quartz cell with a pathlength of 0.1 cm.

EPR spectroscopy. Electron paramagnetic resonance (EPR) spectra were recorded between 5K and 7K using a Bruker ELEXSYS E580 CW X-band spectrometer (Bruker, Silberstreifen, Germany) equipped with an Oxford model 900 EPL liquid helium cryostat (Oxford instruments, Oxfordshire, UK). The magnetic field modulation frequency was 100 kHz; the amplitude was 1 mT; the microwave power was between 1-4 mW and the microwave frequency was 9.42 GHz; the sweep time was 168 s. Samples for the EPR experiments were

prepared in a 1:1 mixture of aqueous 50 mM N-ethyl morpholine (NEM) buffer (pH 7.5) and glycerol (BDH, West Chester, PA) before transfer to a quartz EPR tube. EPR spectra were simulated using EasySpin (v 3.1.1), a computational package developed by Stoll and Schweiger[38] and based on Matlab (The MathWorks, Natick, MA, USA). The model used for the EPR simulations is based on a single high-spin Co^{2+} ion (S = 3/2). The variable parameters were: the *g* values (g_x, g_y and g_z), the line widths (ΔB_x, ΔB_y and ΔB_z), and the zero-field splitting parameters D and E. The fitting procedure was similar to the one previously described by Flores et al.[39]

Magnetic susceptibility. The molecular magnetic susceptibility (χ_M), effective magnetic moment (μ_{eff}) for the partially oxidized Co-SODA, and the time course measurement for the oxidation of reduced Co-SODA after exposure to air were measured via the Evans NMR method by monitoring shifts in the water solvent peaks at either 400 or 500 MHz (^1H) using a Varian Liquid-State NMR instrument.[40,41]

Mass spectrometry. MALDI-MS (matrix assisted laser desorption/ionization mass spectrometry) characterization of apo-SODA was performed on a Voyager DE STR. ESI-MS (electrospray ionization mass spectrometry) of all metallopeptide samples was accomplished using a Thermo Quantum Discovery Max triple-quadrupole mass spectrometer. Measurements were conducted in positive (+) and negative (–) ionization modes, using a methanol/water (50:50 by volume) mobile phase at a flow rate of 10 μL min^{-1} and the following ionization

conditions: spray voltage, 4000 V(+, –); capillary temperature, 270°C; sheath gas pressures, 25 (+) and 15 (–) psi; auxiliary gas pressure, 2 (+, -) psi. Isotope Pattern Calculator v4.0, developed by Junhua Yan, was used for the calculation of the molecular mass with isotopic abundances.

Co K-edge and S K-edge X-ray Absorption Data Collection and Analysis. Solutions of Co-SODA were prepared as 1:1 CoSODA (50 mM NEM buffer, pH 7.5):glycerol samples, injected in aluminum sample holders between windows made from Kapton tape (3M; Minneapolis, MN, catalog no. 1205) and quickly frozen in liquid nitrogen. Data were collected on beamline X3b at the National Synchrotron Light Source (Brookhaven National Laboratories; Upton, NY). The samples were maintained at 20 K throughout data collection in an evacuated He Displex cryostat and collected in fluorescence mode on a Canberra 31 element solid-state Ge detector. Total count rates for all channels were maintained under 30 kHz, and a deadtime correction was not applied. The data were collected in 10 eV steps below the edge (7609 – 7689 eV), 0.5 eV steps in the edge region (7689 – 7759 eV), 2 eV steps in the near-edge region (7759 – 8009 eV) and 5 eV steps in the far edge region (8009 eV – 14 keV). The spectra represent the averaged sum of 3 independent data scans. The sulfur K-edge data were collected as solution samples at room temperature on beamline X19a at the National Synchrotron Light Source (Brookhaven National Laboratories; Upton, NY). Solutions of CoSODA (50 mM NEM buffer, pH 7.5) were injected into Lucite sample holders between two polyester film windows (2.5 μm thickness; SPI

Supplies; West Chester, PA, catalogue no. 01865-AB) adhered to the sample holders using an epoxy resin. Data were collected in a sample chamber that was continuously purged with He(g) and data were recorded in fluorescence mode on a Canberra passivated implanted planar silicon (PIPS) detector. Data were collected from 200 eV below to 300 eV above the edge to obtain a good baseline for data analysis. In the pre-edge region, data were collected in 5 eV steps (2270 – 2465 eV); in the edge region, data were collected in 0.1 eV steps (2465 – 2475 eV); in the far edge region, data were collected in 2 eV steps (2475 – 2765 eV). All data were calibrated to the white line of Na_2SO_4. The spectra presented represent the summed average of 5 scans.

All Co and S K-edge spectra were processed and analyzed as previously described.[22,42] Briefly, S K-edge spectra were obtained by averaging the data sets, applying a baseline, and fitting the pre-edge region to a polynomial function. This baseline was then subtracted from the whole spectrum. The region above the edge jump was fit to a two knot cubic spline, and the data normalized to the edge height. The pre-edge and rising-edge features were modeled as pseudo-Voigt line shapes (a 1:1 sum of Gaussian and Lorentzian line shapes). Co K-edge spectra were processed and analyzed using the XAS data analysis suit *EXAFS123* [43] which operates in Igor Pro[44] (and requires phase and amplitude functions generated within FEFF 8.20.[45] All refinements are based on Fourier-filtered $k^3(\chi)$ data over the energy range of k = 2.0 – 12.0 Å^{-1} and back-transformed over the range of r = 1.0 – 3.0 Å.

Peptide synthesis and purification. The seven amino acid peptide referred to as SODA (ACDLPCG) was synthesized on a Protein Technologies PS3 automated peptide synthesizer using the standard Fmoc/tBu (Fmoc, 9-fluorenylmethoxycarbonyl) protection strategy and HBTU (o-benzotriazole-N,N,N',N'-tetramethyluronium hexafluorophosphate) as coupling agent on Fmoc-gly Wang resin (loading capacity 0.54 mmol/g) at 0.4 mmole scale. During the synthesis, 20% piperidine in DMF (N,N-dimethyl formamide) and 0.4 M N-methyl morpholine in DMF were used as deprotecting agent and activator respectively. Fmoc protected amino acids, Fmoc-Gly wang resin, and HBTU were obtained from Protein Technologies (Tucson, AZ, USA). The peptide was simultaneously deprotected and cleaved from the resin using a mixture consisting of 94% TFA (trifluoroacetic acid), 2.5% water, 2.5% EDT (ethanedithiol) and 1% TIPS (triisopropylsilane) for 2 hours. Following concentration, the crude peptide was precipitated by adding cold (-20ºC) diethyl ether. The crude peptide was purified by reverse-phase HPLC on a Waters 600E system with a photodiode array detector on either a 3x250 mm ODS-A, 300 Å C-18 column from YMC Inc. for analytical scale or a PrepLC 25 mm module C-18 column from Waters for semi-preparative scale. Aqueous acetonitrile gradients containing 0.1% TFA (v/v) were used as the mobile phase. Purity of samples was confirmed by analytical HPLC and molecular weight determined by MALDI-MS. Peptide concentrations were quantified using the procedure of Ellman.[46] Yield = 60%. MALDI-MS (positive ion) $[M]^+$ m/z experimental 678; calculated 677.8.

Synthesis and purification of NHasem1 (CCDLPCGVYDPA) and the subsequent preparation of Co-NHasem1 were performed as described by Shearer *et al*.[22]

Co-SODA preparation in reduced and oxidized forms. Metallopeptide samples were prepared analogously to the procedure described by Neupane *et al*. for the synthesis of the corresponding Ni-metallopeptide.[47] One equivalent of an aqueous solution of Co(II) (ten times concentrated compared to SODA solution) was added dropwise to one equivalent of SODA in 50 mM NEM buffer (pH= 7.5) solution. The concentration of the SODA solution was determined using Ellman's test.[46] Both solutions were degassed and saturated with nitrogen prior to the reaction. The reaction mixture immediately turned green upon addition of the cobalt solution. If exposed to oxygen, the reduced Co-SODA solution rapidly changes to brown.

Reduced Co-SODA: The electronic absorption spectrum (in buffered aqueous solution, pH 7.5) had the following features: λ_{max} nm (ε $M^{-1}cm^{-1}$): 725 (210), 681 (230), 609 (225), 350 (shoulder); 303 (1950). The ESI-MS (negative ion mode) yielded a $[M-H]^-$ peak with an m/z of 731.01 that corresponded well with the calculated mass of 731.1 amu for this species.

Partially oxidized Co-SODA: The features of the electronic absorption spectrum (in buffered aqueous solution, pH 7.5) are as follows: λ_{max} nm (ε $M^{-1}cm^{-1}$): 600 (shoulder), 460 (shoulder), 355 (1100). ESI-MS (positive ion mode) yielded an

$[M+O+3H]^+$ molecular ion peak at 752.04 m/z; the calculated mass was 752.17 amu. The measured effective magnetic moment was μ_{eff} = 4.38 B.M.

Fully oxidized Co-SODA: The electronic absorption spectrum features (in buffered aqueous solution, pH 7.5) included: λ_{max} nm (ε $M^{-1}cm^{-1}$): 570 (shoulder), 450 (shoulder), 340 (1500). The ESI-MS (positive ion mode) yielded an $[M+O+3H]^+$ molecular ion peak at 752.06 m/z, and the calculated mass was 752.17 amu.

2.3. Results and Discussion

Coordination of Co(II) by SODA. The seven amino acid peptide SODA (ACDLPCG) is derived from the nickel enzyme superoxide dismutase and is known to coordinate a Ni(II) ion via the two cysteines together with the amino terminus and a backbone amide nitrogen.[48–50] Thus it seemed likely that a similar coordination set could accommodate Co(II), and the interactions between Co(II) and SODA were investigated via optical spectroscopy under both anaerobic and aerobic conditions. First, an anaerobic aqueous Co(II) solution was added dropwise to a buffered SODA solution (pH 7.5) resulting in a green solution. As shown in **Figure 2.2A**, the UV-vis absorbance spectrum of this reduced, cobalt-bound metallopeptide includes three distinct ligand field (LF) bands in the visible region at 725 nm (ε = 210 $M^{-1}cm^{-1}$), 681 nm (ε = 230 $M^{-1}cm^{-1}$) and 609 nm (ε =

225 M^{-1} cm^{-1}). These bands have the appropriate energies and extinction coefficients for the $^4T_1(P) \leftarrow {}^4A_2(F)$ transitions expected to arise from a tetrahedral Co(II) (d^7) center (**Table 2.1, Figure 2.2A**), and are split, as expected, due to spin-orbit coupling.[51–53] The stoichiometry of the interaction between Co(II) and SODA was determined by monitoring the absorbances at these three wavelengths as a function of added Co(II) as shown in **Figure 2.2B**. Titrations at all three wavelengths are consistent with a 1:1 interaction between Co(II) and SODA. Further evidence for 1:1 binding was provided by mass spectrometry. A $[Co\text{-}SODA]^-$ molecular ion peak with the expected isotopic pattern was observed in a negative-mode ESI-MS experiment (**Figure 2.3**). In addition to the LF bands, two stronger bands at 350 nm (ε = 1450 $M^{-1}cm^{-1}$) and 303 nm (ε = 1950 $M^{-1}cm^{-1}$) were observed in the far UV region of the optical spectrum for reduced Co-SODA (**Figure 2.2A**). Based on comparison to other Co-substituted proteins such as Co-rubredoxin, Co-methionine, and Co liver alcohol dehydrogenase, these higher energy bands likely arise from cysteinyl sulfur to Co(II) charge transfer (CT).[54–56] Comparison of these proteins has demonstrated that each Co-thiolate bond in a metalloprotein or peptide typically contributes ε = 900-1200 $M^{-1}cm^{-1}$ in such a ligand to metal charge transfer (LMCT) transition. Since ε_{303} (Co-SODA)=1950 $M^{-1}cm^{-1}$, it is likely that Co-SODA includes two Co-thiolate bonds.[57]

The CD spectrum of reduced Co-SODA consists of four transitions: a negative band at 280 nm, a positive band at 312 nm, a positive band at 404 nm,

and a negative band at 544 nm (**Figure 2.4, Table 2.1**). The two highest energy bands are likely related to the S→Co LMCT transitions, which are CD active because the first coordination sphere of the cobalt is non-centrosymmetric. The neighboring chiral amino acid based transitions also induce chirality into the metal centered chromophores resulting in the two lower energy features and providing additional evidence that the peptide is involved in coordination of the metal.[47,59]

To evaluate the possibility that the other two ligands to tetrahedral Co(II) in Co-SODA were nitrogenous, FTIR spectra in the region 400-1000 cm^{-1} were collected. Three characteristic ῡ(Co-N) stretching frequencies were observed at 452, 475 and 602 cm^{-1} for Co-SODA which are absent in the spectrum of the SODA apo-peptide (**Figure 2.5**). The two lower energy bands are consistent with symmetric and asymmetric Co-N stretching vibrations for two *cis*-positioned M-N bonds, for M=metal. The highest energy band likely arises from out of plane bending of C=O for a metal-bound amide, which is affected by the M-N bond strength since the two bonds are shared in a ring structure (**Scheme 2.1**).[60,61] Thus, it is very likely that the remaining two ligands of the primary coordination sphere are the amino terminus and a backbone amide, as seen in the Ni-SODA peptide.

Aerobic oxidation of Co-SODA. To investigate the effects of molecular oxygen on the reduced Co-SODA sample, it was exposed to air. The green, reduced Co-SODA was found to be oxygen sensitive; in the presence of air, it turned reddish-brown within a few minutes. The UV-vis spectrum recorded after 30 minutes of

exposure to air consists of a nearly featureless, increase in absorption in the visible region with broad shoulders at 600 and 460 nm (**Figure 2.2A, Table 2.1**). In the far UV region, a sharp band is seen at 355 nm. The prominent LF bands observed for the reduced Co-SODA bleached immediately upon air oxidation, suggesting changes in the tetrahedral coordination geometry around the cobalt center. When this oxidized Co-SODA sample was exposed to air for longer periods (72 hours), additional subtle changes in the optical spectra were observed after 24 hours. The bands of the initially formed oxidized species were subtly shifted to 570 nm, 450 nm, and 340 nm, respectively (**Figure 2.2A, Table 2.1**). After this second oxidized species was formed, no additional spectral changes were observed. These modifications of the optical spectra upon exposure to air suggest a stepwise oxidation of the reduced Co-SODA by oxygen; a partially oxidized intermediate forms first followed later by the fully oxidized product.

CD spectra were also recorded after exposure of the reduced Co-SODA to oxygen. After exposure of the sample to air for 30 minutes, a new spectrum with bands at 267 nm (negative), 306 nm (positive), 420 nm (positive) and 536 nm (negative) arose, suggesting changes in the interactions between the peptide and the cobalt ion. After 24 hours of exposure to air, the CD spectrum was further changed. In particular, both band positions and elliptical polarization (positive or negative) were changed, and a new positive feature appeared at 470 nm (**Figure 2.4**). This suggests further rearrangements in the metal-ligand electronic environment after extended interactions with oxygen. Thus CD spectroscopy

provides evidence complementary to UV-vis absorption spectroscopy that two distinct species are sequentially formed by air oxidation of Co-SODA.

Magnetic susceptibility changes upon exposure of Co-SODA to oxygen. There are two distinct sites in Co-SODA at which oxidation could easily occur: the cysteinyl thiolates and the metal. Oxidation of the metal from Co(II) to Co(III) would result in a change from a paramagnetic (d^7, S=3/2) starting material to a diamagnetic (d^6, S=0) product. Thus we used the Evans NMR method to determine the effect of air oxidation on the magnetic susceptibility of the sample. In this experiment, the shift of a solvent NMR resonance in a sample containing the complex of interest is monitored relative to a pure solvent sample. The frequency difference between the solvent signal in the presence and the absence of the metal complex can be directly correlated to the magnetic susceptibility of the sample. As shown in **Figure 2.6**, the reduced sample is paramagnetic (0 minute data), resulting in two distinct ^{1}H NMR resonances for the pure H_2O and the H_2O in the presence of Co-SODA (For a solution of ~ 1.9 mM metallopeptide in the 500 MHz NMR instrument a shift of 30 Hz was observed). **Figure 2.6** shows analogous H_2O ^{1}H NMR spectra collected after the Co-SODA sample was exposed to air for varying lengths of time. The paramagnetism of the Co-SODA sample continued to be observed for several hours after exposure to air. The molecular magnetic susceptibility (χ_M) of the partially oxidized sample was evaluated using the Evans NMR method.[40,41] The calculated effective magnetic moment (μ_{eff}) was 4.38 Bohr magnetons. Based on the relation: μ_{eff} =

√[n(n+2)],where n= number of unpaired electrons, it is likely that the partially oxidized sample contains at least three unpaired electrons (*i.e.*, an S=3/2 system), corresponding to Co(II). Finally, after 24 hours, the solvent signal collapsed into a single peak indicating that the system became diamagnetic. The persistence of paramagnetism for several hours suggests that the initial oxidation does not change the oxidation state of the cobalt. Instead, only on longer time scales is a diamagnetic, Co(III) species formed.

To explore the hypothesis that the initial site of oxidation of the metallopeptide is the cysteine ligands, attempts were made to detect sulfinate or sulfenate groups via FTIR. Although upon oxidation of the peptide extensive changes in the 1200-900 cm^{-1} region of the spectrum were observed, the bands could not be unambiguously assigned leaving interpretation relatively meaningless.

EPR spectroscopy. NMR experiments demonstrated paramagnetism in the reduced and partially oxidized Co-SODA samples. EPR spectra were recorded for these paramagnetic samples to gain insight into their electron spin distributions and corresponding changes upon oxidation. **Figure 2.7A** shows the EPR spectrum of the reduced Co-SODA sample. The spectrum was simulated using a spin Hamiltonian (see materials and methods) for a high spin Co(II) (d^7 system, S=3/2) system.[62,63] The good agreement between the experimental and simulated data (σ = 0.94%) suggests, as expected, that the spectrum arises from a high spin Co(II) center. The parameters obtained from simulation, g values and zero field splitting

(ZFS) constraints for the reduced Co-SODA species, are shown in **Table 2.2**. The small E/D value indicates the presence of an effectively axial field around the paramagnetic Co(II) center. The EPR spectrum of the partially oxidized sample (**Figure 2.7B, Table 2.2**) was also simulated with an S=3/2 spin Hamiltonian (σ = 1.20%). Although the spectra are quite similar, the g-values for the two species were not identical. This is most clearly seen from their rhombicity parameters [(g_x-g_y/g_z) x 100%], which have values of 18.102 and 12.170 for the reduced and partially oxidized samples, respectively. The decrease in rhombicity after the partial oxidation of the complex is consistent with a change in the coordination geometry of the cobalt with no change in the oxidation state of the metal.

X-ray absorbance spectroscopy. Cobalt X-ray absorbance spectra (XAS) were obtained to confirm the oxidation state and characterize the first coordination sphere of the cobalt in the partially oxidized and completely oxidized samples. In the XAS spectrum of the fully oxidized sample (**Figure 2.8A**), a weak (3.7(1) eV relative to edge height) pre-edge feature at ~7719 eV was observed that arises from the dipole forbidden Co(1s→3d) transition. This transition is ordinarily observed only for cobalt centers in a non-centrosymmetric environment. The edge energy of ~7723 eV corresponds to the presence of a Co(III) center in the fully oxidized metallopeptide sample, consistent with the diamagnetism observed via NMR. The extended X-ray absorbance fine structure (EXAFS) region of the XAS data is best modeled as a pseudo-octahedrally coordinated cobalt center (**Figure 2.8D**) in an $S_2(N/O)_4$ coordination environment (**Figure 2.8B,C**). The two sulfur

scatterers are 2.24 Å from the Co(III) ion. The N/O ligands could be resolved into three shells: two N/O ligands at 2.13 Å, one N/O ligand at 1.97 Å, and one nitrogen ligand at 1.84 Å from the cobalt center. The last one is likely to be a deprotonated amide nitrogen ligand from the peptide backbone. The scatterer at 1.97 Å could be the amino terminus of the peptide, and the ligands at longer distances are likely solvent molecules or other loosely bound amides.

Figure 2.9 compares the XANES regions of the spectra for the fully oxidized and the partially oxidized metallopeptides. An EXAFS spectrum from a partially oxidized sample obtained via an experiment analogous to that shown in **Figure 2.8** is shown in **Figure 2.10**. The edge energy of the partially oxidized sample is 2.9(1) eV lower in energy than that of the fully oxidized sample. These edge energies are consistent with a change from Co(II) in the partially oxidized sample to Co(III) in the fully oxidized sample. The area under the pre-edge feature for the partially oxidized sample is 3.6(2)%, which is also consistent with a six coordinate geometry in the partially oxidized sample. Since the EXAFS data for the partially oxidized sample were of relatively poor quality at high k, the spectrum was only refined over the range 2-11 $Å^{-1}$ and BT. Like the completely oxidized sample, the partially oxidized sample is best fit to a model including two sulfur ligands and four N/O ligands in the first coordination sphere (**Figure 2.10**).

Sulfur K-edge X-ray absorbance spectra of the reduced, partially oxidized and fully oxidized metallopeptides were obtained to unambiguously determine the oxidation states of the cysteinate ligands in each sample. As shown in **Figure**

2.11, the reduced sample contained, as expected, only unoxygenated cysteinate sulfurs; a pre-edge peak at 2470.9(1) eV was observed corresponding to the S(1s) → Co(3d) transition. At higher energy (2472.6(1) eV), the S(1s) □ (C-S(σ*)) transition is observed. In contrast, the S K-edge results suggest the completely oxidized Co(III) complex contains one unmodified cysteinate and one that has been oxidized to a sulfinate (SO_2^-) ligand. The S K-edge spectrum for this sample includes a relatively small pre-edge feature at 2477.8(3) eV together with a strong peak at 2480.8(3) eV. These correspond to SO_2(1s) → Co(3d) and SO_2(1s) → C–S(σ*) transitions, respectively. In addition the S(1s) → Co(3d) transition is observed at 2470.1(1) eV and the S(1s) → (C-S(σ*)) transition at 2473.3(2) eV indicating the presence of a reduced thiolate sulfur ligand. The spectrum of the partially oxidized sample is remarkably similar to that of the completely oxidized metallopeptide and is also consistent with the sulfur being present as thiolate and sulfinate species. These data provide clear spectroscopic evidence that the first step in the oxidiation process is modification of one of the cysteines to form sulfinate. All the Co and S K-edge XAS data is summarized in **Table 2.3**.

2.4. Concluding Remarks

As depicted in **Scheme 2.1**, the data presented herein suggest the tetrahedral high spin d^7 Co(II)-SODA is air oxidized in a two-step process. The immediate changes in the UV-vis and CD spectra upon exposure of Co-SODA to air suggest

oxidation occurs rapidly and results in formation of a pseudo-octahedral species. However, perhaps surprisingly, NMR and EPR spectra indicate that the first oxidation product formed is still paramagnetic with three unpaired electrons. This indicates Co cannot be the first species oxidized. Instead, the S K-edge XAS spectrum of this intermediate shows that the first oxidation occurs at a single cysteine ligand to form a sulfinate. Then, it is only on longer time scales that Co oxidizes to the 3+ oxidation state becoming a diamagnetic low spin d^6 system. EXAFS data suggest this fully oxidized metallopeptide contains a pseudo-octahedrally coordinate Co(III) ion ligated by an unmodified cysteinate as well as an oxidized sulfinate ligand. The remainder of the coordination sphere is four N/O donors present in two pairs at different distances. Two of those are likely to be the peptide ligands from the reduced peptide and the additional ones are expected to be solvent molecules. Thus air oxidation of Co-SODA causes two sequential types of changes: first oxidation of one of the cysteines, followed by oxidation of the metal.

Oxidation of cysteinyl thiolates can result in a number of products including disulfide bonds, sulfinate and sulfenate. Thus the question of how each cysteine in the active site of nitrile hydratase achieves a unique oxidation state comes to the fore, and Co-SODA, in which one cysteinate is modified and the other remains reduced, is an interesting model. For these metalloproteins/peptides, formation of disulfide bonds is likely of little concern due to the relative inertness of Co(II) to substitution reactions. On the other hand, as shown in **Scheme 2.3**, oxidation of a

thiolate sulfur to sulfenate or sulfinate introduces S-O σ* symmetric orbitals to the system. These new orbitals are expected to orient the metal d-orbitals in the equatorial plane as they participate as acceptors in π-bonding with the metal. Additionally, the S-O π* orbitals should be more efficient in formation of σ bonds with the d_z^2 and $d_{x^2-y^2}$ than the reduced thiolates.[64] In short, in the case of Co-SODA, a peptide originally designed to bind not Co but Ni, oxidation of one of the cysteines likely provides more stable bonding. This lowers the energies of the occupied Co d orbitals and increases the driving force for oxidation of the metal to form a low spin d^6 system. Furthermore, binding of S-O ligands likely strains the tetrahedral geometry of Co(II)-SODA towards a more favorable octahedral environment, again providing ideal conditions for oxidation of the metal. We can speculate that once the metal is oxidized in Co-SODA there is relatively little energetic gain from oxidation of the second thiolate so that it remains unmodified.

Comparison of Co-SODA to other model complexes for nitrile hydratase suggests reasons for the unique reactivity of this metallopeptide. Angelosante and coworkers reported the synthesis of an unsymmetrical, square planar S=1 Co(II) complex in which the metal is coordinated in an N_2S_2 environment consisting of two thiolates and two amidates.[65] Interestingly, this complex mimics the asymmetric equatorial coordination environment of nitrile hydratase that consists of two five-membered rings and a single six-membered ring. However, in contrast to Co-SODA, the reported complex does not undergo air oxidation of either the thiolates or the metal.[65] In essence, the square planar complex appears to be too

stable to promote the oxidation. On the other hand, Shearer and coworkers reported the reactivity of an N_2S_3 coordinated Co-metallopeptide known as Co-NHasem1.[22] Like Co-SODA, reduced Co-NHasem1 binds Co(II) in a tetrahedral environment consisting of two thiolates and two amidates. Upon exposure to air, both the metal and two of the three thiolates are oxidized. As shown in Fig. S3, we undertook NMR experiments with Co-NHasem1 to compare its oxidation pathway to that of Co-SODA. Unlike Co-SODA, upon oxidation Co-NHasem1 rapidly forms a diamagnetic Co(III) state. Furthermore, both equatorial thiolates are likely oxidized. The increased rate of metal oxidation in Co-NHasem1 is likely a result, in large part, of the additional axial thiolate ligand and the replacement of an amine with an amide ligand. As shown in **Scheme 2.4**, the strongly σ-donating axial thiolate likely interacts with the metal d_z^2 orbital, changing its character from non-bonding to antibonding – significantly raising its energy. Similarly, the amide of Co-NHasem1 provides stronger π-bonding than the amine of Co-SODA further increasing the ligand field stabilization energy of the N_2S_3 peptide and stabilizing the low spin d^6 oxidized state. Thus oxidation of Co-NHasem1 is considerably more favorable energetically than oxidation of Co-SODA. Essentially, Co-SODA is intermediate between the relatively inert complex of Angelosante and coworkers and the reactive metallopeptide Co-NHasem1. Furthermore, it is likely the tetrahedral geometry of the reduced Co-SODA species and the lack of an axial thiolate that allow it to occupy this unique niche of reactivity.

Finally, we end by speculating as to the applicability of Co-SODA to understanding the details of metal incorporation and protein modification in the natural nitrile hydratase enzyme. Cobalt is generally transported into microbes as Co(II) ion, and it is likely that Co is incorporated into the apo-nitrile hydratase α subunit in this reduced oxidation state.[66,67] Biochemical evidence has arisen that, at least *in vitro*, post-translational modification of the nitrile hydratase protein and oxidation of the metal are autocatlytic.[5] The reactivity of Co-SODA in air lends further credence to such a model. By analogy to Co-SODA, we hypothesize that interaction of the reduced NHase protein with air first results in oxidation of one or both of the equatorial sulfur ligands. Initial binding of the metal in a geometry that is more tetrahedral than square planar geometry would likely promote the specific protein modifications. The modified bonding with the oxidized ligands could then provide the driving force for a subtle change in geometry and oxidation of the metal to the active form of the enzyme. At the moment, these ideas are hypothetical, but further investigation of both the enzyme and relevant model complexes is expected to clarify the remaining unknowns of this unique biosynthetic process.

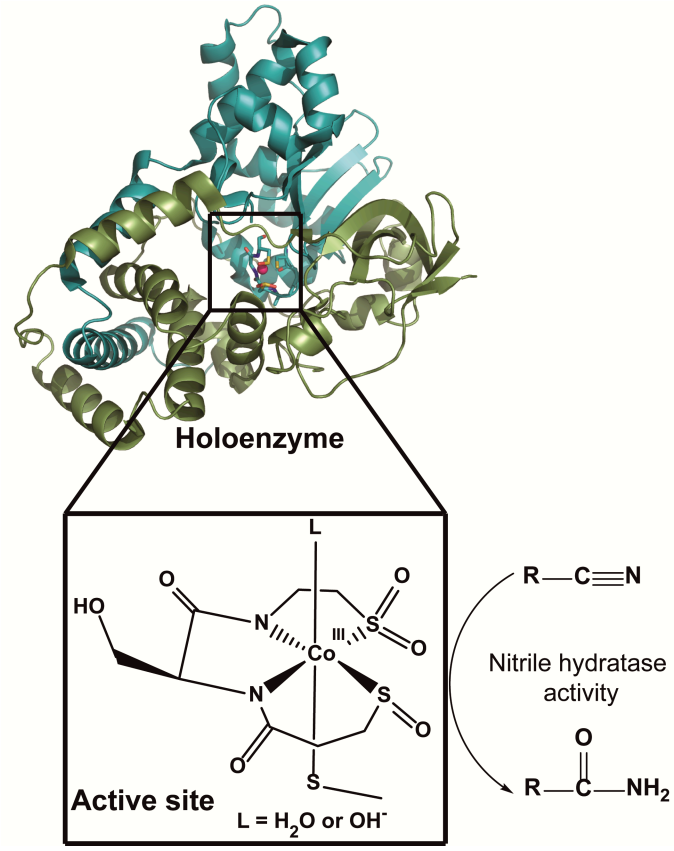

Figure 2.1. Co(III)-nitrile hydratase enzyme and its active site. Heterodimeric cobalt nitrile hydratase enzyme and its metal active site (PDB code: 1UGP, figure prepared using PyMOL software [The PyMOL Molecular Graphics System, Version 0.99rc6, Schrödinger, LLC]). The green color corresponds to the α chain and the blue color to the β chain, respectively.

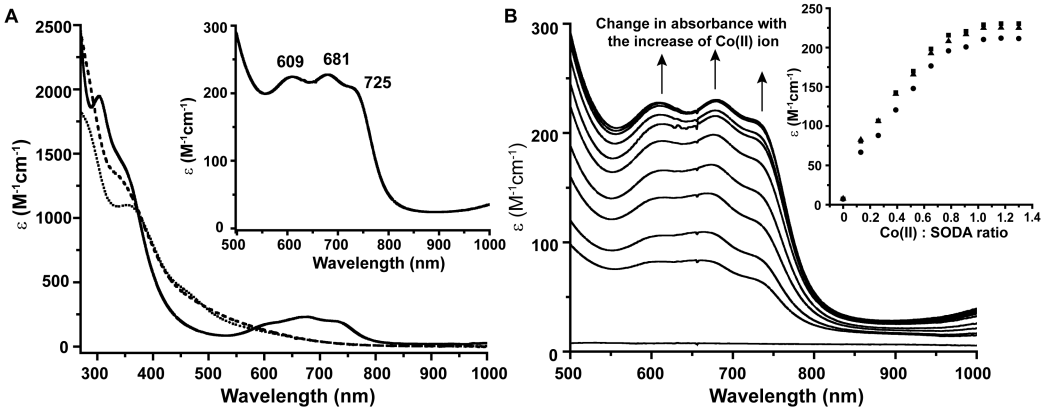

Figure 2.2. Comparative optical spectra and titration curve for Co-SODA. **(A)** UV-vis spectrum of Co-SODA (solid black line), partially oxidized Co-SODA (dotted black line, 30 minutes of air oxidation), completely oxidized Co-SODA (dashed black line, 24 hours of air exposure) All solutions are in aqueous 50 mM NEM buffer at pH 7.5. The inset shows an enlargement of the region between 500 and 1000 nm featuring bands associated with ligand field (LF) transitions for reduced Co-SODA. **(B)** Spectral changes in the UV-vis spectrum of SODA upon stepwise addition under anaerobic conditions of an aqueous solution (50 mM NEM buffer, pH 7.7) of Co(II). The inset shows the binding curves extracted at three different wavelengths from the spectra (squares 681 nm, circles 725 nm, and triangles 609 nm). The ratios of Co(II):SODA for which spectra are shown are 0:1, 0.13:1, 0.26:1, 0.39:1, 0.52:1, 0.65:1, 0.78:1, 0.91:1, 1.04:1, 1.17:1, and 1.3:1.

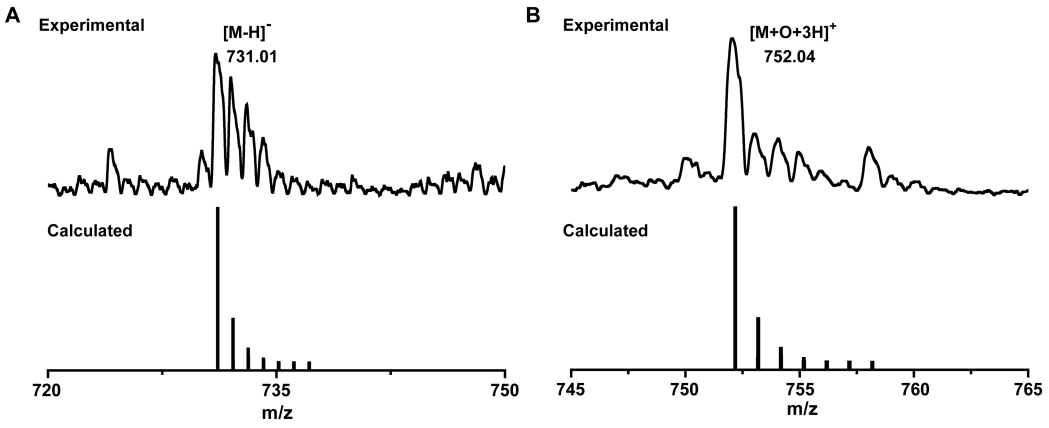

Figure 2.3. **Comparative ESI-mass spectra for Co-SODA.** Experimental and calculated ESI-MS spectra from (A) Co-SODA (reduced; negative ion mode) and (B) Co-SODA (oxidized; positive ion mode).

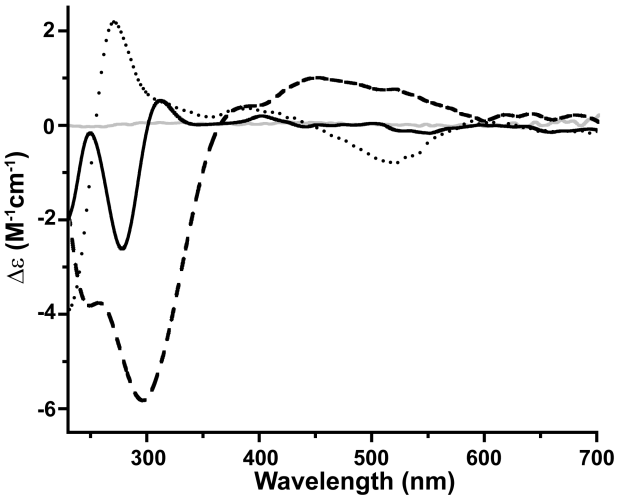

Figure 2.4. Comparative CD spectra for Co-SODA. CD spectra for reduced Co-SODA (solid black line), partially oxidized Co-SODA (dotted black line), completely oxidized Co-SODA (dashed black line) and the SODA apo-peptide (solid grey line). All metallopeptide samples were in aqueous 50 mM NEM buffer at pH 7.5.

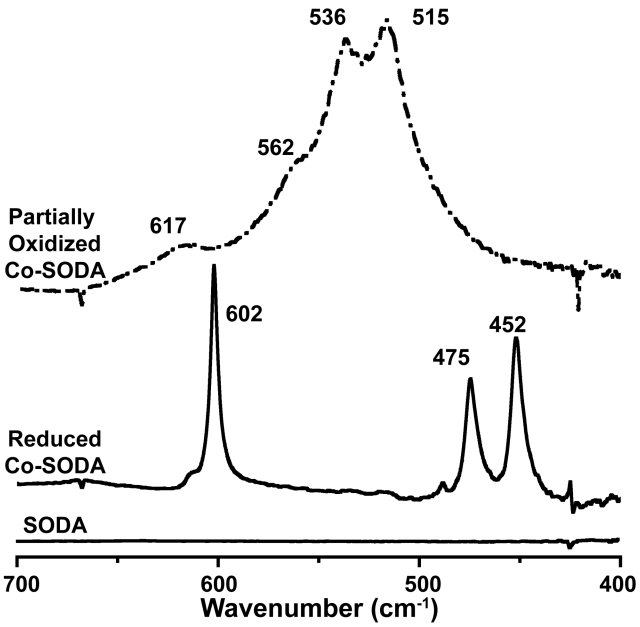

Figure 2.5. Comparative FTIR spectra for Co-SODA. FTIR absorption spectra from the SODA apo-peptide (solid line at the bottom), reduced Co-SODA (solid line in the middle), and the partially oxidized Co-SODA (dash-dotted line) in the 400-700 cm^{-1} region.

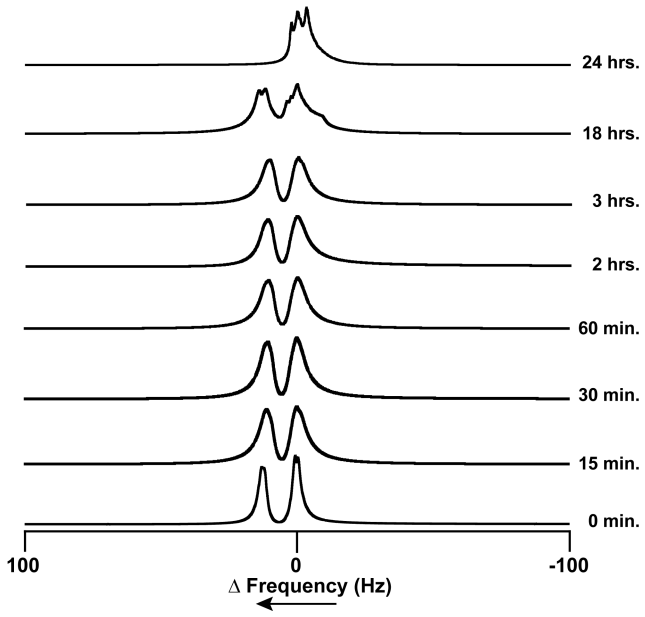

Figure 2.6. Time course magnetic susceptibility experiment for Co-SODA. ^{1}H NMR resonances as a function of time exposed to air for H_2O in an aqueous sample of reduced Co-SODA [in an NMR tube (O.D. ~ 3mm)]. The sample was placed within another NMR tube (O.D. ~ 5 mm) containing pure H_2O, and the resonances are referenced such that the frequency of the signal of the blank H_2O (measured independently) is zero.

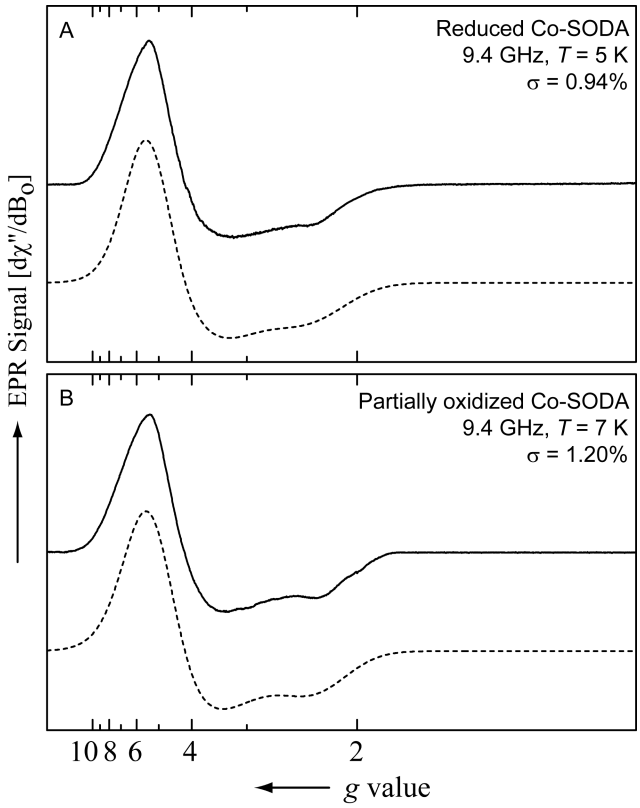

Figure 2.7. Comparative EPR spectra for Co-SODA. Continuous wave (CW) EPR spectra of (A) reduced Co-SODA (in aqueous 50 mM NEM buffer at pH 7.5) at 5 K and (B) partially oxidized Co-SODA sample (in aqueous 50 mM NEM buffer at pH 7.5) at 7 K. The experimental data and the simulated data are shown as solid black line and dotted lines, respectively.

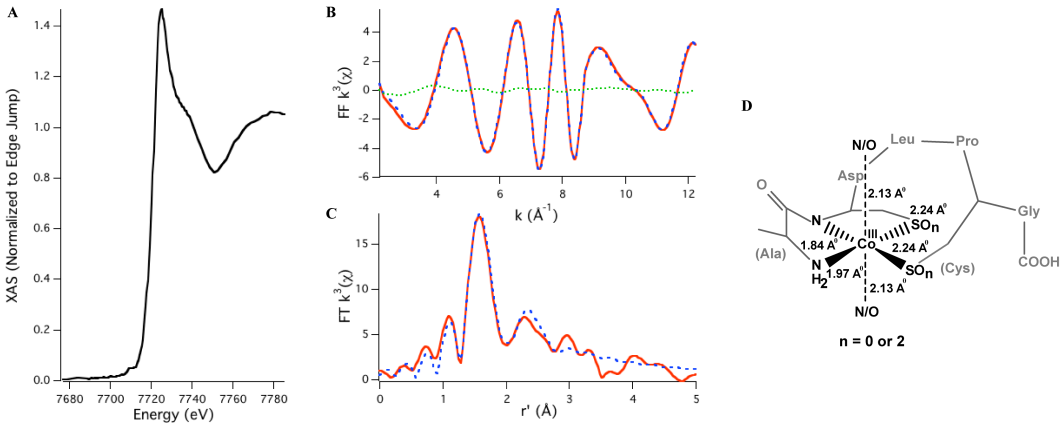

Figure 2.8. XAS results for fully oxidized Co-SODA. (A) XANES region of the Co K-edge X-ray absorption spectrum of fully oxidized Co-SODA. (B) FF k^3 data and (C) FT k^3 data (experimental data, simulated data, and the difference spectrum are represented as the red solid line, blue dashed line, and green dotted line, respectively). (D) Primary coordination geometry around cobalt in oxidized Co-SODA and metal-ligand bond distances from EXAFS. Refinement parameters: Co–S, n = 2 (restrained), r = 2.241(13) Å, σ^2 = 0.0009(2) Å^2; Co–N, n = 2 (restrained), r = 2.130(9) Å, σ^2 = 0.0012(4) Å^2; Co–N, n = 1 (restrained), r = 1.968(7) Å, σ^2 = 0.0011(8) Å^2; Co–N, n = 1 (restrained), r = 1.844(6) Å, σ^2 = 0.0011(4) Å^2; Co–C, n = 5 (restrained), r = 2.50(2) Å, σ^2 = 0.0016(2) Å^2; E_o = 7725.1 eV.

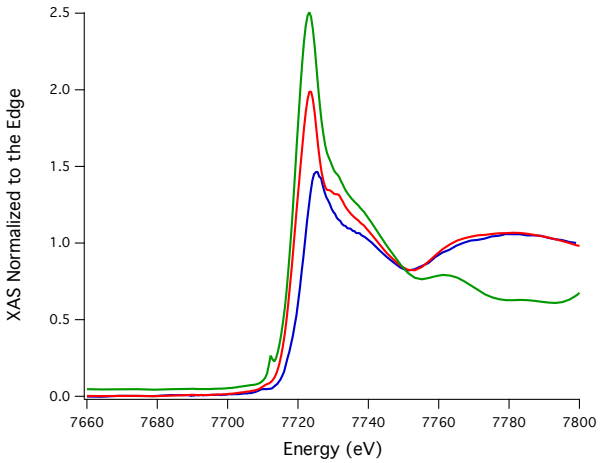

Figure 2.9. Comparative XANES spectra for Co-SODA. Comparison of the XANES region of the X-ray absorption spectrum of reduced (green), partially oxidized (red), and fully oxidized Co-SODA (blue).

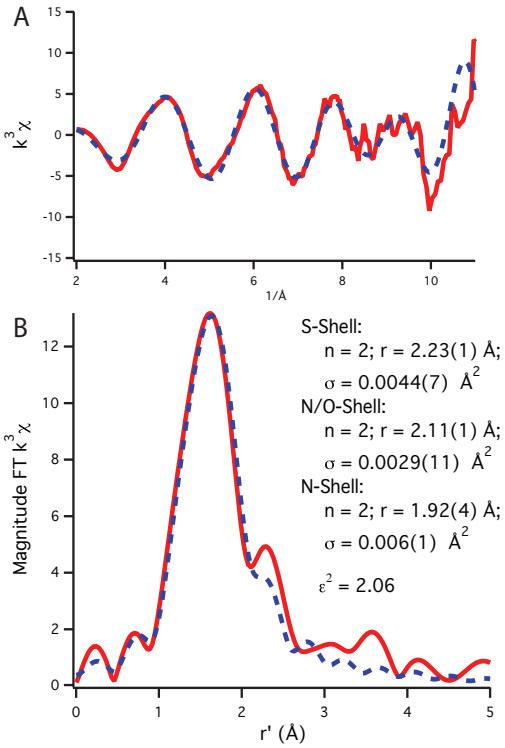

Figure 2.10. EXAFS region of the X-ray absorption spectrum of partially oxidized Co-SODA. (A) FF k^3 data and (B) FT k^3 data (experimental data and simulated data are represented as the red solid line and the blue dotted line, respectively).

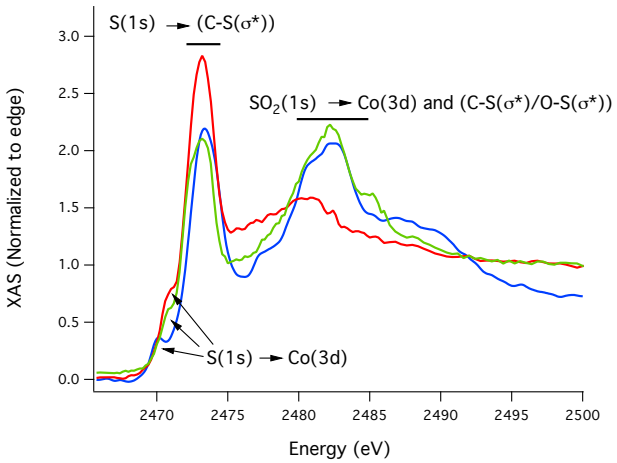

Figure 2.11. Comparative sulfur XAS spectra for Co-SODA. S K-edge X-ray absorption spectra of fully reduced (red), partially oxidized (green) and fully oxidized (blue) CoSODA.

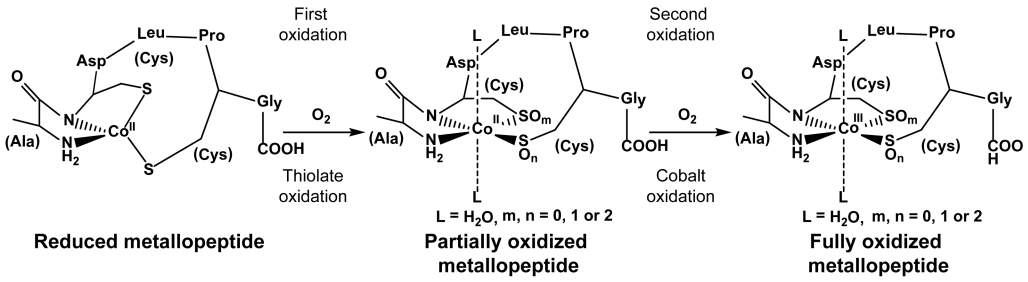

Scheme 2.1. **Hypothesized sequence for oxidation of Co(II)-SODA in air.**

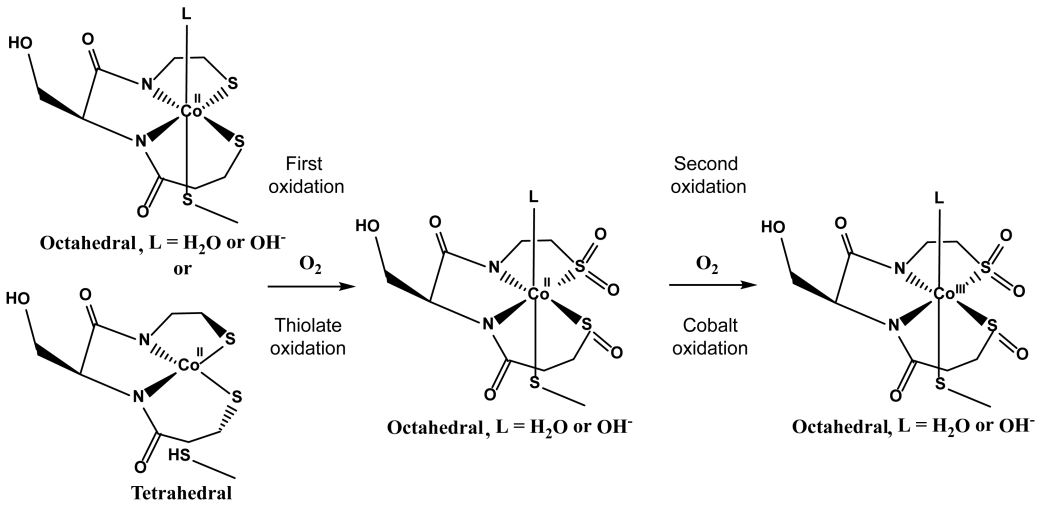

Scheme 2.2. Hypothetical sequence for *in vivo* oxidation of Co-NHase.

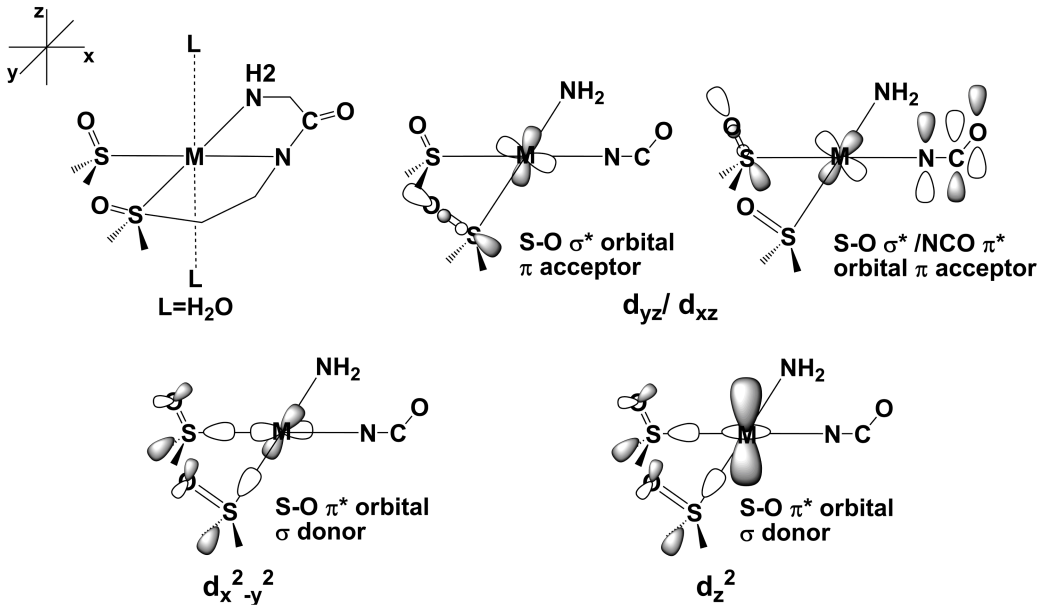

Scheme 2.3. Diagram of possible interactions between SO and Co frontier orbitals.

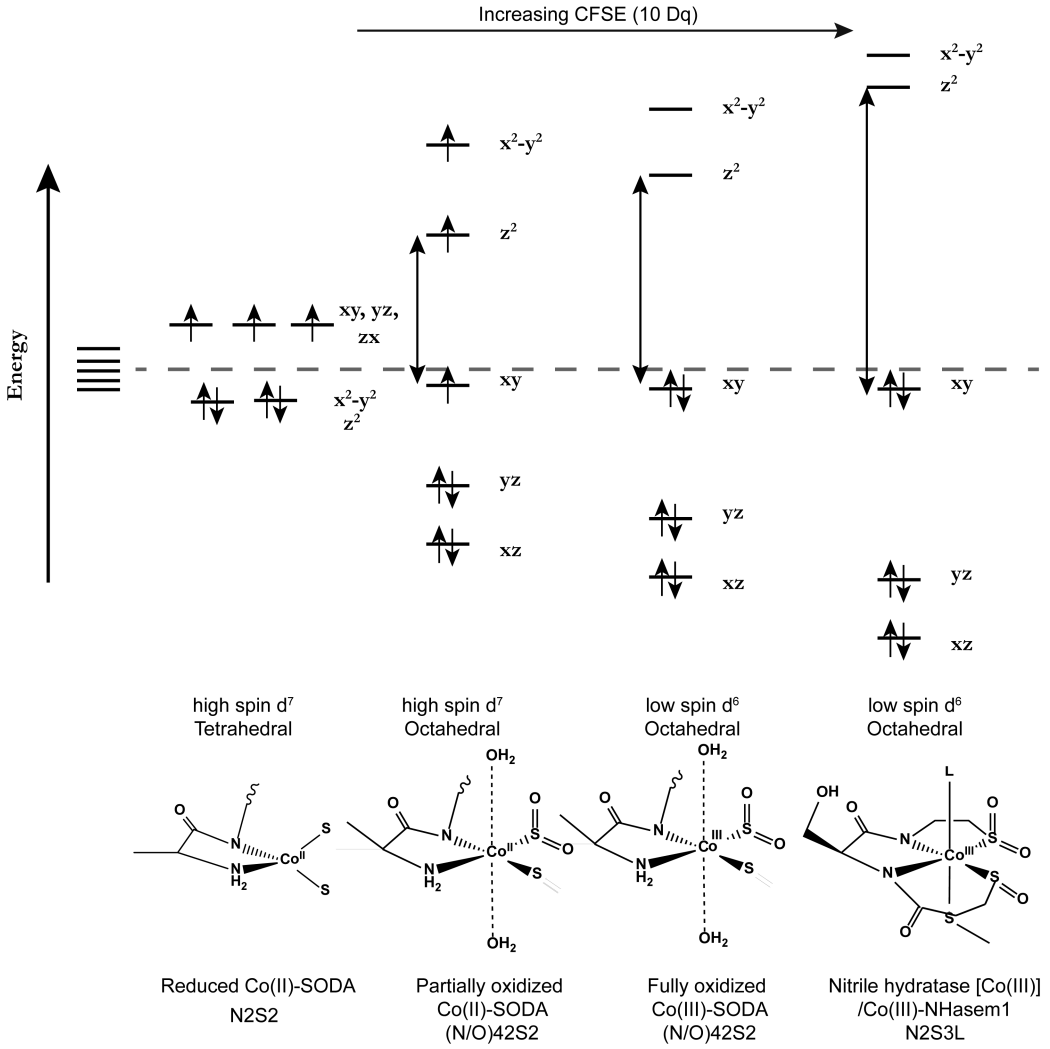

Scheme 2.4. Energy diagrams for the d orbitals of Co for various geometries and oxidation states.

Table 2.1: Optical and CD data for various Co-SODA species

Sample	Electronic absorption [λ (nm), ε (M^{-1} cm^{-1})]	CD absorption [λ (nm), Δε (M^{-1} cm^{-1})]
Reduced Co-SODA	725 (210), 681 (230), 609 (225), 350 (shoulder, 1450), 303 (1950)	544 (-0.15), 404 (0.20), 312 (0.54), 280 (-2.58)
Partially oxidized Co-SODA	600 (shoulder, 140) 460 (shoulder, 430) 355 (1100)	536 (-0.8) 420 (0.37) 306 (2.18) 267 (-3.92)
Fully oxidized Co-SODA	570 (shoulder, 195) 450 (shoulder, 480) 340 (1500)	536 (0.7) 470 (0.96) 414 (shoulder, 0.36) 328 (-5.88) 286 (-3.87)

Table 2.2: Parameters used in the simulation of the EPR spectra for various Co-SODA species

Parameters[a]	Co(II)-SODA	
	Reduced	**Partially oxidized**
g_x (±0.001)	2.527	2.476
g_y	2.111	2.199
g_z	2.298	2.276
ΔB_x (MHz)	3480	3695
ΔB_y	5544	6096
ΔB_z	2824	2491
D (MHz)	$\geq 5 \times 10^8$	$\geq 5 \times 10^8$
E/D	0.02	- 0.02
$[(g_x-g_y/g_z) \times 100\%]$	18.102	12.170

[a] The simulation parameters were the following: the principal g values (g_x, g_y and g_z), the line widths (ΔB_x, ΔB_y and ΔB_z) and the zero-field splitting parameters, D and E.

Table 2.3: Summary of K-edge energies from Co and S XAS

Sample	Co K-edge energy (eV)		S K-edge energy (eV)			
	Co (1s→3d)	Co edge	S(1s)→ Co(3d)	S(1s)→ C-S (σ*)	SO_2(1s)→ Co(3d)	SO_2(1s)→ C–S(σ*)
Reduced Co-SODA	7719.3(2)	7720.1(3)	2470.9(2)	2472.6(2)	N/A	N/A
Partially oxidized Co-SODA	7719.2(1)	7720.1(4)	2470.4(2)	2473.2(2)	2477.6(7)	2480(1)
Fully oxidized Co-SODA	7719.4(1)	7723.2(3)	2470.1(2)	2473.2(2)	2477.8(6)	2480(1)

2.5. References

1. Paulsen, C. E. & Carroll, K. S. Orchestrating Redox Signaling Networks through Regulatory Cysteine Switches. *ACS Chem. Biol.* **5**, 47–62 (2009).

2. Claiborne, A. *et al.* Protein-Sulfenic Acids: Diverse Roles for an Unlikely Player in Enzyme Catalysis and Redox Regulation. *Biochem.* **38**, 15407–15416 (1999).

3. Dickinson, B. C. & Chang, C. J. Chemistry and biology of reactive oxygen species in signaling or stress responses. *Nat. Chem. Biol.* **7**, 504–511 (2011).

4. Nagashima, S. *et al.* Novel non-heme iron center of nitrile hydratase with a claw setting of oxygen atoms. *Nat. Struct. Mol. Biol.* **5**, 347–351 (1998).

5. Arakawa, T. *et al.* Structural Basis for Catalytic Activation of Thiocyanate Hydrolase Involving Metal-Ligated Cysteine Modification. *J. Am. Chem. Soc.* **131**, 14838–14843 (2009).

6. Arakawa, T. *et al.* Structure of Thiocyanate Hydrolase: A New Nitrile Hydratase Family Protein with a Novel Five-coordinate Cobalt(III) Center. *J. Mol. Biol.* **366**, 1497–1509 (2007).

7. Katayama, Y. *et al.* Thiocyanate Hydrolase Is a Cobalt-Containing Metalloenzyme with a Cysteine-Sulfinic Acid Ligand. *J. Am. Chem. Soc.* **128**, 728–729 (2005).

8. Huang, W. *et al.* Crystal structure of nitrile hydratase reveals a novel iron centre in a novel fold. *Structure* **5**, 691–699 (1997).

9. Miyanaga, A., Fushinobu, S., Ito, K. & Wakagi, T. Crystal Structure of Cobalt-Containing Nitrile Hydratase. *Biochem. Biophys. Res. Commun.* **288**, 1169–1174 (2001).

10. Nakasako, M. *et al.* Tertiary and Quaternary Structures of Photoreactive Fe-Type Nitrile Hydratase from Rhodococcus sp. N-771: Roles of Hydration Water Molecules in Stabilizing the Structures and the Structural Origin of the Substrate Specificity of the Enzyme. *Biochem.* **38**, 9887–9898 (1999).

11. Song, L. *et al.* High resolution X-ray molecular structure of the nitrile hydratase from Rhodococcus erythropolis AJ270 reveals posttranslational oxidation of two cysteines into sulfinic acids and a novel biocatalytic nitrile hydration mechanism. *Biochem. Biophys. Res. Commun.* **362**, 319–324 (2007).

12. Murakami, T. *et al.* Post-translational modification is essential for catalytic activity of nitrile hydratase. *Protein Sci.* **9**, 1024–1030 (2000).

13. Endo I., Odaka M. & Yohda M. An enzyme controlled by light: the molecular mechanism of photoreactivity in nitrile hydratase. *Trends Biotechnol.* **17**, 244–248 (1999).

14. Zhou, Z., Hashimoto, Y. & Kobayashi, M. Nitrile Degradation by *Rhodococcus*: Useful Microbial Metabolism for Industrial Productions. *Actinomycetologica* **19**, 18–26 (2005).

15. Kobayashi, M., Nagasawa, T. & Yamada, H. Enzymatic synthesis of acrylamide: a success story not yet over. *Trends Biotechnol.* **10**, 402–408 (1992).

16. Noveron, J. C., Olmstead, M. M. & Mascharak, P. K. Co(III) Complexes with Carboxamido N and Thiolato S Donor Centers: Models for the Active Site of Co-Containing Nitrile Hydratases. *J. Am. Chem. Soc.* **121**, 3553–3554 (1999).

17. Kovacs, J. A. Synthetic Analogues of Cysteinate-Ligated Non-Heme Iron and Non-Corrinoid Cobalt Enzymes. *Chem. Rev.* **104**, 825–848 (2004).

18. Kung, I. *et al.* How Do Oxidized Thiolate Ligands Affect the Electronic and Reactivity Properties of a Nitrile Hydratase Model Compound? *J. Am. Chem. Soc.* **122**, 8299–8300 (2000).

19. Shearer, J., Kung, I. Y., Lovell, S., Kaminsky, W. & Kovacs, J. A. Why Is There an 'Inert' Metal Center in the Active Site of Nitrile Hydratase? Reactivity and Ligand Dissociation from a Five-Coordinate Co(III) Nitrile Hydratase Model. *J. Am. Chem. Soc.* **123**, 463–468 (2000).

20. Galvez, C., Ho, D. G., Azod, A. & Selke, M. Reaction of a Coordinated Cysteinato Ligand with Singlet Oxygen: Photooxidation of (Cysteinato-N,S)bis(ethylenediamine)cobalt(III). *J. Am. Chem. Soc.* **123**, 3381–3382 (2001).

21. Rat, M. *et al.* Clean oxidation of thiolates to sulfinates in a four-coordinate CoIII complex with a mixed carboxamido N–thiolato S donor set: relevance to nitrile hydratase. *J. Inorg. Biochem.* **84**, 207–213 (2001).

22. Shearer, J., Callan, P. E. & Amie, J. Use of Metallopeptide Based Mimics Demonstrates That the Metalloprotein Nitrile Hydratase Requires Two Oxidized Cysteinates for Catalytic Activity. *Inorg. Chem.* **49**, 9064–9077 (2010).

23. Masitas, C. A., Kumar, M., Mashuta, M. S., Kozlowski, P. M. & Grapperhaus, C. A. Controlled Sulfur Oxygenation of the Ruthenium Dithiolate (4,7-Bis-(2′-methyl-2′-mercaptopropyl)-1-thia-4,7-diazacyclononane)RuPPh$_3$ under Limiting O_2 Conditions Yields Thiolato/Sulfinato, Sulfenato/Sulfinato, and Bis-Sulfinato Derivatives. *Inorg. Chem.* **49**, 10875–10881 (2010).

24. Farmer, P. J. *et al.* Isotopic labeling investigation of the oxygenation of nickel-bound thiolates by molecular oxygen. *J. Am. Chem. Soc.* **114**, 4601–4605 (1992).

25. Mirza, S. A., Pressler, M. A., Kumar, M., Day, R. O. & Maroney, M. J. Oxidation of nickel thiolate ligands by dioxygen. *Inorg. Chem.* **32**, 977–987 (1993).

26. Farmer, P. J., Verpeaux, J.-N., Amatore, C., Darensbourg, M. Y. & Musie, G. Reduction-Promoted Sulfur-Oxygen Bond Cleavage in a Nickel Sulfenate as a Model for the Activation of [NiFe] Hydrogenase. *J. Am. Chem. Soc.* **116**, 9355–9356 (1994).

27. Noveron, J. C., Olmstead, M. M. & Mascharak, P. K. A Synthetic Analogue of the Active Site of Fe-Containing Nitrile Hydratase with Carboxamido N and Thiolato S as Donors: Synthesis, Structure, and Reactivities. *J. Am. Chem. Soc.* **123**, 3247–3259 (2001).

28. Kaasjager, V. E. *et al.* Unique Reactivity of a Tetradentate N2S2 Complex of Nickel: Intermediates in the Production of Sulfur Oxygenates. *Inorg. Chem.* **41**, 1837–1844 (2002).

29. Lee, C.-M., Hsieh, C.-H., Dutta, A., Lee, G.-H. & Liaw, W.-F. Oxygen Binding to Sulfur in Nitrosylated Iron−Thiolate Complexes: Relevance to the Fe-Containing Nitrile Hydratases. *J. Am. Chem. Soc.* **125**, 11492–11493 (2003).

30. Lee, C.-M. *et al.* Nitrosylated Iron−Thiolate−Sulfinate Complexes with {Fe(NO)}6/7 Electronic Cores: Relevance to the Transformation between the Active and Inactive NO-Bound Forms of Iron-Containing Nitrile Hydratases. *Inorg. Chem.* **44**, 6670–6679 (2005).

31. Chohan, B. S. & Maroney, M. J. Selective Oxidations of a Dithiolate Complex Produce a Mixed Sulfonate/Thiolate Complex. *Inorg. Chem.* **45**, 1906–1908 (2006).

32. Grapperhaus, C. A., Darensbourg, M. Y., Sumner, L. W. & Russell, D. H. Template Effect for O2 Addition across cis-Sulfur Sites in Nickel Dithiolates. *J. Am. Chem. Soc.* **118**, 1791–1792 (1996).

33. Galardon, E., Giorgi, M. & Artaud, I. Oxygenation of thiolates to S-bonded sulfinate in an iron(III) complex related to nitrile hydratase. *Chem. Commun.* 286–287 (2004).doi:10.1039/B312318A

34. Bourles, E., Alves de Sousa, R., Galardon, E., Giorgi, M. & Artaud, I. Direct Synthesis of a Thiolato-S and Sulfinato-S Co^{III} Complex Related to the Active Site of Nitrile Hydratase: A Pathway to the Post-Translational Oxidation of the Protein. *Angew. Chem. Int. Ed.* **44**, 6162–6165 (2005).

35. Zhou, Z., Hashimoto, Y., Shiraki, K. & Kobayashi, M. Discovery of Posttranslational Maturation by Self-Subunit Swapping. *Proc. Natl. Acad. Sci. USA* **105**, 14849–14854 (2008).

36. Zhou, Z. *et al.* Unique Biogenesis of High-Molecular Mass Multimeric Metalloenzyme Nitrile Hydratase: Intermediates and a Proposed Mechanism for Self-Subunit Swapping Maturation. *Biochem.* **49**, 9638–9648 (2010).

37. Zhou, Z., Hashimoto, Y. & Kobayashi, M. Self-Subunit Swapping Chaperone Needed for the Maturation of Multimeric Metalloenzyme Nitrile Hydratase by a Subunit Exchange Mechanism Also Carries Out the Oxidation of the Metal Ligand Cysteine Residues and Insertion of Cobalt. *J. Biol. Chem.* **284**, 14930–14938 (2009).

38. Stoll, S. & Schweiger, A. EasySpin, a comprehensive software package for spectral simulation and analysis in EPR. *J. Magn. Reson.* **178**, 42–55 (2006).

39. Flores, M. *et al.* Protein-Cofactor Interactions in Bacterial Reaction Centers from Rhodobacter sphaeroides R-26: II. Geometry of the Hydrogen Bonds to the Primary Quinone $Q_A^{\cdot -}$ by ^1H and ^2H ENDOR Spectroscopy. *Biophys. J.* **92**, 671–682 (2007).

40. Evans, D. F. 400. The determination of the paramagnetic susceptibility of substances in solution by nuclear magnetic resonance. *J. Chem. Soc.* 2003–2005 (1959).doi:10.1039/JR9590002003

41. Grant, D. H. Paramagnetic Susceptibility by NMR: The 'Solvent Correction' Reexamined. *J. Chem. Educ.* **72**, 39 (1995).

42. Shearer, J., Dehestani, A. & Abanda, F. Probing Variable Amine/Amide Ligation in Ni^{II}N2S2 Complexes Using Sulfur K-Edge and Nickel L-Edge X-ray Absorption Spectroscopies: Implications for the Active Site of Nickel Superoxide Dismutase. *Inorg. Chem.* **47**, 2649–2660 (2008).

43. Shearer, J. & Scarrow, R. S. *EXAFS123*. (University of Nevada, Reno, 2011).

44. *Igor Pro*. (WaveMetrics, Inc.: Lake Oswego, OR, 2011).
45. Ankudinov, A. L., Ravel, B., Rehr, J. J. & Conradson, S. D. Real-space multiple-scattering calculation and interpretation of x-ray-absorption near-edge structure. *Phys. Rev. B* **58**, 7565–7576 (1998).

46. Ellman, G. L. A colorimetric method for determining low concentrations of mercaptans. *Arch. Biochem. Biophys* **74**, 443–450 (1958).

47. Neupane, K. P., Gearty, K., Francis, A. & Shearer, J. Probing Variable Axial Ligation in Nickel Superoxide Dismutase Utilizing Metallopeptide-Based Models: Insight into the Superoxide Disproportionation Mechanism. *J. Am. Chem. Soc.* **129**, 14605–14618 (2007).

48. Choudhury, S. B. *et al.* Examination of the Nickel Site Structure and Reaction Mechanism in Streptomyces seoulensis Superoxide Dismutase. *Biochem.* **38**, 3744–3752 (1999).

49. Wuerges, J. Crystal structure of nickel-containing superoxide dismutase reveals another type of active site. *Proc. Natl. Acad. Sci. USA* **101**, 8569–8574 (2004).

50. Barondeau, D. P., Kassmann, C. J., Bruns, C. K., Tainer, J. A. & Getzoff, E. D. Nickel Superoxide Dismutase Structure and Mechanism. *Biochem.* **43**, 8038–8047 (2004).

51. Lever, A. B. *Inorganic Electronic Spectroscopy*. (Elsevier: 1986).

52. Petros, A. K., Shaner, S. E., Costello, A. L., Tierney, D. L. & Gibney, B. R. Comparison of Cysteine and Penicillamine Ligands in a Co(II) Maquette. *Inorg. Chem.* **43**, 4793–4795 (2004).

53. Petros, A. K., Reddi, A. R., Kennedy, M. L., Hyslop, A. G. & Gibney, B. R. Femtomolar Zn(II) Affinity in a Peptide-Based Ligand Designed To Model Thiolate-Rich Metalloprotein Active Sites. *Inorg. Chem.* **45**, 9941–9958 (2006).

54. May, S. W. & Kuo, J.-Y. Preparation and properties of cobalt(II) rubredoxin. *Biochem.* **17**, 3333–3338 (1978).

55. Vasak, M., Kaegi, J. H. R., Holmquist, B. & Vallee, B. L. Spectral studies of cobalt(II)- and nickel(II)-metallothionein. *Biochem.* **20**, 6659–6664 (1981).

56. Drum, D. E. & Vallee, B. L. Optical properties of catalytically active cobalt and cadmium liver alcohol dehydrogenases. *Biochem. Biophys. Res. Commun.* **41**, 33–39 (1970).

57. VanZile, M. L., Cosper, N. J., Scott, R. A. & Giedroc, D. P. The Zinc Metalloregulatory Protein Synechococcus PCC7942 SmtB Binds a Single Zinc Ion per Monomer with High Affinity in a Tetrahedral Coordination Geometry. *Biochem.* **39**, 11818–11829 (2000).

58. Greenfield, N. J. & Timasheff, S. N. Enzyme Ligand Complexes: Spectroscopic Studie. *Crit. Rev. Biochem. Mol. Biol.* **3**, 71–110 (1975).

59. Nakashini, K., Berova,, N. & Woody, R., W. *Circular Dichroism: Principles and Applications*. (VCH publishers: 1994).

60. Condrate, R. A. & Nakamoto, K. Infrared Spectra and Normal Coordinate Analysis of Metal Glycino Complexes. *J. Chem. Phys.* **42**, 2590–2598 (1965).

61. Kincaid, J. R. & Nakamoto, K. Vibrational spectra and normal coordinate analysis of bis(glycino) complexes with Ni(II), Cu(II) and Co(II). *Spectrochim. Acta, Part A* **32**, 277–283 (1976).

62. Rizzi, A. C. *et al.* Structure and Magnetic Properties of Layered High-Spin Co(II)(*l*-threonine)$_2$(H_2O)$_2$. *Inorg. Chem.* **42**, 4409–4416 (2003).

63. Pietrzyk, P., Srebro, M., Radoń, M., Sojka, Z. & Michalak, A. Spin Ground State and Magnetic Properties of Cobalt(II): Relativistic DFT Calculations Guided by EPR Measurements of Bis(2,4-acetylacetonate)cobalt(II)-Based Complexes. *J. Phys. Chem. A* **115**, 2316–2324 (2011).

64. Dey, A. *et al.* Sulfur K-Edge XAS and DFT Studies on NiII Complexes with Oxidized Thiolate Ligands: Implications for the Roles of Oxidized Thiolates in the Active Sites of Fe and Co Nitrile Hydratase. *Inorg. Chem.* **46**, 4989–4996 (2007).

65. Angelosante, J. *et al.* Synthesis and characterization of an unsymmetrical cobalt(III) active site analogue of nitrile hydratase. *J. Biol. Inorg. Chem.* **16**, 937–947 (2011).

66. Komeda, H., Kobayashi, M. & Shimizu, S. A Novel Transporter Involved in Cobalt Uptake. *Proc. Natl. Acad. Sci. USA* **94**, 36–41 (1997).

67. Okamoto, S. & Eltis, L. D. The biological occurrence and trafficking of cobalt. *Metallomics* **3**, 963–970 (2011).

Chapter 3

Reactivity of bio-inspired model complexes with small molecules: Incorporation of cyanide into synthetic cobalt and copper containing metallopeptides

*Arnab Dutta[†§], Marco Flores[†], Souvik Roy[†§], Jennifer C. Schmitt[‡], Alexander G. Hamilton[†], Hilairy Hartnett[†∞], Jason Shearer[‡], Anne K. Jones[†§]**

[†]Department of Chemistry and Biochemistry, [§]Center for Bio-Inspired Solar Fuel Production, [∞] School of Earth and Space Exploration; Arizona State University, Tempe, AZ 85287

[‡]Department of Chemistry, University of Nevada, Reno, Nevada 89557

3.0. Abstract

In this chapter, the heptapeptide SODA (ACDLPCG) is shown to bind not only its natural metal, nickel, but also Co(II) and Cu(II). Both of these peptides are reactive, showing binding of an external cyanide ligand. Spectroscopic evidence suggests that cyanide binding occurs at the metallocenter and does not involve displacement of any of the original peptide ligands. Thus, metal-bound SODA retains enough flexibility to facilitate reorientation to allow access of a new ligand and formation of a modified metal geometry.

3.1. Introduction

An N_2S_2 coordination motif is widely found throughout biology as a binding site for a variety of metallocenters including structurally important sites, oxidation/reduction catalysts, and Lewis acid catalysts. Nickel binds in a square planar N_2S_2 binding site in cluster A of acetyl-CoA synthase carbon monoxide dehydrogenase (CODH/ACS) (activates CO) and nickel superoxide dismutase (NiSOD) (interacts with superoxide anion).[1–4] The redox active copper of type-I copper proteins is coordinated by an N_2S_2 motif; it forms an entatic state consisting of a trigonal planar base together with a weak axial ligand.[5–7] The zinc finger binding motif consists of a tetrahedrally coordinated zinc in a site comprised of two histidines and two cysteines; remarkably this site also binds other first row transitional metals (Mn^{2+}, Fe^{2+}, Co^{2+}, Ni^{2+}, and Cu^{2+}) with variable specificity.[8] The N_2S_2 binding motif is also a substructure within the N_2S_3 binding site of Co(III) in Co nitrile hydratases (NHase).[9] This wide range of metal binding ability is facilitated by the presence of both hard nitrogen and soft sulfur ligands in this motif. Additionally, this motif is likely widespread in biology because of the ubiquity of functional groups in proteins that can serve as ligands including amines, amides, or histidines for nitrogen and cysteine or methionine for sulfur.

Shearer *et al.* demonstrated square planar Ni(II) binding to a N_2S_2 coordinating, twelve amino acid containing peptide maquette derived from the N-terminus of Ni superoxide dismutase and investigated its reactivity towards superoxide anion.[10] Tietze and his group extended this work to show binding of

cyanide ion to the same Ni-metallopeptide in solution.[11] In this study, we have used a truncated seven amino acid version of this peptide, SODA (ACDLPCG,)[10] as a ligand for Co(II) and Cu(II). The flexibility of this peptide allows it to interact uniquely with all three metals using the same ligand set, but the coordination geometry of the resulting metallocenters depends on the identity of the metal. In a first step toward catalytic functionality, both of these peptides are also shown to be able to coordinate cyanide without loss of any of the original ligands. This study shows that delicate, synchronized changes in the metal-peptide coordination geometry can be observed in biomimetic metallopeptide complexes.

3.2. Experimental Section:

General

All inorganic syntheses were performed under a nitrogen atmosphere using a double-manifold Schlenk vacuum line. Unless otherwise specified, chemicals and solvents of the highest available grades were obtained from Sigma-Aldrich (Milwaukee, WI) and used as received. Aqueous solutions were prepared using purified water (resistivity 18.2 MΩ cm).

Physical Measurements

Optical, FTIR, and CD spectroscopy

UV-vis measurements were executed on a Hewlett-Packard 8453 spectrophotometer using quartz cuvettes with a 1 cm pathlength. FTIR (Fourier transformed infrared) spectra of the samples were recorded on a Thermo Nicolet

Avatar-360 spectrometer in KBr pellets. The pellets were prepared in an anaerobic glove box (Vacuum atmospheres). A KBr pellet without sample was used as a reference. For the samples, each spectrum is an average of 512 scans at 1 cm^{-1} resolution. Circular dichroism (CD) spectroscopy was performed on a Jasco-815 spectropolarimeter using a rectangular quartz cell with a pathlength of 0.1 cm. Electron paramagnetic resonance (EPR) spectra were recorded between 5 K and 50 K using a Bruker ELEXSYS E580 CW X-band spectrometer (Bruker, Silberstreifen, Germany) equipped with an Oxford model 900 EPL liquid helium cryostat (Oxford instruments, Oxfordshire, UK). The magnetic field modulation frequency was 100 kHz; the amplitude was 1 mT; the microwave power was between 1-4 mW; the microwave frequency was 9.42 GHz; the sweep time was 168 s. Samples for EPR experiments were prepared using a 1:1 mixture of an aqueous solution of 50 mM NEM (pH 7.5) and glycerol (BDH, West Chester, PA) before transferring to a quartz EPR tube. EPR spectra were simulated using EasySpin (v 3.1.1), a computational package developed by Stoll and Schweiger[12] based on Matlab (The MathWorks, Natick, MA, USA). The model used for the EPR simulations considered either a single high-spin Co^{2+} ion (S = 3/2) or a Cu^{2+} ion (S=1/2). The fitting parameters were the following: the *g* values (g_x, g_y and g_z), the line widths (ΔB_x, ΔB_y and ΔB_z), hyperfine coupling constants (A_x, A_y and A_z; only for Cu(II) systems), and the zero-field splitting parameters (D and E; only for Co(II) systems). The fitting procedure was similar to the one previously described by Flores *et al.*[13] ESI-MS (electrospray ionization mass spectrometry) for metallopeptides was accomplished using a Thermo Quantum Discovery Max

triple-quadrupole mass spectrometer. Measurements were conducted in positive (+) and negative (–) ionization modes, using a methanol/water (50:50 by volume) mobile phase at a flow rate of 10 μL min^{-1} and the following ionization conditions: spray voltage, 4000 V(+, –); capillary temperature, 270 °C; sheath gas pressures, 25 (+) and 15 (–) psi; auxiliary gas pressure, 2 (+, -) psi. MALDI-MS (matrix assisted laser desorption/ ionization mass spectrometry) characterization of peptide and cyanide bound metallopeptides was performed on a Voyager DE STR. Isotope Pattern Calculator v4.0 developed by Junhua Yan was used for the calculation of the molecular mass with isotopic abundances.

Peptide synthesis and purification

The seven amino acid peptide referred to as SODA (ACDLPCG) was synthesized and characterized as described in ***Chapter 2***.

Co-SODA

Cobalt and copper containing metallopeptide samples were prepared under anaerobic conditions using the following the procedure reported by Neupane *et al.* for the synthesis of the analogous Ni-metallopeptide.[14] One equivalent of an aqueous solution of $CoCl_2 \cdot 6H_2O$ (ten times concentrated relative to the SODA solution) was added dropwise to SODA in 50 mM NEM buffer (pH= 7.5). The concentration of the SODA solution was determined using Ellman's test.[15] Both solutions were degassed and saturated with nitrogen prior to mixing. The reaction immediately turned green upon addition of the cobalt solution and the binding of the metal to the peptide. Electronic absorption spectrum (in buffered aqueous

solution, pH 7.5) λ_{max} nm (ε $M^{-1}cm^{-1}$): 725 (210), 681 (230), 609 (225), 350 (shoulder); 303 (1950). ESI-MS (negative ion) $[M-H]^-$ m/z experimental 731.01, calculated 731.1.

Co(CN)-SODA

One equivalent of aqueous KCN solution (20 mM) was added dropwise to the green Co-SODA solution to produce a yellowish green solution. The resultant mixture was stirred for 2 hours under nitrogen. The solution was lyophilized before analyzing. Electronic absorption spectrum λ_{max} nm (ε $M^{-1}cm^{-1}$): 735 (98), 644 (235), 590 (226), 395 (shoulder), 355 (2600); 300 (shoulder). FTIR (KBr): ν_{CN} = 2108 cm^{-1}. ESI-MS (positive ion): $[M+2O]^+$ m/z experimental 792.11, calculated 792.16.

Cu-SODA

In a manner analogous to the preparation of Co-SODA, the light brown Cu-SODA was synthesized by adding $CuCl_2 \bullet 2H_2O$ to an SODA solution. Electronic absorption spectrum λ_{max} nm (ε $M^{-1}cm^{-1}$): 550 (275), 445 (400), ESI-MS (negative ion) $[M-H]^-$ m/z experimental 734.97, calculated 735.1.

Cu(CN)-SODA

Following a similar procedure to that used for the synthesis of Co(CN)-SODA, one equivalent of KCN was added to an aqueous solution of Cu-SODA to produce Cu(CN)-SODA. Electronic absorption spectrum λ_{max} nm (ε $M^{-1}cm^{-1}$): 540 (175), 320 (shoulder), 260 (shoulder). FTIR (KBr): ν_{CN} = 2108 cm^{-1}. ESI-MS (positive ion): $[M+4O]^+$ m/z experimental 825.89, calculated 826.11.

3.3. Results

Previous work has shown that the peptide SODA (ACDLPCG) binds Ni(II) and Co(II) (Chapter 2).[10] The goal of this study was to explore the coordination of Co(II) and Cu(II) by SODA and the reactivity of the resulting metallopeptides with the small molecule CN^-.

Co-SODA and its reaction with CN^-

SODA was prepared and purified as described previously using solid phase peptide synthesis and HPLC.[16] **Figure 3.1** shows the UV-vis spectrum upon addition of one equivalent of Co(II) to an aqueous solution of SODA with 50 mM NEM buffer (pH 7.5). As we have previously described, the UV-vis spectrum of Co-SODA includes three distinct bands in the visible region at 725, 681, and 609 nm as well as a band at 303 nm in the UV.[17] These features indicate that the peptide coordinates the Co(II) ion in a tetrahedral first coordination sphere including two sulfur-donor ligands. Additionally, we previously concluded via evaluation of the Co-N stretching vibrations in the FTIR spectrum that the first coordination sphere of Co-SODA likely also contains the amino terminus of the peptide and an amide from the peptide backbone. The SODA sequence is derived from the N-terminal sequence of the enzyme Ni-superoxide dismutase in which the nickel is coordinated in a similar first coordination sphere lending further credence to the proposed binding of Co to SODA.

Upon addition of one equivalent of CN^- to Co-SODA, two significant changes in the UV-vis spectrum were observed: a substantial drop in the intensity of the

lowest energy feature (from ε_{725}=210 M^{-1} cm^{-1} for Co-SODA to ε_{735}= 98 M^{-1} cm^{-1} for Co(CN)-SODA) and the appearance of a sharp band at 355 nm (**Figure 3.1, Table 3.1**). This suggests that, upon addition of CN^-, Co-SODA is modified and possibly coordinates the CN^-, and we will refer to the species generated as Co(CN)-SODA. In considering the chemical structure of Co(CN)-SODA, we first note that the absorbance near 300 nm is virtually unaffected by the binding of CN^-. This transition arises from a cysteinyl sulfur to Co(II) charge transfer, and the extinction coefficient can be closely correlated with the number of sulfur ligands.[18] This suggests that Co(CN)-SODA, like Co-SODA, possesses two sulfur-donor ligands coordinated to the metal. The lower energy d-d bands (500-800 nm) are generated from the spin-orbit coupled $^4T_1(P) \leftarrow {}^4A_2(F)$ transitions of a tetrahedral Co(II) (d^7) center.[19] Thus it is interesting to note that all three are still present in the spectrum of Co(CN)-SODA, but the lowest in energy drops in intensity. **Figure 3.2A** shows the FTIR spectrum of Co(CN)-SODA in the Co-N stretching region. Bands attributable to Co-N stretching (symmetric and asymmetric) and out of plane carbonyl bending are observed at 452, 475 and 602 cm^{-1}, respectively. These indicate that the two nitrogen donor ligands present in Co-SODA are retained in Co(CN)-SODA.[20,21] Taken together, these data suggest that although different from the Co-SODA starting material, Co(CN)-SODA also contains two Co-S bonds as well as two Co-N bonds, one of which arises from an amine and the other from an amide.

To address the question of whether a CN^- ligand is present in Co(CN)-SODA, FTIR spectra in the region in which CN stretches are expected were obtained

(Figure 3.2B). The C-N bond vibration of free CN^- is found at 2078 cm^{-1}. A higher energy band at 2108 cm^{-1}, not present in the spectrum of Co-SODA (**Figure 3.2B**), was present in the spectrum of Co(CN)-SODA. This strongly suggests that a metal bound CN^- is present in Co(CN)-SODA. Formation of a σ-bond between CN^- and the Co should transfer electron density from the anti-bonding HOMO of CN^- into a metal-based orbital simultaneously increasing the bond order of the ligand. This is consistent with the higher energy CN stretching vibration observed and suggests that π-bonding in the system is minimal.[22] Furthermore, the MALDI-MS spectrum of Co(CN)-SODA included a signal attributable to CN^- coordinated metallopeptide upon addition of two oxygen atoms ($[M+2O]^+$, **Figure 3.3A**) that was not present in the spectrum of Co-SODA (data not shown). The additional oxygen atoms can be accounted for by the fact that the sulfurs of this sample are easily oxidized.

Additional evidence for electronic changes upon binding of CN^- to Co-SODA was provided by determination of the circular dichroism spectra. There are four distinct features in the CD spectrum of Co-SODA: a negative band at 544 nm, a positive band at 404 nm, a positive band at 312 nm, and a negative band at 280 nm (**Figure 3.4, Table 3.1**). By comparison, several differences were found in the CD spectrum of Co(CN)-SODA. Upon binding CN^-, the weak band at 544 nm bleached and a new negative band emerged near 344 nm. The intensities and precise positions of several other bands were also changed: the bands at 404 and 312 nm shifted to 410 and 302 nm, respectively; the sharp band at 280 nm split into two bands near 266 and 240 nm. The high energy bands in the far-UV region

arise from S→Co LMCT transitions. These are CD active due to the presence of a non-centrosymmetric cobalt center in both the CN^- bound and unbound forms of the metallopeptide. Induction of chirality from the neighboring amino acid chromophores into metal based ligand field transitions causes the electronic transitions in the visible region to also be CD active.[23,24] With this in mind, the changes in both the UV and visible regions of the CD spectra suggest changes in the interactions between the cysteine thiolates and the Co(II) center as well as modifications in the coordination geometry and subsequent electronic distribution around the cobalt center after the addition of cyanide to Co-SODA.

EPR spectroscopy was used to provide a more nuanced picture of the electronic structure of the Co in both Co-SODA and Co(CN)-SODA. The EPR spectrum from Co-SODA, shown in **Figure 3.5A**, could be simulated using a spin Hamiltonian of an S=3/2 system, as expected for a high spin Co(II) system with three unpaired electrons (**Table 3.2**).[25,26] The simulated spectrum matches well the experimental data (σ = 0.94%). **Table 3.2** shows the g values and zero field splitting (ZFS) constraints for Co-SODA, acquired from the simulated data. A pseudo-axial field around the paramagnetic Co(II) center is suggested from the small E/D value obtained for Co-SODA. This interpretation is consistent with the optical spectroscopic data which suggested the presence of a tetrahedral Co(II) (d^7 system, S=3/2) center in Co-SODA. The spectrum from Co(CN)-SODA also features an axially oriented paramagnetic signal (**Figure 3.5B**) which can be simulated with an S=3/2 system arising from a Co=3/2 center similar to that used to simulate the data from Co-SODA. However, the g-values for the cyanide

adduct are different from Co-SODA. One explanation is that the unpaired electron spin of the cobalt center reorients following the addition of cyanide (**Table 3.2**).

Cu-SODA and its reaction with CN^-

Addition of one equivalent of Cu(II) to SODA resulted in a new species with a band at 560 nm and a shoulder at 445 nm in the UV-vis spectrum, suggesting that Cu(II) coordinates the peptide (**Figure 3.6, Table 3.1**). When considering the first coordination sphere of the metal in the peptide, we note that the position and moderate intensity of the bands are consistent with Cu(d^9) ← S LMCT transitions.[7,27] Furthermore, like Co-SODA, the low energy region of the Cu-SODA FTIR spectrum shown in **Figure 3.2** also possesses the three bands expected for mixed amide/amine coordination of a metal. This data suggests that both the two thiolate sulfurs and two nitrogen atoms from the peptide also ligate Cu(II) in Cu-SODA. Additional evidence for formation of this complex was provided by ESI mass spectrometry. The anticipated molecular ion peak $[M-H]^-$ for Cu(II) ligated peptide Co-SODA, *i.e.* a 1:1 Cu to peptide complex, was observed with an experimental value of 734.97 m/z (**Figure 3.3**).

As shown in **Figure 3.2**, addition of one equivalent of KCN to Cu-SODA resulted in a new band in the FTIR spectrum at 2108 cm^{-1}. This band is in the region expected for stretching modes of the CN^- ligand. Furthermore, it is 30 cm^{-1} higher in energy than the analogous vibrational mode for free CN^-, strongly suggesting that the ligand is coordinated to the Cu(II) ion. MALDI-MS provides additional evidence that the CN^- coordinates the metallopeptide to form a species that we will refer to as Cu(CN)-SODA. A molecular ion $[M+4O]^+$ for the cyanide

coordinated and oxidized metallopeptide with an experimental m/z value of 825.99 was observed (**Figure 3.3B**). We note that, the MALDI-MS results suggest that Cu(CN)-SODA is relatively easily oxidized, *i.e.* incorporation of four oxygen atoms was observed. This may be a result of substantial electron density accumulated at the Cu center that arises from the strong σ-donating propensity of the CN^- ligand.

Changes in the other spectroscopic properties of Cu(CN)-SODA relative to Cu(SODA) were evaluated to determine the electronic properties of the former. Considering first the UV-vis spectra, as shown in **Figure 3.6**, the higher energy band of Cu—SODA at 445 nm bleached upon addition of CN^-, and the 560 nm band blue-shifted to 540 nm. However, as shown in **Figure 3.2**, binding of CN^- to Cu-SODA did not impact the FTIR spectrum in the region between 400 and 600 cm^{-1}. This suggests that the nitrogen coordination of the metal is relatively unchanged by the introduction of CN^- to the metallopeptide. On the other hand, the positions of Cu(d^9)←S LMCT transitions are known to be significantly influenced by the relative orientation of the copper half-filled d orbital and the p_σ or p_π orbitals of the sulfur.[7,27] Thus the changes in the UV-vis spectrum can be explained by a change in the geometry of the metallopeptide upon CN^- addition that modifies the relative geometries of the S and Cu(II) orbitals.

The CD spectrum of Cu-SODA consists of four major features: a broad negative band near 570 nm, a positive band at 492 nm, a weak negative feature at 415 nm, and a sharp positive band near 318 nm (**Figure 3.7, Table 3.1**). By comparison, the CD spectrum of Cu(CN)-SODA also displays four transitions,

but their positions are shifted to 590 nm (negative), 504 nm (positive), 362 nm (negative), and 307 nm (positive) (**Figure 3.7**). The intensities of both the lowest and highest energy transitions (near 590 nm and 307 nm, respectively) for Cu(CN)-SODA are significantly lower than the corresponding transitions for Cu-SODA (**Figure 3.7**). Like the features in the UV-vis spectrum, the lower energy bands in the CD spectrum likely arise from $Cu_d \leftarrow S_\pi$ and $Cu_d \leftarrow S_\sigma$ transitions.[7,27] Thus, the modifications in the position and intensities of these CD features also suggest structural reorientation of the ligand environment around the copper center after the introduction of cyanide into Cu(CN)-SODA.

The X-band EPR spectrum of Cu-SODA obtained at 50 K showed an axial signal for the Cu(II) (d^9, S=1/2, I=3/2) bound metallopeptide system (**Figure 3.8A**). The data could be simulated well (σ = 4.98%) using an S=1/2 spin Hamiltonian. The g values and the hyperfine coupling constants (A) for Cu-SODA determined from this simulation are listed in **Table 3.3**. The simulated g values suggest that the unpaired electron density is axially distributed along the Cu(II) ion. The high A_x value (~208 x 10^{-4} cm^{-1}) indicates a strong interaction between the electron spin and the copper nuclear spin, suggesting that the unpaired electron density resides mostly on the copper. The experimental data also show weak superhyperfine coupling (~13 x 10^{-4} cm^{-1}) due to the presence of ^{14}N atoms (I=1) in the copper coordination sphere (**Figure 3.9**) again confirming the presence of nitrogenous ligands. The Cu(CN)-SODA EPR spectrum could be simulated with an S=1/2 spin Hamiltonian corresponding to a Cu(II) (d^9, S=1/2, I=3/2) (**Figure 3.8B**). Following cyanide addition, the g-values were almost

unaltered for the Cu-metallopeptide, but the hyperfine coupling constants and line broadening parameters were changed significantly (**Table 3.3**). Superhyperfine splitting of the EPR signals due to peptide based N atoms was also observed for Cu(CN)-SODA.

3.4. Discussion and conclusions

Previous work has shown that the seven amino acid peptide SODA (ACDLPCG) coordinates both Ni(II) and Co(II) in an N_2S_2 coordination sphere consisting of the two cysteinyl thiolates, the amino terminus of the peptide and a backbone amide. The Ni metallopeptide is square planar whereas the Co species is tetrahedral suggesting that there is significant flexibility inherent in the metal binding ability of SODA. In this work, we have demonstrated via a combination of UV-vis, FTIR, CD and EPR spectroscopies as well as mass spectrometry that the same peptide can also coordinate Cu(II). Analysis of the spectroscopic data can also be used to define the geometry of the Cu-SODA metallopeptide. The optical spectrum of Cu-SODA includes both $Cu_d \leftarrow S_\pi$ and $Cu_d \leftarrow S_\sigma$ LMCT transitions. The presence of both these bands indicates that the thiolate sulfurs are interacting with the Cu(II) via both σ- and π-modes. In addition, a very weak d-d transition is also observed as a broad shoulder near 700 nm. The appearance of this ligand field band suggests that the sulfur p-orbitals contribute significantly enough to the both d_{xz} and d_{yz} orbitals of Cu(II) to cause this otherwise forbidden d-d transition to be observed. Related transitions are also observed in the CD

spectrum. Furthermore, the FTIR spectrum of Cu-SODA shows the three expected nitrogen-related vibrational modes characteristic of mixed amine/amide coordination of the metal. Together these data suggest that Cu-SODA contains a relatively covalent Cu(II) center coordinated, like Ni-SODA and Co-SODA, in an N_2S_2 first coordination sphere.[7,27,28] Preliminary XAS spectra from Cu-SODA are also consistent with this hypothesis and suggest the metal geometry is a distorted four coordinate structure with a trigonal planar base, much like a type I copper center.[29] However, we note that the covalent interactions between the Cu and sulfur ligands is superior in the case of the natural type-I copper centers, as is indicated by the occurrence of very strong $Cu_d \leftarrow S_\pi$ LMCT bands ($\varepsilon \sim 5000$ M-1 cm^{-1}) along with weaker EPR hyperfine splitting constant (A_x) values ($\sim 15 \times 10^{-4}$ cm^{-1}).[7,27]

Tietze *et al.* demonstrated that the square planar metallopeptide Ni-SODA binds cyanide to form square pyramidal Ni(CN)-SODA.[11] Herein, we have shown that cyanide addition to the Co- and Cu- analogs of Ni-SODA also results in stark changes in the spectroscopy of the metallopeptides. Evidence for coordination of the CN^- by the metallocenter was provided by FTIR spectroscopy. The FTIR spectrum of Co(CN)-SODA includes a band attributable to a metal bound CN^- coordinated primarily via a σ-interaction. On the other hand, the UV-vis spectrum of Co(CN)-SODA includes LF transitions in the visible region that are similar to those of Co-SODA. This provides evidence that both of the sulfur ligands remain intact in the cyano-peptide. Similarly, the nitrogen-based stretching frequencies in the 400-650 cm^{-1} region are unaffected by coordination of the CN^- confirming that

both nitrogenous ligands are also retained. On the other hand, following cyanide addition the CD spectrum has an increase in molar ellipticity for the extrinsic bands in the visible region. Additionally, the EPR spectrum has a decrease in the span of the g-values. Taking all of these observations into account, it is likely that Co(CN)-SODA has a square pyramidal structure with a distorted N_2S_2-pyramidal base and cyanide apex.

Spectroscopic evidence also suggests that Cu-SODA binds CN^- at the metallocenter without loss of any of the original metal ligands. First, FTIR data reveal that even for Cu(CN)-SODA, cyanide acts as a σ-donating ligand as in the Co- and Ni-analogs. Second, upon binding CN^-, the intensity of the $Cu_d \leftarrow S_\pi$ LMCT band of Cu-SODA decreases and the energy is blue shifted by 20 nm. Third, the $Cu_d \leftarrow S_\sigma$ LMCT and Cu(II) based d-d transitions are diminished in Cu(CN)-SODA and become almost undetectable. This indicates a reduction in the covalency of the interaction between the Cu(II) and the thiolate sulfurs. This observation is also supported by the decrease in the molar ellipticities of the metal-based CD bands. Taken together, this is sufficient evidence to generate a hypothesis that the addition of cyanide to Cu-SODA forces a penta- coordinated Cu(II) center in Cu(CN)-SODA. Nonetheless, the original ligand geometry of Cu-SODA is likely not retained. Instead, in the cyano-peptide the thiolates are likely relatively non-planar, explaining the loss of favorable σ- and π-type Cu-S interactions. In short, cyanide addition decreases the covalency of the Cu(II)-sulfur interactions. This hypothesis is supported by preliminary XAS data for

Cu(CN)-SODA that indicate the presence of a five coordinated copper center with a change in the K-edge energy corresponding to an increase in the partial oxidation state of Cu relative to Cu-SODA.

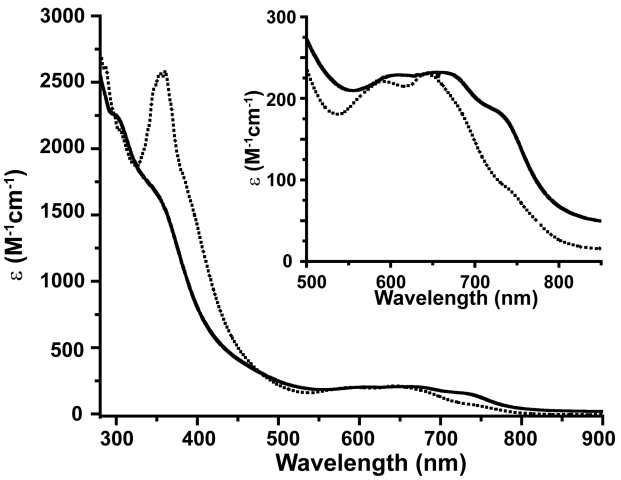

Figure 3.1. **Changes in optical absorbance spectra for Co-SODA following cyanide addition.** UV-vis spectra from Co-SODA (solid line) and Co(CN)-SODA (dotted line). Spectra were recorded in 50 mM aqueous NEM buffer (pH 7.5). The inset shows a magnification of the 500-800 nm region.

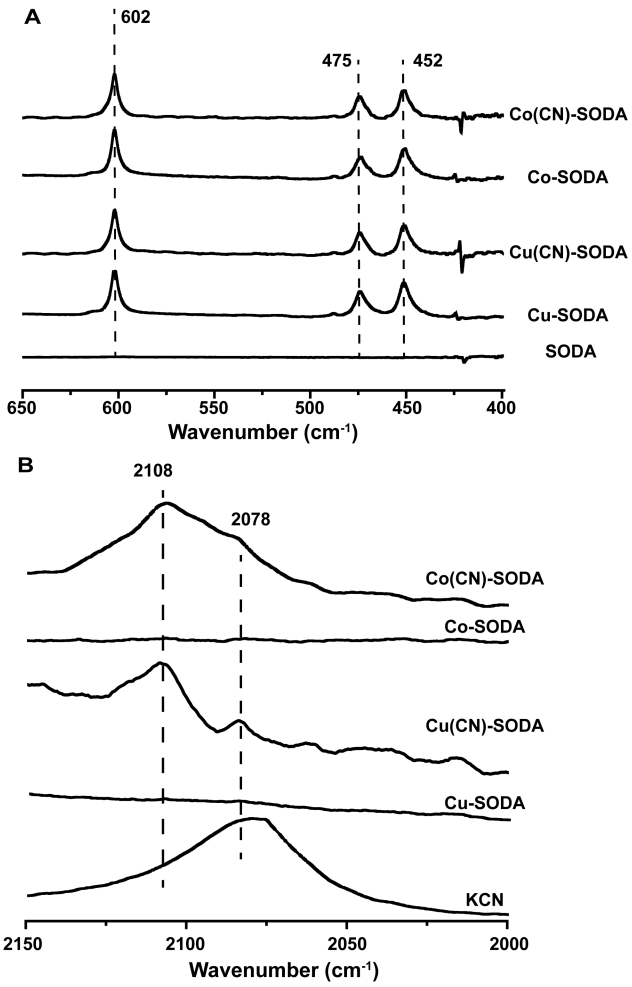

Figure 3.2. **Comparative FTIR spectra for Co- and Cu-SODA following cyanide addition.** Infrared spectra for Co(CN)-SODA, Co-SODA, Cu(CN)-SODA, Cu-SODA, and SODA in the 650-400 cm^{-1} region (A) and Co(CN)-SODA, Co-SODA, Cu(CN)-SODA, Cu-SODA, and KCN in the 2150-2000 cm^{-1} region (B).

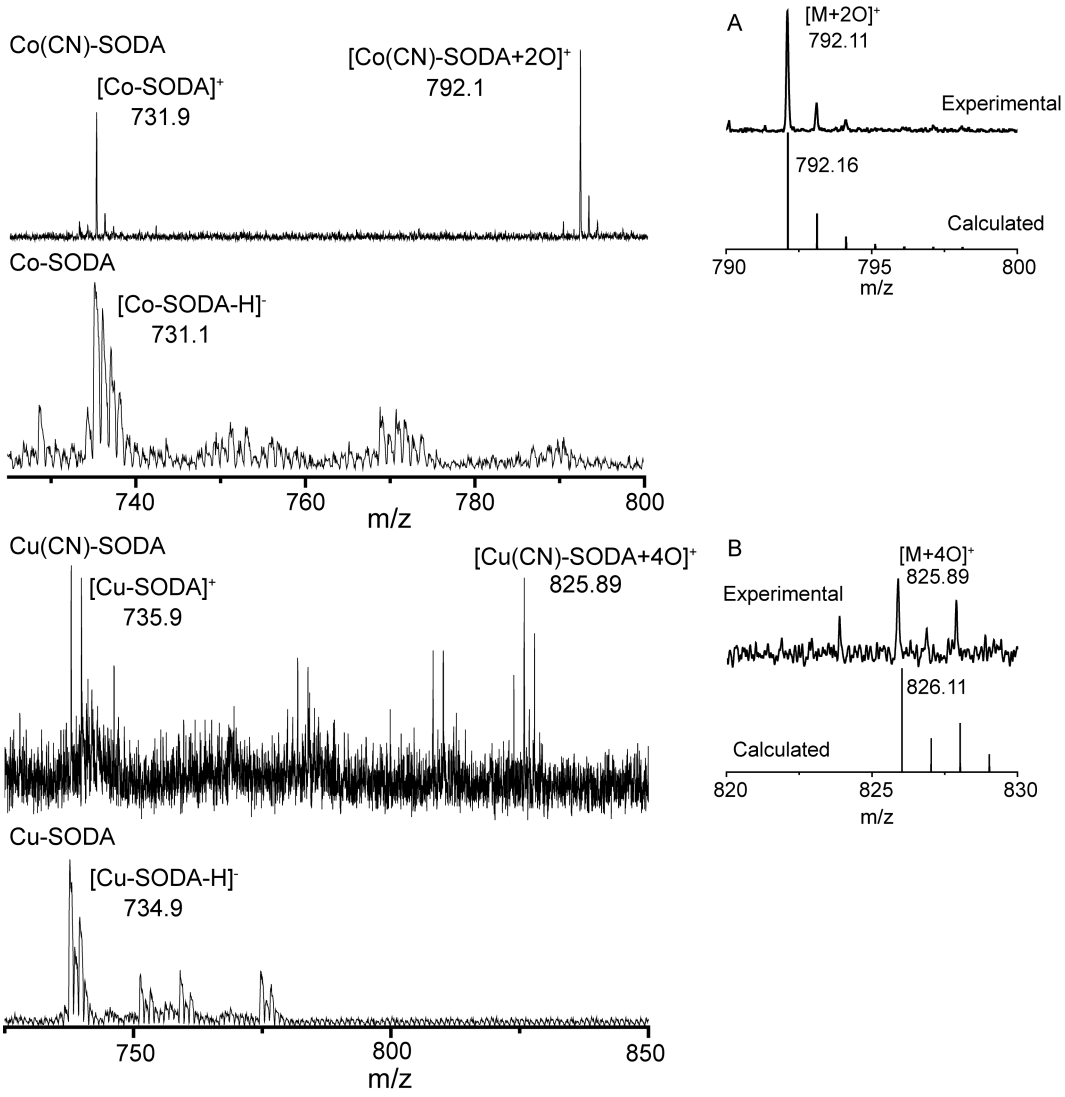

Figure 3.3. Comparative ESI-mass spectra for cyanide bound and parent Co- and Cu-SODA. Experimental and calculated salient molecular ion peaks for (A) Co(CN)-SODA and (B) Cu(CN)-SODA are shown in inset. Data were recorded with samples in aqueous, 50 mM NEM buffer (pH 7.5) solution (negative ion mode was used for Co-SODA and Cu-SODA whereas positive ion mode was used for cyanide bound metallopeptides).

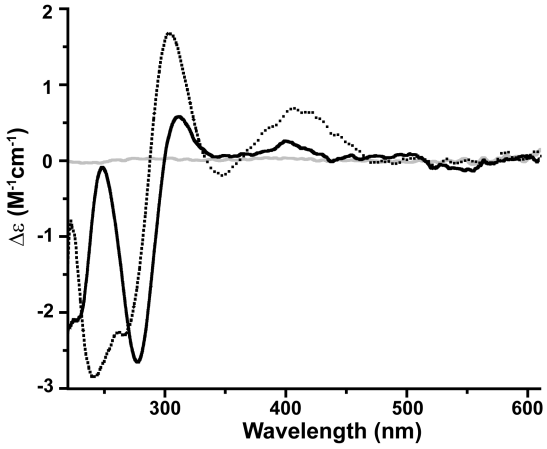

Figure 3.4. **Changes in CD spectra for Co-SODA following cyanide addition.** CD spectra from Co-SODA (solid line), Co(CN)-SODA (dotted line), and SODA apopeptide (solid grey line) in NEM buffer (50 mM, pH 7.5).

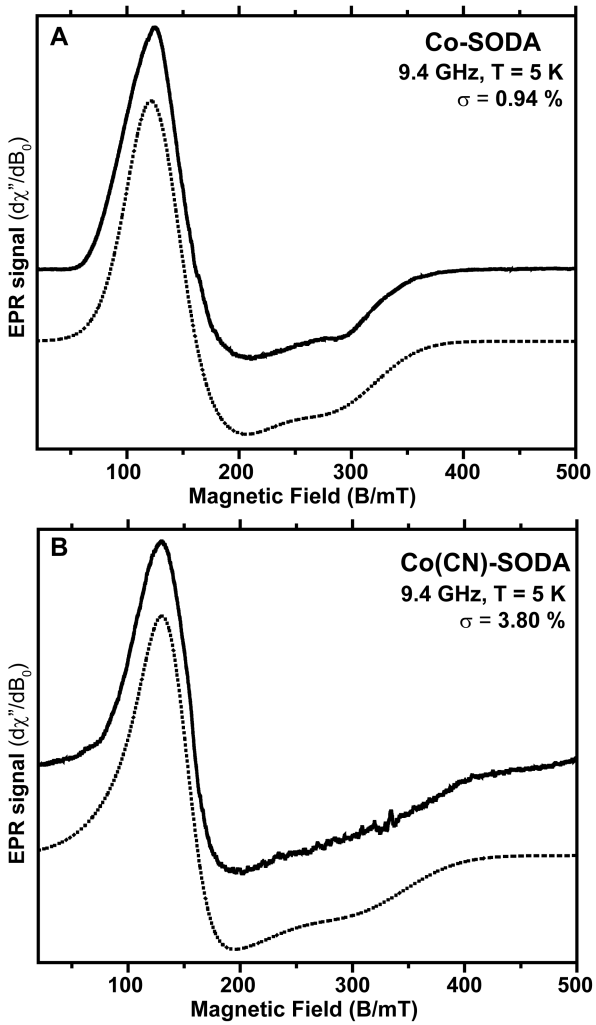

Figure 3.5. EPR spectra comparison between Co-SODA and Co(CN)-SODA. Continuous wave (CW) X-band EPR spectra of experimental (solid line) and simulated data (dotted line) for (A) Co-SODA and (B) Co(CN)-SODA at 5 K. EPR spectra for both samples were recorded in 1:1 mixtures of glycerol and aqueous 50 mM NEM buffer solution at pH 7.5.

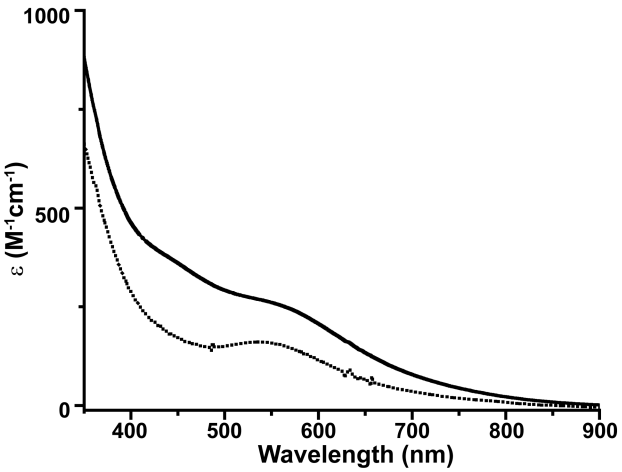

Figure 3.6. Changes in optical absorbance spectra for Cu-SODA following cyanide addition. UV-vis spectra from Cu-SODA (solid line) and Cu(CN)-SODA (dotted line). Spectra were recorded in 50 mM aqueous NEM buffer (pH 7.5).

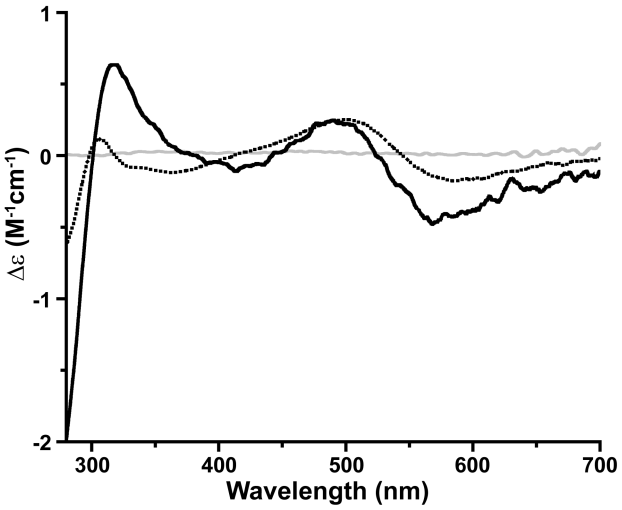

Figure 3.7. **Changes in CD spectra for Cu-SODA following cyanide addition.** CD spectra from Cu-SODA (solid line) and Cu(CN)-SODA (dotted line), and SODA apopeptide (solid grey line) in NEM buffer (50 mM, pH 7.5).

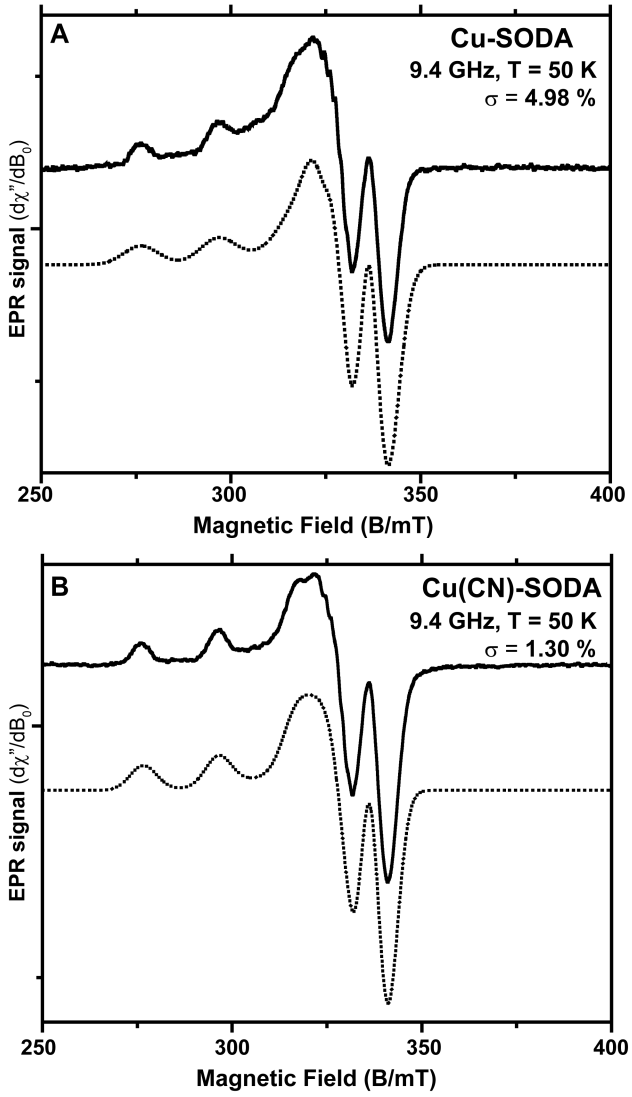

Figure 3.8. EPR spectra comparison between Cu-SODA and Cu(CN)-SODA. Continuous wave (CW) X-band EPR spectra of (A) Cu-SODA (50 K) and (B) Cu(CN)-SODA (7 K). Experimental data are shown as a solid line and simulated data as a dotted line. Samples were in a 1:1 mixture of glycerol and aqueous 50 mM NEM buffer at pH 7.5.

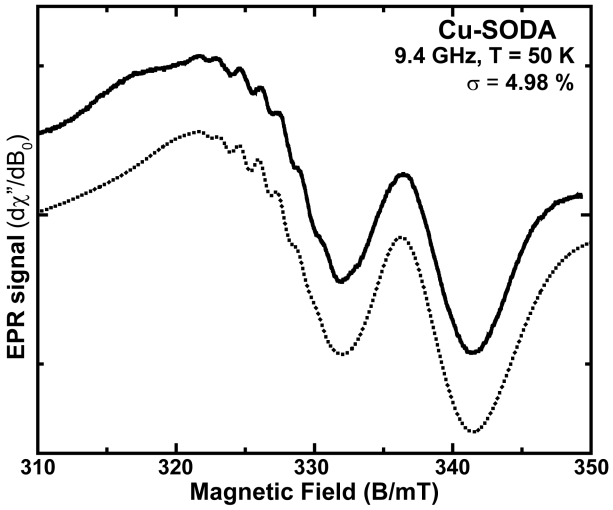

Figure 3.9. Superhyperfine splitting in EPR spectrum for Cu-SODA. Enlargement of the continuous wave (CW) X-band EPR spectrum from Cu(CN)-SODA in the 310-350 mT region to allow observation of the superhyperfine splitting by nitrogen nuclei. Conditions are as described in Figure 3.8.

Table 3.1: UV-vis absorption and CD data

Sample	Electronic absorption [λ (nm), ε (M^{-1} cm^{-1})]	CD absorption [λ (nm), Δε (M^{-1} cm^{-1})]
Co-SODA	725 (210), 681 (230), 609 (225), 350 (shoulder, 1700); 303 (2250)	544 (-0.15), 404 (0.20), 312 (0.54), 280 (-2.58)
Co(CN)-SODA	735 (98), 644 (235), 590 (226), 395 (shoulder), 355 (2600); 300 (shoulder)	410 (0.7), 344 (-0.2), 303 (1.65), 266 (-2.3), 240 (-2.9)
Cu-SODA	700 (shoulder) 560 (275), 445 (400)	570 (-0.47), 492 (0.25), 415 (-0.10), 318 (0.64)
Cu(CN)-SODA	540 (175), 320 (shoulder), 260 (shoulder).	590 (-0.17), 504 (0.25), 362 (-0.12), 307 (0.12)

Table 3.2: Parameters used in the simulation of the EPR spectra of Co-SODA and Co(CN)-SODA

Parameter	Sample	
	Co-SODA	**Co(CN)-SODA**
g_x (±0.001)	2.527	2.292
g_y	2.111	2.263
g_z	2.298	2.156
ΔB_x (MHz)	3480	3215
ΔB_y	5544	2522
ΔB_z	2824	8229
D (MHz)	≥ 5 x 10^8	≥ 5 x 10^8
E/D	0.02	- 0.02

Table 3.3: Parameters used in the simulation of the EPR spectra of Cu-SODA and Cu(CN)-SODA

Parameters	Sample	
	Cu-SODA	**Cu(CN)-SODA**
g_x (±0.001)	2.198	2.200
g_y	2.056	2.068
g_z	2.036	2.033
ΔB_x (MHz)	326.7	251.8
ΔB_y	141.2	244.5
ΔB_z	97.8	139.7
A_x (x 10^{-4} cm^{-1})	208.2	203.7
A_y (x 10^{-4} cm^{-1})	33.3	22.6
A_z (x 10^{-4} cm^{-1})	12.4	3.2

3.5. References

1. Choudhury, S. B. *et al.* Examination of the Nickel Site Structure and Reaction Mechanism in Streptomyces seoulensis Superoxide Dismutase. *Biochem.* **38**, 3744–3752 (1999).

2. Wuerges, J. Crystal structure of nickel-containing superoxide dismutase reveals another type of active site. *Proc. Natl. Acad. Sci. USA* **101**, 8569–8574 (2004).

3. Barondeau, D. P., Kassmann, C. J., Bruns, C. K., Tainer, J. A. & Getzoff, E. D. Nickel Superoxide Dismutase Structure and Mechanism. *Biochem.* **43**, 8038–8047 (2004).

4. Doukov, T. I., Iverson, T. M., Seravalli, J., Ragsdale, S. W. & Drennan, C. L. A Ni-Fe-Cu center in a bifunctional carbon monoxide dehydrogenase/acetyl-CoA synthase. *Science* **298**, 567–572 (2002).

5. Sykes, A. Plastocyanin and the Blue Copper Proteins. *Struct. Bond.* **75**, 175–224 (1991).

6. Solomon, E. I. & Hadt, R. G. Recent advances in understanding blue copper proteins. *Coord. Chem. Rev.* **255**, 774–789 (2011).

7. Solomon, E. I. Spectroscopic Methods in Bioinorganic Chemistry: Blue to Green to Red Copper Sites. *Inorg. Chem.* **45**, 8012–8025 (2006).

8. Chen, X. H., Chu, M. H. & Giedroc, D. P. Spectroscopic characterization of Co(II)-, Ni(II)-, and Cd(II)-substituted wild-type and non-native retroviral-type zinc finger peptides. *J. Biol. Inorg. Chem.* **5**, 93–101 (2000).

9. Kovacs, J. A. Synthetic Analogues of Cysteinate-Ligated Non-Heme Iron and Non-Corrinoid Cobalt Enzymes. *Chem. Rev.* **104**, 825–848 (2004).

10. Neupane, K. P., Gearty, K., Francis, A. & Shearer, J. Probing Variable Axial Ligation in Nickel Superoxide Dismutase Utilizing Metallopeptide-Based Models: Insight into the Superoxide Disproportionation Mechanism. *J. Am. Chem. Soc.* **129**, 14605–14618 (2007).

11. Tietze, D. *et al.* New Insight into the Mode of Action of Nickel Superoxide Dismutase by Investigating Metallopeptide Substrate Models. *Chem. Eur. J.* **15**, 517–523 (2009).

12. Stoll, S. & Schweiger, A. EasySpin, a comprehensive software package for spectral simulation and analysis in EPR. *J. Magn. Reson.* **178**, 42–55 (2006).

13. Flores, M. *et al.* Protein-Cofactor Interactions in Bacterial Reaction Centers from Rhodobacter sphaeroides R-26: II. Geometry of the Hydrogen Bonds to the Primary Quinone $Q_A^{\cdot -}$ by ^1H and ^2H ENDOR Spectroscopy. *Biophys. J.* **92**, 671–682 (2007).

14. Neupane, K. P., Gearty, K., Francis, A. & Shearer, J. Probing Variable Axial Ligation in Nickel Superoxide Dismutase Utilizing Metallopeptide-Based Models: Insight into the Superoxide Disproportionation Mechanism. *J. Am. Chem. Soc.* **129**, 14605–14618 (2007).

15. Ellman, G. L. A colorimetric method for determining low concentrations of mercaptans. *Arch. Biochem. Biophys* **74**, 443–450 (1958).

16. Dutta, A., Hamilton,, G., A., Hartnett, H. & Jones, A. K. Construction of heterometallic clusters in a small peptide scaffold, as [NiFe]-hydrogenase models: development of a synthetic methodology. *Inorg. Chem.*(2012).doi:10.1021/ic2026818

17. Dutta, A. *et al.* Chapter 2 (this thesis) Unpublished data.

18. Vasak, M., Kaegi, J. H. R., Holmquist, B. & Vallee, B. L. Spectral studies of cobalt(II)- and nickel(II)-metallothionein. *Biochem.* **20**, 6659–6664 (1981).

19. Lever, A. B. *Inorganic Electronic Spectroscopy*. (Elsevier: 1986).

20. Condrate, R. A. & Nakamoto, K. Infrared Spectra and Normal Coordinate Analysis of Metal Glycino Complexes. *J. Chem. Phys.* **42**, 2590–2598 (1965).

21. Kincaid, J. R. & Nakamoto, K. Vibrational spectra and normal coordinate analysis of bis(glycino) complexes with Ni(II), Cu(II) and Co(II). *Spectrochim. Acta, Part A* **32**, 277–283 (1976).

22. Nakamoto, K. *Infrared and Raman Spectra of Inorganic and Coordination compounds*. (John Wiley & Sons: Milawukee, Wisconsin, 1986).

23. Greenfield, N. J. & Timasheff, S. N. Enzyme Ligand Complexes: Spectroscopic Studie. *Crit. Rev. Biochem. Mol. Biol.* **3**, 71–110 (1975).

24. Nakashini, K., Berova,, N. & Woody, R., W. *Circular Dichroism: Principles and Applications*. (VCH publishers: 1994).

25. Rizzi, A. C. *et al.* Structure and Magnetic Properties of Layered High-Spin Co(II)(*l*-threonine)$_2$(H_2O)$_2$. *Inorg. Chem.* **42**, 4409–4416 (2003).

26. Pietrzyk, P., Srebro, M., Radoń, M., Sojka, Z. & Michalak, A. Spin Ground State and Magnetic Properties of Cobalt(II): Relativistic DFT Calculations Guided by EPR Measurements of Bis(2,4-acetylacetonate)cobalt(II)-Based Complexes. *J. Phys. Chem. A* **115**, 2316–2324 (2011).

27. Solomon, E. I. & Lever, A. B. P. *Inorganic Electronic Structure and Spectroscopy*. **I and II**, (Wiley Interscience: Hoboken, New Jersey, 2006).

28. Stibrany, R. T. *et al.* Charge-Transfer Spectra of Structurally Characterized Mixed-Valence Thiolate-Bridged Cu(I)/Cu(II) Cluster Complexes. *Inorg. Chem.* **41**, 5203–5215 (2002).

29. Shearer, Jason. *Personal communication* (2012).

Chapter 4

Construction of heterometallic clusters in a small peptide scaffold as [NiFe]-hydrogenase models: development of a synthetic methodology

Arnab Dutta[†§], *G. Alexander Hamilton*[†], *Hilairy Ellen Hartnett*[†∞], *Anne Katherine Jones*[†§*]

†Department of Chemistry and Biochemistry; §Center for Bio-Inspired Solar Fuel Production; ∞School of Earth and Space Exploration; Arizona State University; Tempe, AZ 85287; USA; Tel: 480-965-0356; Fax: 480-965-2747

Reproduced with permission from Inorganic Chemistry (ASAP article, DOI: 10.1021/ic2026818) Copyright 2012 American Chemical Society

(Appendix A)

4.0. Abstract

[NiFe]-hydrogenases are enzymes that catalyze the reversible interconversion of protons and hydrogen at a heterobimetallic site containing Ni and Fe. This organometallic site has served as an inspiration for the synthesis of a number of biomimetic complexes, but, unfortunately, most close structural mimics have shown little to no reactivity with either of the substrates for hydrogenases. This suggests that interactions between the metallo-active site and the protein scaffold are crucial in tuning reactivity. As a first step towards development of peptide-based models, in this paper I demonstrate a synthetic strategy for construction of peptide coordinated, cysteinyl thiolate bridged Ni-M complexes in which M is a hetero-organometallic fragment. I utilize the seven amino acid peptide ACDLPCG as a scaffold for construction of these peptide-coordinated metallocenters. This peptide binds Ni in an N_2S_2 environment consisting of the amino terminus, an amide nitrogen, and the two cysteinyl thiolates. I show that these thiolates serve as reactive sites for formation of heterometallic complexes in which they serve as bridging ligands. The method is general, and a number of heterometallic fragments including $Ru(\eta^6\text{-arene})^{2+}$, $M(CO)_4$(piperidine) for M=Mo and W, and $Fe_2(CO)_6$ were successfully incorporated, and the resulting metallopeptides characterized via a range of spectroscopic techniques. This methodology serves as the first step to construction of hydrogenase peptidomimetics that incorporate defined outer coordination sphere interactions intended to tune reactivity.

4.1 Introduction:

Hydrogenases, the metalloenzymes responsible for the biological interconversion of hydrogen and protons, have received widespread attention for their potential uses in technological applications.[1] As shown in **Figure 4.1**, [NiFe]-hydrogenases feature a biologically unusual organometallic active site in which a tetrathiolate coordinated Ni shares two bridging cysteine thiolates (represented as SR) with an $Fe(CO)(CN)_2$ moiety.[2,3] This motif has inspired the synthesis of a rich variety of thiolate bridged Ni-M compounds that serve, to varying degrees, as structural or functional models of the enzyme active site.[4,5] The typical synthetic route to such compounds combines a $Ni^{II}(SR)_2$ precursor with a hetero-fragment with labile ligands that can be exchanged for the thiolates. The identity of the second fragment can be quite diverse, encompassing mono- as well as bi- nuclear metallocenters and a wide range of ligand sets.[6–11]

Despite the intense interest in hydrogenases, many open questions remain regarding their mechanisms, and evidence is mounting that the protein matrix may play crucial roles in tuning the reactivity of the inorganic active site.[12–14] Artificial metalloproteins are proving to be a powerful tool for understanding metal-containing active sites at a molecular level and exploring the roles played by the protein matrix in modulating the physical properties of a metallocenter.[15–24] Although protein design has made the introduction of a single metal ion or preformed cofactors such as hemes or [FeS] clusters into an artificial scaffold more accessible, means for introducing multiple distinct metals and/or

organometallic complexes are in their infancy.[25–28] Inspired by the metalloclusters of carbon monoxide dehydrogenases, Holm and coworkers reported the first attempts to create peptide-coordinated, bridged assemblies in which two metallocenters, a mononuclear nickel center and a [4Fe4S] cluster were connected by a covalent bridge, a cysteine ligand.[25] Similarly, Green and coworkers reported utilization of the resin bound peptide CGC as an N_2S_2 coordinating ligand for nickel and its derivatization with $W(CO)_5$ and $Rh(CO)_2^+$ to produce heterobimetallic complexes.[29] However, this tripeptide provides little opportunity to tailor interactions with the metallocenter. To develop peptide models for [FeFe]-hydrogenases, methods have been developed to introduce [(μ-SRS)$[Fe(CO)_3]_2$] derivatives into peptides using both natural cysteine and an artificial dithiol modification[30–33] but, to date, peptide-based models of [NiFe]-hydrogenases are scarce. Jain and coworkers have constructed mononuclear $[Ni(P^{Ph}{}_2N^R{}_2)_2]^{2+}$ complexes in which R is a mono or dipeptide, but their synthetic strategy necessarily imposes four-fold symmetry on the peptide components and prevents direct modification of the metal first coordination sphere.[34]

In this paper, we report the use of a small peptide as a scaffold for construction of heterometallic clusters. The enzyme nickel superoxide dismutase (NiSOD) binds a mononuclear Ni(II) in a square-planar N_2S_2 first coordination sphere consisting of two cysteinyl thiolates, the amino terminus of the protein, and an amide nitrogen derived from the protein backbone. Oxidation of the Ni center to Ni(III) induces binding of the N-terminal histidine and a change to a square-based pyramidal geometry.[35–37] Interestingly, most of the interactions

critical for binding Ni to this protein are provided by the first seven amino acids in the sequence: HCDLPCG. In fact, Neupane and coworkers demonstrated that this heptapeptide alone is sufficient to coordinate Ni, and the resulting complex maintained superoxide dismutase activity. Furthermore, replacement of the axial histidine ligand by alanine did not prevent formation of the Ni complex although the loss of the fifth ligand destabilized the Ni(III) state.[38] Here, we report the utilization of Ni-coordinated ACDLPCG, the alanine variant of the Ni-binding hook that we will refer to as NiSODA, as a fragment for construction of [NiFe]-hydrogenase models. As shown in **Scheme 4.1**, the cysteinyl thiolates of this metallopeptide can exchange labile ligands on heterometallic complexes. Synthesis and characterization of a range of model complexes for [NiFe]-hydrogenases of different metal composition, nuclearity, and terminal ligand set will be presented, demonstrating the generality of this methodology for production of peptide-based heterobimetallic complexes.

4.2. Experimental Section

General

All inorganic syntheses were performed on a double-manifold Schlenk vacuum line under a nitrogen atmosphere. Unless otherwise specified, all chemicals and solvents were obtained from Sigma-Aldrich and were of the

highest grade available. Aqueous solutions were prepared using purified water (resistivity 18.2 MΩ cm).

Physical Measurements

MALDI-MS (matrix-assisted laser desorption/ ionization-mass spectrometry) characterization of peptides was performed on a Voyager DE STR in the Proteomics and Protein Chemistry Laboratory at Arizona State University using α-Cyano-4-hydroxycinnamic acid in acetonitrile/water (50:50 by volume) as the matrix. ESI-MS (electrospray ionization-mass spectrometry) was performed using a Thermo Quantum Discovery Max triple-quadrupole mass spectrometer in the Environmental Biogeochemistry Laboratory at Arizona State University. Measurements were conducted in positive (+) and negative (–) ionization modes using a methanol/water (50:50 by volume) mobile phase at a flow rate of 10 μL min^{-1} and the following ionization conditions: spray voltage, 4000 V(+, –); capillary temperature, 270°C; sheath gas pressures, 25 (+) and 15 (–) psi; auxiliary gas pressure, 2 (+, –) psi. Isotope pattern calculator v4.0 (developed by Junhua Yan) was used to simulate the molecular mass spectral data. NMR spectra were recorded at 400 MHz (^1H) using Varian Liquid-State NMR instruments in $CDCl_3$ solutions (99.8%, Cambridge Isotopes Laboratories Inc.) containing 0.1% TMS (tetramethylsilane) or in D_2O (99.9%, Cambridge Isotopes Laboratories Inc.) unless otherwise noted. UV-vis measurements were performed using a Hewlett-Packard 8453 spectrophotometer using quartz cuvettes with a 1 cm pathlength. FTIR (Fourier transformed infrared) spectra were recorded on a

Thermo Nicolet Avatar-360 spectrometer either as KBr pellets or as a dry film on a CaF_2 window. Each spectrum is an average of 250 scans (for KBr pellets) or 264 scans (for dry film samples) at 1 cm^{-1} resolution. Circular dichroism (CD) spectroscopy was performed on a Jasco 710 or J-815 spectropolarimeter using a rectangular quartz cell with a pathlength of 0.1 cm. Metal concentrations were determined using ICP-MS on a Thermo Finnigan X-Series quadrupole ICP-MS in CCT mode (for Fe) and normal mode (for Ni, Mo, Ru, and W), using 7% H_2 in He as the collision cell gas. Indium, bismuth, and germanium were used as internal standards. Iron was measured at masses 54, 56 and 57 and Ni at masses 58 and 60, molybdenum at 95 and 97, ruthenium at 101 and 102, and tungsten at 182 and 184. Samples were digested in concentrated nitric acid in Teflon beakers. After digestion, samples were dried and dissolved in 0.32M HNO_3 for measurements. X-ray photoelectron spectroscopy (XPS) data were acquired using a VG 220i-XL system. The X-ray source uses a monochromated Al K_α line at 1486.6 eV. The base pressure of the system is 7 x 10^{-10} mbar, and spectra were acquired at approx. 1 x 10^{-9} mbar. Powder samples were pressed into indium (In) foil for transfer into the system. XPS spectra were calibrated to the C1s peak position (at 285.0 eV for CH_3) and analyzed using CasaXPS software (version 2.3.15, Casa Software Ltd.).

Peptide synthesis and purification

The seven amino acid peptide referred to as SODA (ACDLPCG) was synthesized and characterized as described in ***Chapter 2***.

Metallopeptide complexes synthesis

NiSODA

NiSODA was synthesized in 50 mM N-ethylmorpholine (NEM) buffer (pH 7.5) from $NiCl_2$ (anhydrous) as described by Neupane *et al*.[38] The concentration of NiSODA was determined spectroscopically using $\varepsilon_{\lambda 459}$=427 M^{-1} cm^{-1} and purity confirmed via analytical HPLC (**Figure 4.2**)

NiSODA-$Fe_2(CO)_6$

10 mg of $Fe_3(CO)_{12}$ in 3 mL MeOH was added to 2.5 mL of 1.2 mM solution of NiSODA in 50 mM NEM buffer, pH 7.5 and stirred at room temperature for 15 minutes. The mixture was subsequently heated to 70ºC for 2.5 hrs. The solution turned reddish brown. After cooling, the solution was centrifuged and filtered through 0.8/0.2 μm Acrodisc syringe filter (Pall corporations) to remove the green precipitate. The solution was evaporated under reduced pressure to remove the methanol. The remaining aqueous solution was purified by analytical HPLC (0-100% acetonitrile gradient in water). The purified NiSODA-$Fe_2(CO)_6$ sample was lyophilized and then rehydrated to the desired concentration before spectroscopic characterization. As a control experiment, an analogous reaction between SODA and $Fe_3(CO)_{12}$ was also performed. After reaction, the SODA- $Fe_2(CO)_6$ complex was isolated by filtering unreacted $Fe_3(CO)_{12}$ and removing the methanol under reduced pressure.

NiSODA-[$Mo(CO)_4$(piperidine)]$_2$ and NiSODA-[$W(CO)_4$(piperidine)]$_2$

NiSODA-$[M(CO)_4(piperidine)]_2$ (M=Mo, W) complexes were prepared via two different methods. First, one equivalent (2.5 mg) of $W(CO)_4(piperidine)_2$ was dissolved in 50 ml methanol. This anaerobic solution was then added slowly to a 2 mL solution of 2.68 mM NiSODA in 50mM NEM buffer (pH 7.5) at room temperature. The mixture was then refluxed (65°C) for 2 hours. After cooling, the methanol was removed under reduced pressure, and the remaining aqueous solution was lyophilized to obtain a solid powder. Unreacted $W(CO)_4(piperidine)_2$ was removed by dissolving the mixture in water and filtering out the insoluble $W(CO)_4(piperidine)_2$. The water-soluble part was then purified via HPLC. NiSODA-$[Mo(CO)_4(piperidine)]_2$ was also synthesized using an analogous procedure. In the second method, a concentrated sample of $M(CO)_4(piperidine)_2$ was prepared in N,N'-dimethylformamide (DMF). Then one equivalent of NiSODA in aqueous NEM buffer (pH 7.5) was added to the solution at room temperature. After addition, the v/v ratio of aqueous solution to DMF was 20:1. The mixture was heated at 65ºC for 2 hours, and the rest of the experiment was performed as for the first method. Both methods gave comparable results.

[NiSODA-Ru(η^6-p-cymene)$(H_2O)_3$]$(NO_3)_2$ and [NiSODA-Ru(η^6-C_6Me_6)$(H_2O)_3$]$(NO_3)_2$

Ru(η^6-p-cymene)$(H_2O)_3(NO_3)_2$ was prepared as described in reference 39.[39] Similarly, [Ru(η^6-C_6Me_6)$(H_2O)_3$]$(NO_3)_2$ was prepared as described Jahncke *et al*.[40] A 1 mL aqueous solution of 3.3 mM Ru(η^6-arene)$(H_2O)_3^{2+}$ (arene= C_6Me_6 or p-cymene) was added to 3 mL of 1.1 mM NiSODA in 50 mM NEM, pH 7.5 buffer and stirred at room temperature for four hours. Purification of the complexes was

achieved using reversed phase HPLC on the analytical scale. Aqueous acetonitrile gradients (0-100%, without TFA) were used as the mobile phase. The acetonitrile concentration was increased at a rate of 1% min^{-1} and the flow rate was 0.50 mL min^{-1}. Purified *[NiSODA-Ru(η^6-C_6Me_6)(H_2O)$_3$](NO_3)$_2$* eluted from the column at 27.0 min. See also **Figure 4.2** for chromatograms.

4.3. Results and Discussion

The general strategy developed in this work for the synthesis of peptide coordinated heterometallic (Ni-M) complexes is summarized in **Scheme 4.1**. First, Ni was incorporated into purified SODA in 50 mM NEM buffer at pH 7.5 as described by Neupane and coworkers.[38] Metal incorporation was confirmed by UV-vis spectroscopy [$\varepsilon_{459\ nm}$(NiSODA)= 427 M^{-1} cm^{-1}] (**Figure 4.5**) and MALDI mass spectrometry (**Figure 4.3**). NiSODA was then used as a metalloligand for exchange reactions with iron, tungsten, molybdenum and ruthenium complexes with labile ligands. When considering this general synthetic strategy, two properties of NiSODA are important to note. First, NiSODA is only sparingly soluble in organic solvents. Second, Ni is coordinated to SODA only at circumneutral pH (6-8). If the pH is too high, insoluble nickel (II) hydroxide forms, and, if the solution is too acidic, the cysteinyl ligands are not deprotonated. Thus, one of the unique challenges of preparing organometallic peptide

complexes of this type is identifying appropriate solvents for both components of the reaction.

NiFe complexes

Metal carbonyls have been used to great effect in models of hydrogenases with the advantage that FTIR spectroscopy can be employed to probe the resulting complexes. Schröder and coworkers described the synthesis and reactivity of a trimetallic $[Ni(\mu\text{-}SR)_2Fe_2(CO)_6]$ cluster by reaction of a nickel tetrathiolate complex with $Fe_3(CO)_{12}$.[41,42] Unlike most models of [NiFe]-hydrogenases, the trimetallic Schröder complex catalyzes proton reduction. A related trimetallic compound, Compound 3A shown in **Scheme 1**, is expected to form from the reaction of NiSODA and $Fe_3(CO)_{12}$. The expected metallopeptide features two terminal nitrogen-based ligands to the Ni and two thiolates bridging between the nickel and a diiron-hexacarbonyl fragment. As a test of the ability to utilize the cysteine thiolates of NiSODA as bridging ligands in a heterometallic complex, we synthesized the NiSODA-$Fe_2(CO)_6$ complex analogue of the Schröder complex by the reaction at high temperature of NiSODA and $Fe_3(CO)_{12}$ in a mixture of methanol and water. After reaction, the NiSODA-$Fe_2(CO)_6$ complex was purified by analytical HPLC (**Figure 4.2**), and all spectroscopic measurements were performed with purified samples. ESI-MS was used to confirm that the mass of the isolated product matched that of the anticipated trimetallic complex (**Figure 4.4**). In addition to the anticipated molecular ion (1010.6 m/z for $[M\text{-}H]^-$),

several heavier peaks were also observed in the mass spectrum. These peaks are likely the result of air oxidation of the thiols. This process may be accelerated by the harsh ionization conditions employed for ESI-MS. However, we also note that not all species are detected with equal efficiency via ESI-MS so that peak intensities cannot be correlated with relative concentrations in the sample. Peaks associated with the loss of several CO ligands, commonly observed for metal carbonyls, were also detected. Furthermore, the modeled isotope pattern for each set of peaks, uniquely determined by the isotopic abundances of each of the elements in the complex, closely matches the experimental data. Thus there can be little doubt that the complex contains all three metals. The Ni:Fe ratio of the purified metalloprotein was determined to be 1:2.1 via metal quantization using ICP-MS. This result again confirms the expected metal composition.

Figure 4.5 compares the UV-vis spectra of Ni-SODA and NiSODA-$Fe_2(CO)_6$. A strong metal-to-ligand charge transfer (MLCT) band around 335 nm and a weak d-d transition at 470 nm (**Figure 4.5**) are seen in the spectrum of NiSODA-$Fe_2(CO)_6$ but not in the Ni-SODA starting material.[43] This pair of features is commonly associated with the so-called butterfly Fe-S core of an $(\mu\text{-}SR)_2Fe_2(CO)_6$ fragment. Since we have previously shown that $Fe_3(CO)_{12}$ can react with two cysteines in peptides to form $Fe_2(RS)_2(CO)_6$, we considered it necessary to ensure that the diiron butterfly core complex did not arise simply from SODA-$Fe_2(CO)_6$, *i.e.*, a nickel-free complex.[30] As a control, $Fe_3(CO)_{12}$ was reacted with SODA, *i.e.,* without a coordinated Ni, to establish whether an SODA-$Fe_2(CO)_6$ complex could be formed. The dotted line in **Figure 4.5** demonstrates that indeed,

a diiron product with the expected UV-vis features was formed. The retention time of this nickel-free, diiron complex (42 minutes) is substantially different from the trimetallic peptide (30 minutes) (data not shown). Additionally, the charge transfer band was shifted to slightly lower energy (328 nm to 334 nm) for SODA-$Fe_2(CO)_6$ relative to the trimetallic NiSODA-$Fe_2(CO)_6$ complex. Thus considering together the UV-vis, mass spectrospic and metal quantitation data, we conclude that the reaction with NiSODA did result in trimetallic peptide. We attribute the subtle shift in the *circa* 330 nm charge transfer band of the trimetallic to the altered electronic environment created by sharing the electron density of the sulfurs with the neighboring Ni ion. Furthermore, based on the presence of this charge transfer band, there can be no doubt that the $Fe_2(CO)_6$ fragment is coordinated to the cysteinyl sulfurs.

Figure 4.6 compares the CD spectra of Ni-SODA, NiSODA-$Fe_2(CO)_6$, and SODA-$Fe_2(CO)_6$ in the visible region (400-600 nm). The CD spectrum of NiSODA consists of a negatively signed feature at 475 nm and two positive features at higher energies. The negatively signed feature is unchanged in the spectrum of NiSODA-$Fe_2(CO)_6$, but the positive features are shifted to higher energy and an additional one has emerged. It is worth noting that the spectrum of SODA-$Fe_2(CO)_6$ is completely flat, providing additional evidence for a trimetallic product in the reaction of NiSODA with $Fe_3(CO)_{12}$. Neupane and coworkers reported the spectra for NiSODA and related nickel-containing peptides with several variations at the N-terminus,[38] and the spectrum of NiSODA matches that reported. It is consistent with a chiral, square planar N_2S_2 environment for the

nickel (**Figure 4.6**). Neupane and coworkers demonstrated that the negatively signed feature is an excellent reporter on the nature of the nitrogen coordination; it shifts dramatically (2,150 cm^{-1}) upon conversion of the terminal amine to an amide producing a bis-amide coordination sphere.[44] The observation that this feature is virtually unchanged by addition of the $Fe_2(CO)_6$ fragment to NiSODA suggests that the nitrogen coordination of the nickel is relatively unchanged in the trimetallic complex. On the other hand, the positive features have been attributed to sulfur-based transitions. The dramatic change in this region of the CD spectrum provides additional evidence that coordination of the $Fe_2(CO)_6$ fragment occurs through the cysteinyl sulfurs.

FTIR spectroscopy has proven invaluable for characterizing metal carbonyls in peptides/proteins because there are no interfering peptide vibrations at similar frequencies (circa 2000 cm^{-1}). FTIR spectra of [SODA-$Fe_2(CO)_6$] and [NiSODA-$Fe_2(CO)_6$] revealed bands at 2074 cm^{-1}, 2038 cm^{-1} and 2002 cm^{-1} (**Figure 4.7**). These frequencies are nearly identical to those reported for related peptidyl bis-thiolate ligated $Fe_2(CO)_6$ complexes,[30,31] and demonstrate conclusively not only that the carbonyl ligands are retained in the products, but also that their bonding to iron is not significantly influenced by the nickel. Additionally, the number and intensities of these bands demonstrate the formation of a complex with pseudo C_{2v} symmetry.[43] In considering how or if the peptide modifies the properties of the coordinated metallocenter, it is interesting to compare the FTIR spectra of NiSODA-$Fe_2(CO)_6$ and the analogous tetrathiolate $Ni(SR)_2(\mu\text{-}SR')_2Fe_2(CO)_6$ complex reported by Schröder. The tetrathiolate complex also has an FTIR

spectrum with three peaks in the CO vibration region at 2035, 1995, and 1955 cm^{-1}. Thus, as expected, both complexes are pseudo C_{2v} when considering only the $Fe_2(CO)_6$ fragment. However, the frequencies of the tetrathiolate complex are systematically shifted by approximately 40 cm^{-1} to lower energy. This can be explained by the significant sharing of electron density between the Ni and Fe parts of the complex. However, those of NiSODA-$Fe_2(CO)_6$ are nearly identical to the well known μ-($S(CH_2)_3S$)-$Fe_2(CO)_6$ complex and suggest that there is very little electronic interaction between the Ni and the diiron fragments. The question of why there is not appreciable electronic interaction between the Ni and diiron parts of the complex in the peptide then comes naturally to the fore. Although one might ordinarily be tempted to look to the first coordination spheres of the metal, the exchange of the two terminal thiolates at the nickel for amine/amide coordination alone is probably not sufficient for this electronic change. Instead, we hypothesize that the steric hindrance imposed by the peptide occludes one side of the nickel. The likely effect is that the nickel, bridging sulfur, and iron atoms are no longer coplanar. Instead, the square planar nickel is in one plane, and the bridging thiolates and irons form a second plane. If this assumption is correct, the electronic communication between the nickel and the irons is almost completely severed since each metal interacts with a different orbital of the sulfur.

NiW and NiMo complexes

Darensbourg and coworkers have systematically characterized the electronic and steric parameters of square planar NiN_2S_2 complexes as bidentate, S-donor

ligands to $W(CO)_4$ complexes by comparison of the ν(CO) stretching frequencies.[45] By analogy, we have also considered the reaction of NiSODA with $[M(CO)_4(piperidine)_2]$ (M=Mo,W) to generate heterobimetallic Ni-W and Ni-Mo complexes (Compound 3b in **Scheme 4.1**). Analytical HPLC of the reaction mixtures suggested that a single, much slower-running (*i.e.*, more hydrophobic), major product was formed in each reaction, and the product could be purified using HPLC (**Figure 4.2**). Although by analogy to previous work we anticipated formation of a bimetallic species by cysteine thiolate substitution of both piperidine ligands, mass spectrometry indicated formation of heavier complexes. As shown in **Figure 4.8**, modeling of the isotopic distribution patterns observed in the MALDI-TOF spectra suggests that the products contained a single Ni and two Mo or W ions consistent with formation of (μ-NiSODA-κS:κS´)$[M(CO)_4(piperidine)]_2$ complexes. We note that intact parent ions were not detected for the complexes in the mass spectra; instead, ions corresponding to loss of a single piperidine (for W) or four CO ligands (for Mo) from the trimetallic complexes were observed. This is not unusual as the harsh ionization conditions of MALDI often dissociate loosely bound ligands, like carbonyls, from metal complexes. In short, the mass spectra suggest that only a single piperidine ligand was substituted in each reaction to generate a trinuclear cluster. Furthermore, the Ni:M ratios for M=Mo and W were determined to be 1:2.2 and 1:2.0, respectively, using ICP-MS, providing additional evidence for trinuclear complexes.

As was the case for the NiFe complex already described, CD spectra in the visible region demonstrated that the Ni-N_2S_2 center remained intact in both the Mo and W products, and the sulfur-based transitions were dramatically changed by coordination of a heterometallic fragment (**Figure 4.9**). UV-vis spectroscopy was also used to characterize the electronic environment of both the Ni and the W or Mo heterometal. As shown in **Figure 4.10**, broad transitions were observed in the spectra of both NiSODA and NiSODA-$[M(CO)_4(piperidine)]_2$ (M=W or Mo) at 465 nm and 550 nm. These features have been described as characteristic of square planar nickel in an N_2S_2 geometry. Inspection of the remaining features in the UV-vis spectra provides insights into the nature of the bonding of the peptide to the W or Mo fragment. Considering first the spectrum of the W precursor, $W(CO)_4(piperidine)_2$, it consists of two groups of features: a d-d transition visible band at 400 nm and two UV transitions at 255 and 300 nm arising from MLCT bands from the metal d orbitals to the CO π^* orbitals. Since there are two inequivalent sets of CO ligands, *trans-* and *cis-* to the nitrogens, two MLCT transitions are observed. Relative to the strongly σ-donating piperidine ligand, a cysteinyl alkyl thiolate is expected to be weakly σ and π donating. Thus replacement of a piperidine by cysteine upon formation of the peptide coordinated complex is expected to raise the energy of the d_π orbitals and stabilize the d_{σ^*} orbitals resulting in red shifts of both the d-d and the MLCT transitions (See also **Scheme 4.2** for a qualitative MO diagram of relevant orbitals). As shown in **Figure 4.10A**, these shifts are observed for NiSODA-$[W(CO)_4(piperidine)]_2$

providing strong evidence that the peptide coordinates the W via a thiolate. Additionally, replacement of only one of the piperidine ligands with cysteine, as suggested by the MALDI data, should create three sets of CO ligands since the ligands *trans* to the peptide and the piperidine are no longer equivalent. The observation of three MLCT bands (at 260, 280 and 320 nm) for NiSODA-$[W(CO)_4(piperidine)]_2$ relative to the two seen for the starting material also suggests that only one of the piperidine ligands was exchanged during the reaction. Similar features in the optical spectrum of NiSODA-$[Mo(CO)_4(piperidine)]_2$ (**Figure 4.10B**) provide evidence that an analogous Mo complex was formed.

Further information regarding the binding mode of the cysteines was obtained by probing the binding energies of the sulfur 2p core electrons in NiSODA and NiSODA-$[Mo(CO)_4(piperidine)]_2$ via X-ray photoelectron spectroscopy (XPS). Signals corresponding to both oxidized and reduced forms of sulfur could be detected in the samples due to air oxidation, and, for both of these sulfur signals, a 1.0-1.3 eV increase in binding energy was observed upon comparison of NiSODA to the heterometallic complex (**Figure 4.11, Table 4.1**) This is consistent with the results of Walton and coworkers that the binding energy of an S $2p_{3/2}$ electron increases by at least +0.5 eV upon conversion from a terminal to a bridging position and provides additional evidence that the cysteinyl sulfurs are bridging ligands in NiSODA-$[Mo(CO)_4(piperidine)]_2$.[46,47]

Figure 4.12A shows an FTIR spectrum from [NiSODA-$W(CO)_4(piperidine)]_2$ in the CO stretching region. Several attempts were made to obtain spectra for the

Mo complex, but signals were very weak and are thus not discussed here. For [NiSODA-$W(CO)_4$(piperidine)]$_2$, four strong bands are observed: 2003, 1930, 1885, and 1847 cm^{-1}. A weaker band at 1970 cm^{-1} was also found. The bands are higher in energy than those of the precursor Mo/W complexes indicating a decrease in metal backbonding into the π^* orbital upon coordination of a poorer electron donor, cysteine thiolate. The presence of these bands confirms retention of the CO ligands in the NiW peptide. Furthermore, according to the arguments below, the number of bands provides additional evidence for formation of a trinuclear complex. In work analogous to that presented here, Ainscough and coworkers described the FTIR spectra of *cis*-$W(CO)_4XY$ complexes in which X was an amine and Y a thiolate.[48] These complexes also produced four CO stretching bands at frequencies of approximately 2018, 1900, 1880, and 1845 cm^{-1}. Assuming pseudo-C_{2v} symmetry about the W, these bands can be assigned as having a_1, a_1, b_1, and b_2 symmetry. Asali and coworkers also described a series of [$W(CO)_4$(pip)]$_2$Z complexes in which Z is a bidentate phosphine or dithiolate ligand.[49–51] These compounds also had four CO stretching frequencies, and it is likely that these are analogous to the strong bands observed in our experiment. We assign the weaker 1970 cm^{-1} band found in our spectrum to the single asymmetric stretch anticipated for a *trans*- $W(CO)_4XY$ complex.[52,53]

Figure 4.12B shows the FTIR spectra from [NiSODA-$M(CO)_4$(piperidine)]$_2$ (M=Mo, W) and NiSODA in the region 400-650 cm^{-1}. NiSODA has three vibrations in this region at 600, 472, and 450 cm^{-1}. Two of these (472 and 450 cm^{-1}) are believed to arise from Ni-N stretching and the third (600 cm^{-1}) from

out-of-plane bending of the C=O of the coordinated amide.[54,55] These bands were systematically shifted to higher wavenumbers to 605, 475, and 453 cm^{-1} upon coordination of the Mo or W fragment. This suggests that sharing of electron density through the bridging sulfurs impacts the strengths of the Ni-N bonds. In short, the Mo/W fragment is expected to withdraw electron density from the Ni-S bonds. The Ni fragment then compensates with stronger Ni-N bonding as reflected in the IR stretches.

Although not the intended reaction products, the trimetallic clusters generated here are not without precedent in the literature. A similar trimetallic (μ-N_2S_2-κS:κS')$[W(CO)_5]_2$ has been reported.[56] In the case of reactions with NiSODA, it is likely there are both steric and thermodynamic reasons for the formation of trimetallic Ni-M (M=Mo, W) complexes as opposed to binuclear ones. First, the transition state for a 1:1 reaction between NiSODA and $[M(CO)_4(piperidine)_2]$ (M=Mo, W) may require accommodating both the bulky sides chains of the SODA peptide and the not-yet-displaced piperidine ligands in a structure that is too sterically cramped to be energetically accessible. On the thermodynamic side, it is important to consider that piperidine is a strong σ-donating ligand, but the alkyl thiolate sulfurs are expected to be relatively weak σ- and π-donating ligands. Thus, replacement of both piperidine ligands may be enthalpically unfavorable. Similarly, tethering of both sides of the Mo or W complex to the peptide in a 1:1 complex should cause a substantial decrease in entropy that will also favor the 1:2 reaction. On the other hand, it is natural to also ask why, in contrast, our Ni-Ru reactions (described below) produced bimetallic complexes.

In these reactions, water ligands on the Ru precursor complex are replaced by the relatively stronger σ-donating cysteine thiolates providing a much greater enthalpic driving force. Substitution of the water molecules by cysteinates from the ruthenium fragment also increases the entropy of the system.

NiRu complexes

Two related, dinuclear Ni-Ru(arene) complexes were identified as synthetic targets: [NiSODA-Ru(η^6-*p*-cymene)(H_2O)](NO_3)$_2$ and [NiSODA-Ru(η^6-C_6Me_6)(H_2O)](NO_3)$_2$ (Compound 3C in **Scheme 1**). As described by Ogo and coworkers, analogous complexes utilizing the N,N'-dimethyl-N,N'-bis(2-mercaptoethyl)-1,3,-propanediamine ligand as an N_2S_2 coordination environment for the nickel were highly water soluble and, in the case of the hexamethylbenzene complex, cleaved hydrogen to form a bridging hydride species.[6]

NiRu complexes were generated by the reaction of NiSODA in NEM buffered aqueous solution (pH 7.5) with [Ru(η^6-arene)(H_2O)$_3$](NO_3)$_2$ where the arene was either hexamethylbenzene or *p*-cymene. The hexamethylbenzene complex was then purified for further analysis via reverse-phase analytical HPLC (Chromatogram is shown in **Figure 4.2**). MALDI-TOF spectra of the reaction products showed that complexes of the expected molecular weights were formed (m/z = 996 and 969 for hexamethylbenzene and *p*-cymene complexes, respectively.). Furthermore, these spectra had the isotope pattern expected for a

heterobimetallic Ni-Ru complex (**Figure 4.13**), and the Ni:Ru ratio determined via ICP-MS was 1:0.9. **Figure 4.14** shows ^{1}H-NMR spectra for SODA, NiSODA, [NiSODA-Ru(η^6-C_6Me_6)(H_2O)](NO_3)$_2$, and the ruthenium precursor used in synthesis of the heterometallic complex. As shown in **Figure 4.14B**, binding of Ni to SODA resulted in a broadening and shifting in particular of the resonances of the β-protons of the cysteines confirming interaction of the cysteinyl sulfurs with Ni. Upon addition of the Ru-hexamethylbenzene fragment, a sharp resonance at 2.08 ppm appeared that can be attributed to the resonance of the methyl-protons of the hexamethylbenzene ring (**Figure 4.14C**), providing further evidence that this ligand was retained in the product. The position of this methyl resonance was shifted from 2.22 ppm in the starting compound to 2.08 ppm in the product. Interestingly, Ogo and colleagues also reported that the methyl resonance shifted upfield in their analogous NiRu complex to 2.15 or 2.18 ppm depending on the counter ion present.[6] Thus it is likely that the Ru fragments in that organometallic complex and in the peptide reported here are in similar electronic environments.

UV-Vis, CD and FTIR spectroscopy were also used to characterize the electronic environment of the products. **Figure 4.15** shows the UV-Vis spectrum of the heterobimetallic (NiRu) hexamethylbenzene complex, and data from the *p*-cymene complex can be found in the Appendix (**Figure 4.16**). Although the spectra of the heterobimetallic complexes consist of a superposition of relatively broad peaks especially in the visible region, features arising primarily from each of the individual metal fragments were observed and help to confirm retention of the expected ligand sets. For example, the broad transitions observed at 460 nm

and 545 nm are characteristic of Ni in a square planar N_2S_2 geometry and are also seen in the spectrum of the starting NiSODA complex. Similarly, the band centered at 400 nm is likely to arise from a Ru-based ligand field (LF) transition.[57] Despite shared features between the precursor complexes and the heterobimetallic complexes, it is important to note that the spectrum from the bimetallic complex is not simply a linear combination of the spectra of the individual components. Instead, the precise maximum of each feature is shifted by interaction of the two metal fragments. For example, the 400 nm band in the heterobimetallic complex is blue-shifted relative to the starting Ru-arene complex likely due to interaction of the Ru fragment with the sulfur ligands. The CD spectra for the heterobimetallic NiRu complexes are shown in **Figure 4.17**. As for the other compounds described in this work, the negative feature at 475 nm was unchanged by binding of the Ru-fragments, shifting only 5 nm to lower energy. However, the higher energy positive features were significantly changed providing evidence that the Ru fragment is coordinated via the sulfur ligands. Finally, as described for the Mo/W complexes, the Ni–N stretching modes of the NiRu complexes were slightly higher in energy than those of NiSODA (**Figure 4.18**).

4.4. Concluding Remarks

We have demonstrated that NiSODA reacts with a range of heterometallic fragments with different metals, nuclearities, and ligand sets to form peptide-coordinated hydrogenase mimics. Spectroscopic evidence suggests that in all cases the N_2S_2 coordination of the Ni is maintained and the sulfurs are the reactive

sites, forming bridges to the heterometallic fragment. Additionally, the unique vibrational frequencies of metal carbonyls can be used to demonstrate incorporation of heterometallic fragments and evaluate the donor ability of the nickel fragment. This synthetic approach is similar to that reported for other [NiFe]-hydrogenase small molecule mimics, and opens countless opportunities to construct water-soluble hydrogenase mimics and compare their properties to those of both the enzymes and small molecules. Furthermore, this method parallels the biosynthesis of the hydrogenase active site, believed to proceed via incorporation of the Fe fragment with its diatomic ligands into the apo-enzyme followed by transfer of the Ni atom from a metallochaperone to complete the active site.[58] This suggests that a model peptide could be used as an *in vitro* substrate for biosynthetic studies.

Hydrogenases are not the only known heterometallic enzymes. In fact, this group includes a number of bioenergetically and technologically important enzymes catalyzing small molecule transformations such as acetylcoenzyme A synthase-carbon monoxide dehydrogenase (ACS-CODH),[59–61] nitrogenase,[62,63] and the oxygen evolving complex (OEC) of photosystem II.[64,65] There is significant interest in developing bioinspired, homogeneous, molecular catalysts corresponding to each of these enzymes, and this work provides a starting point for constructing peptide-based mimics. Peptide-based systems offer several crucial advantages over traditional models including the opportunity to alter the aqueous solubility of relevant inorganic complexes[30,31,66] and the chance to tailor functionally important outer coordination sphere interactions.[34] In particular, there

are remarkable parallels between our synthetic hybrid bioinorganic/organometallic site and the acetylcoenzyme A synthase (ACS) active site, the A-cluster. That center consists of a [4Fe4S] cluster bridged to a binuclear center. The nickel site distal to the iron-sulfur cluster has very similar coordination to the nickel to NiSODA, consisting of two cysteinyl and two amide nitrogen ligands. Interestingly, the metal binding site proximal to the iron-sulfur cluster can be variously occupied by a nickel, copper or zinc ion sharing the cysteinyl sulfurs with the distal nickel in the same arrangement as the complexes that were constructed in this work.[60,67] In essence, the distal site can be thought of as a metallosynthon for coordination of heterometallic fragments. By analogy, our results may have direct relevance also to the biosynthesis of ACS, and it may be the case that the proximal metal site in ACS can be used to coordinate novel metallocenters creating new bioinorganic/organometallic catalysts with unique reactivities.

In this work, we have created five distinct heterometallic peptides. In the cases of the NiRu and NiFe peptides, complexes analogous to the known small molecules were formed. However, in the cases of the reactions with Mo and W fragments, unexpected trinuclear complexes were formed due to both steric and thermodynamic constraints imposed by the peptide. This suggests that reactions of even small metallopeptides may have novel products, and metallopeptides will serve as crucial models for metalloprotein catalysis.

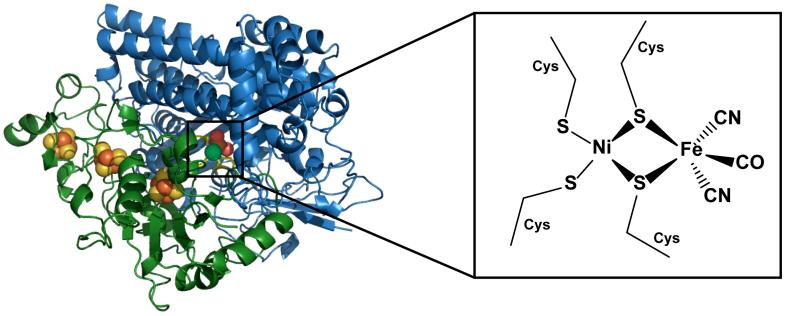

Figure 4.1: **Active site structure of [NiFe]-hydrogenases**. The [NiFe] active site containing large subunit is shown in blue and the [FeS]-containing small subunit in green. Prosthetic groups are shown in ball and stick representation. The chemical structure of the active site is expanded in the black box. The figure was prepared using PyMOL software using overall ribbon structure of the [NiFe]-hydrogenase from *Desulfovibrio gigas* (PDB ID: 1FRV) [The PyMOL Molecular Graphics System, Version 0.99rc6, Schrödinger, LLC].

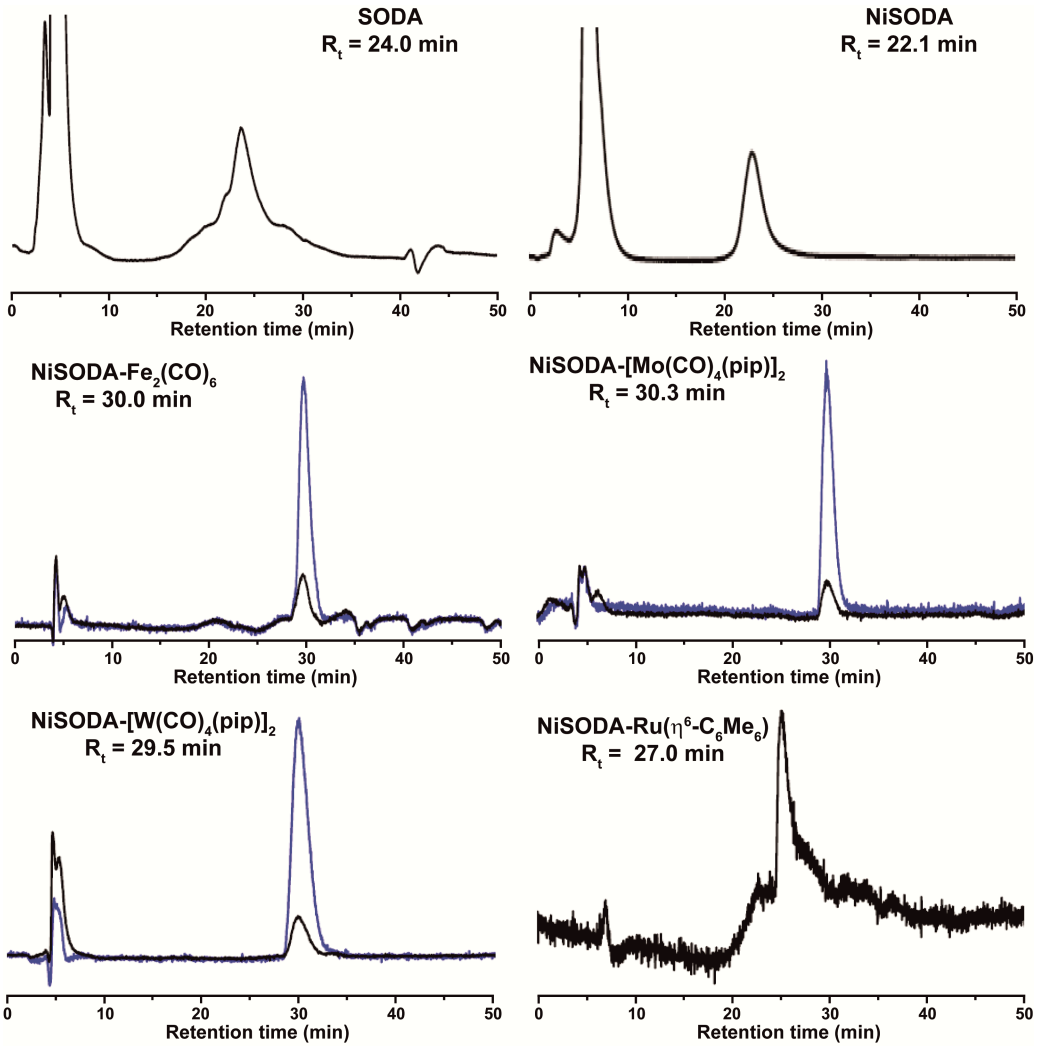

Figure 4.2. Analytical HPLC chromatograms for SODA apopetide and other metallopeptides. Probe wavelengths during HPLC: SODA (220 nm: black), NiSODA (220 nm: black), NiSODA-$Fe_2(CO)_6$ (275 nm: black and 330 nm: blue), NiSODA-$[Mo(CO)_4(pip)]_2$ (275 nm: black and 320 nm: blue), NiSODA-$[W(CO)_4(pip)]_2$ (275 nm: black and 320 nm: blue), and NiSODA-Ru(η^6-C_6Me_6) (275 nm: black). Experimental conditions: 0-50% neat acetonitrile in water in 50 minutes with a 1% gradient and flow rate = 0.5 mL/min.

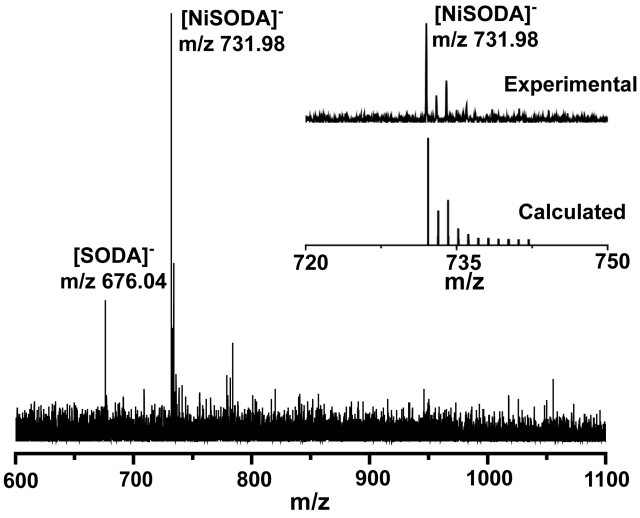

Figure 4.3. MALDI-TOF mass spectrum for NiSODA. Experimental and calculated ESI mass spectra from the NiFe complex molecular ion are shown in inset. Data were recorded in negative ion mode with matrix 4- hydroxyl α-cyano cinnamic acid.

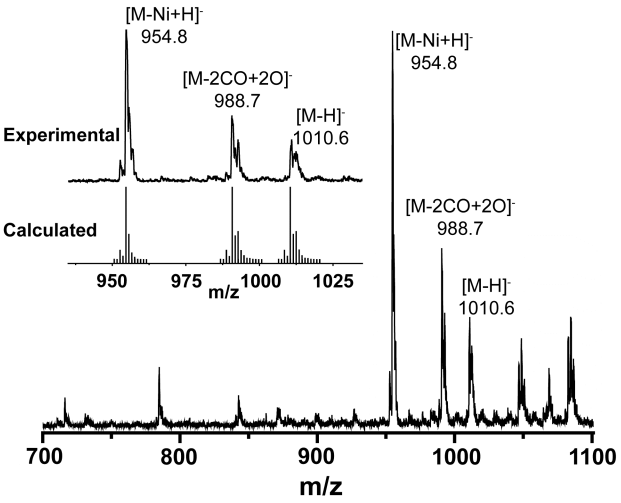

Figure 4.4. ESI-mass spectrum for NiSODA-$Fe_2(CO)_6$. Experimental and calculated ESI mass spectra from the NiFe complex are shown with identities of salient peaks labeled adjacent to the peak. Data were recorded in negative ion mode in aqueous solution, methanol mixture (1:1).

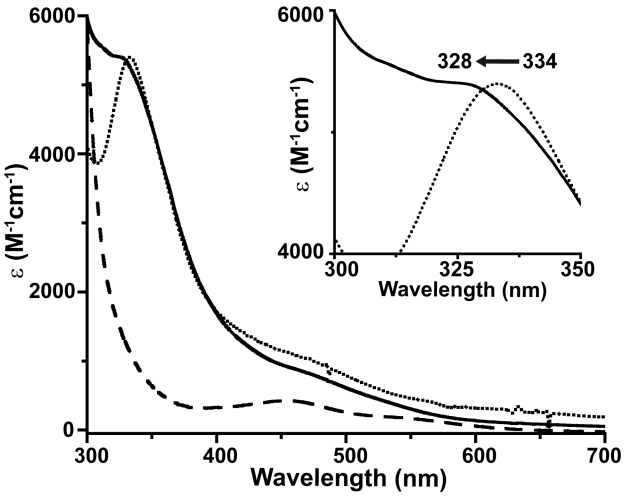

Figure 4.5. Comparative optical spectra for NiSODA-$Fe_2(CO)_6$. UV-vis spectra from NiSODA (dashed line), SODA-$Fe_2(CO)_6$ (dotted line), and NiSODA-$Fe_2(CO)_6$ (solid line). Spectra were recorded in 50 mM aqueous NEM buffer (pH 7.5). In the inset, the MLCT band region is magnified to show the difference between SODA-$Fe_2(CO)_6$ (dotted line), and NiSODA-$Fe_2(CO)_6$ (solid line).

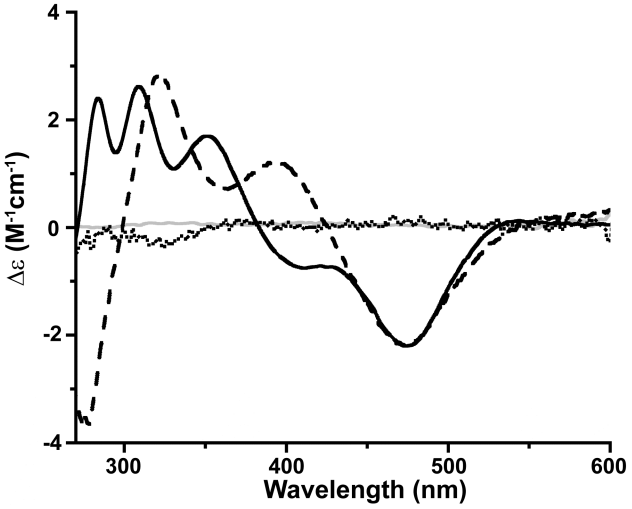

Figure 4.6. Comparative CD spectra for NiSODA-$Fe_2(CO)_6$. CD spectra from NiSODA (dashed line), [NiSODA-$Fe_2(CO)_6$] (solid line), and SODA-$Fe_2(CO)_6$ (dots) in NEM buffer (50 mM, pH 7.5). The apopeptide solution alone is shown in grey.

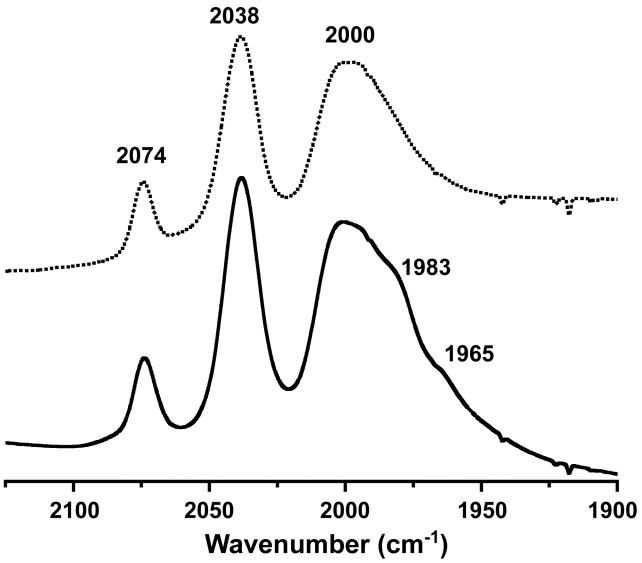

Figure 4.7. Comparative FTIR spectra for SODA-$Fe_2(CO)_6$. The CO stretching frequencies are shown for [SODA-$Fe_2(CO)_6$] (dotted line) and [NiSODA-$Fe_2(CO)_6$] (solid line). The samples were prepared as dried films on a CaF_2 window.

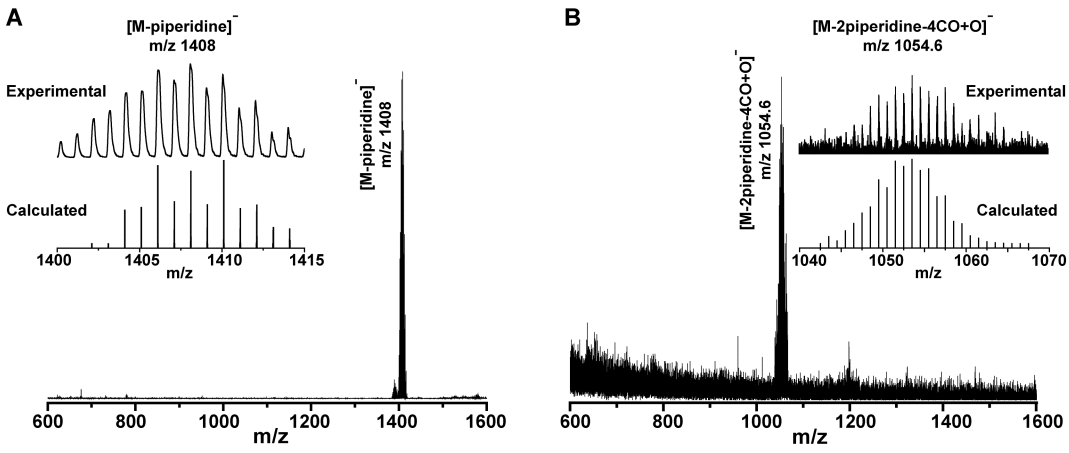

Figure 4.8. Comparative MALDI-mass spectra for NiSODA-[M(CO)$_4$(piperidine)]$_2$ (M=Mo, W). Experimental and calculated MALDI-TOF mass spectra for (A) NiSODA-[W(CO)$_4$(piperidine)]$_2$ and (B) NiSODA-[Mo(CO)$_4$(piperidine)]$_2$ in aqueous, 50 mM NEM buffer (pH 7.5) solution (data recorded in negative ion mode).

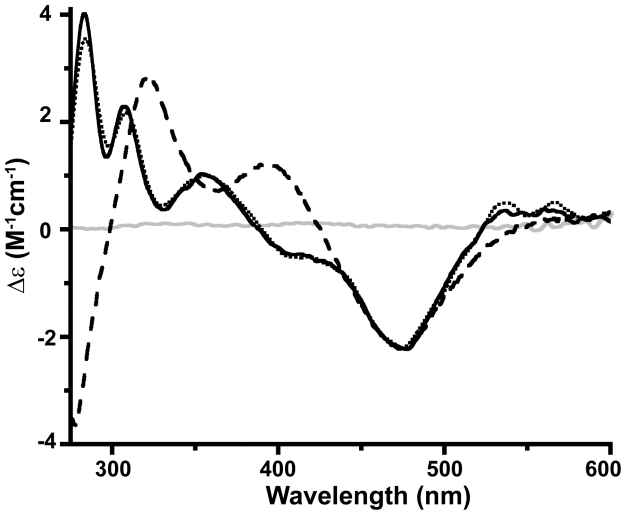

Figure 4.9. Comparative CD spectra for NiSODA-[M(CO)$_4$(piperidine)]$_2$ (M=Mo, W). CD spectra from NiSODA (dashed line), NiSODA-[W(CO)$_4$(piperidine)]$_2$ (solid line), and NiSODA-[Mo(CO)$_4$(piperidine)]$_2$ (dots) in NEM buffer (50 mM, pH 7.5). The apopeptide solution alone is shown in grey.

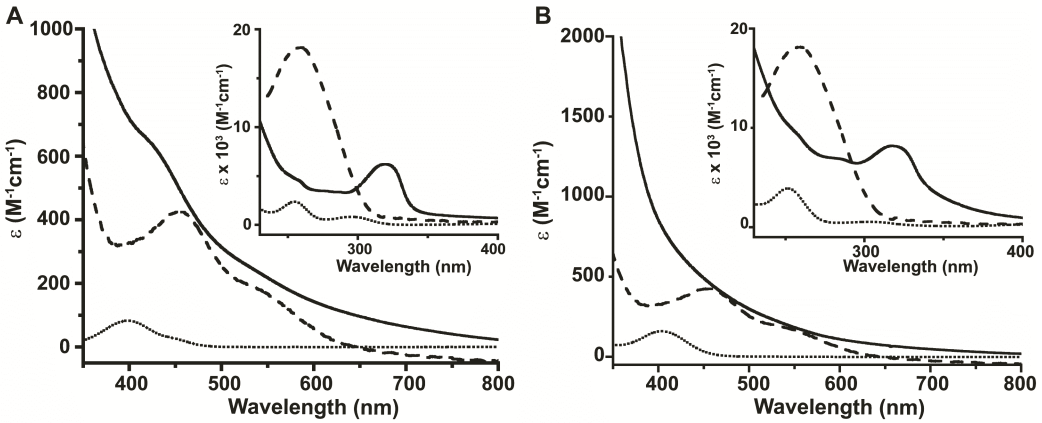

Figure 4.10. Comparative UV-vis spectra for NiSODA-[M(CO)$_4$(piperidine)]$_2$ (M=Mo, W). UV-vis spectra for NiSODA in 50 mM aqueous NEM buffer solution (dashed line), W(CO)$_4$(piperidine)$_2$ (A) or Mo(CO)$_4$(piperidine)$_2$ (B) in methanol (dotted line) and NiSODA-[W(CO)$_4$(piperidine)]$_2$ (A) or NiSODA-[W(CO)$_4$(piperidine)]$_2$ (B) in 50 mM aqueous NEM buffer solution (solid line).

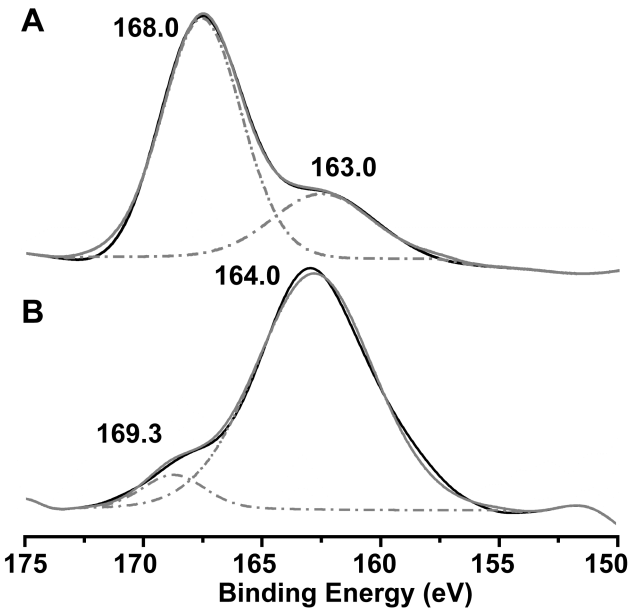

Figure 4.11. Sulfur $2p_{3/2}$ binding energy spectra from (A) NiSODA and (B) NiSODA-$[Mo(CO)_4(piperidine)]_2$. Experimental data are shown as a solid black line. Data were smoothed using an SG quadratic function fitting five points at a time with the CasaXPS software. The same software was used to construct the best fit to the data based on two components (an oxidized, higher energy, and a reduced, lower energy, sulfur species) with the contribution of each component allowed to vary. The two components of the best fit are shown as dash-dot, and the sum of these components as a solid grey line.

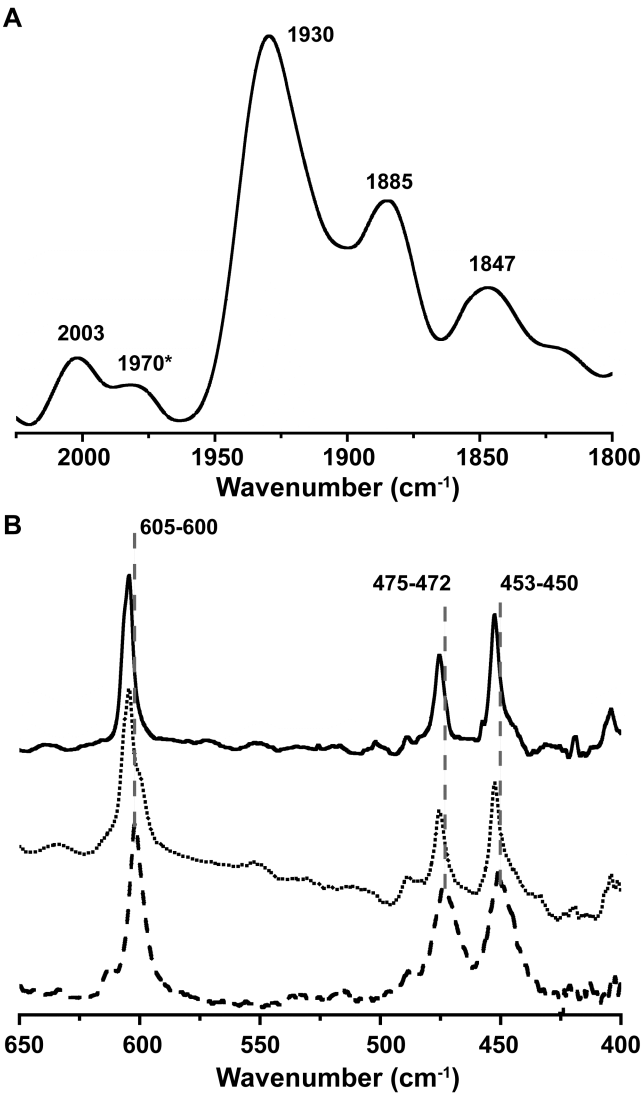

Figure 4.12. **Comparative FTIR spectra for NiSODA-[$M(CO)_4$(piperidine)]$_2$ (M=Mo, W).** FTIR spectra from NiSODA-[$W(CO)_4$(piperidine)]$_2$ (solid line), NiSODA-[$Mo(CO)_4$(piperidine)]$_2$ (dotted line), and NiSODA (dashed line) complexes in the (A) 2025-1800 cm^{-1} region and (B) 650-400 cm^{-1} region. The spectrum in Panel A was obtained from a dried peptide film on a single CaF_2 window. Due to IR absorption by CaF_2 at low wavenumbers, spectra in Panel B were obtained from samples in KBr pellets.

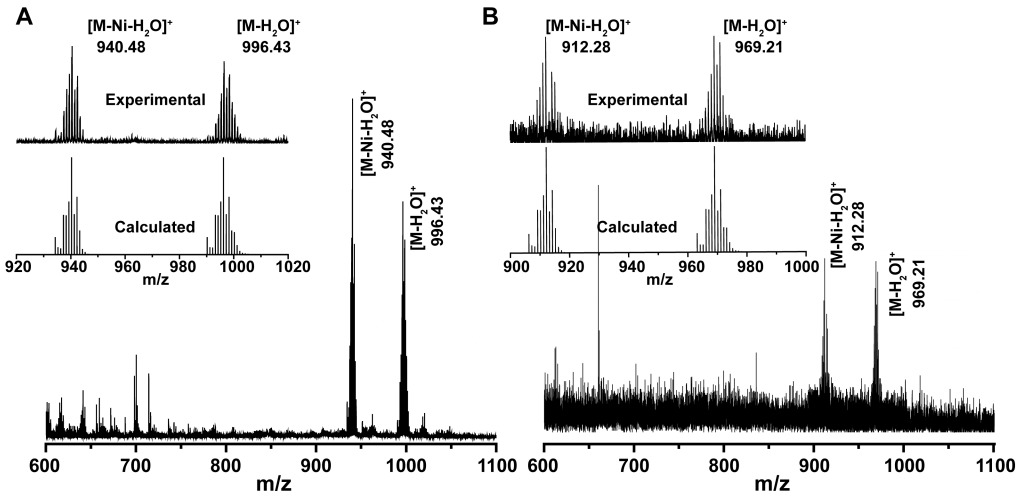

Figure 4.13. Comparative MALDI-mass spectra for NiSODA-Ru(arene) complexes. Experimental and calculated MALDI-TOF mass spectra of (A) [NiSODA-Ru(η^6-C_6Me_6)(H_2O)](NO_3)$_2$ and (B) [NiSODA-Ru(η^6- p-cymene)(H_2O)](NO_3)$_2$ complexes in aqueous solution buffered with 50 mM NEM. Data were recorded in positive ion mode).

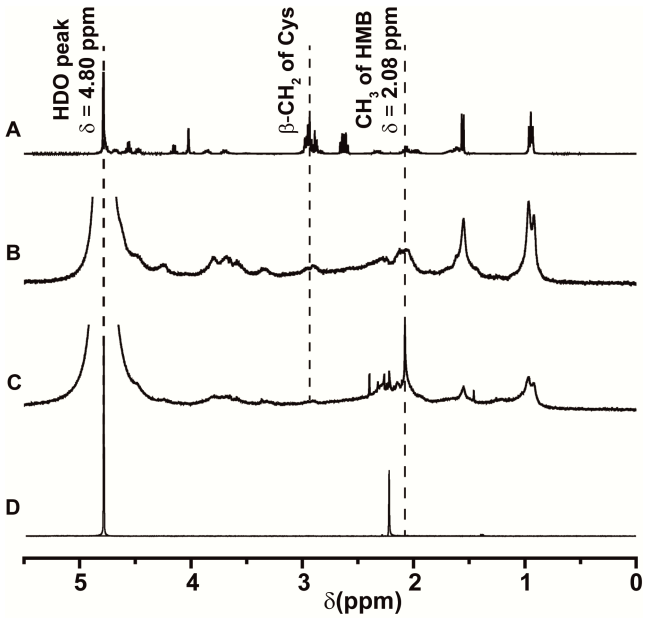

Figure 4.14. Comparative proton NMR spectra after insertion of Ni and Ru(η^6-C_6Me_6) in SODA. ^{1}H NMR spectra of (A) SODA, (B) NiSODA, (C) [NiSODA-Ru(η^6-C_6Me_6)(H_2O)](NO_3)$_2$, and (D) [Ru(η^6-C_6Me_6)(H_2O)$_3$](SO_4) in D_2O. Chemical shifts were referenced to the solvent (HDO) peak at δ=4.80 ppm.

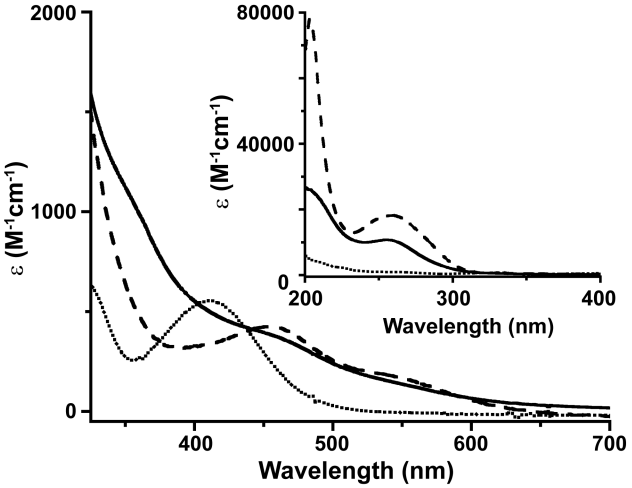

Figure 4.15. **Comparative optical spectra for NiSODA- Ru(η^6-C_6Me_6) complex.** UV-visible spectra for NiSODA (dashed line), [Ru(η^6-C_6Me_6)$(H_2O)_3$]$(NO_3)_2$ (dotted line), and [NiSODA-Ru(η^6-C_6Me_6)(H_2O)]$(NO_3)_2$ (solid line). Spectra were obtained at pH 7.5 in 50 mM NEM buffer. The inset shows the absorbance in the UV region.

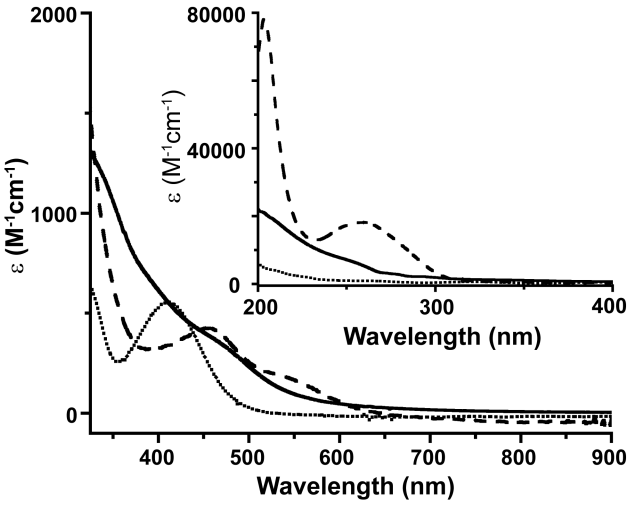

Figure 4.16. **Comparative optical spectra for NiSODA- Ru(η^6-p-cymene) complex.** UV-visible spectra for NiSODA (dashed line), [Ru(η^6-p-cymene)$(H_2O)_3$]$(NO_3)_2$ (dotted line), and [NiSODA-Ru(η^6-p-cymene)(H_2O)]$(NO_3)_2$ (solid line). Spectra were obtained at pH 7.5 in 50 mM NEM buffer. The inset shows the absorbance in the UV region.

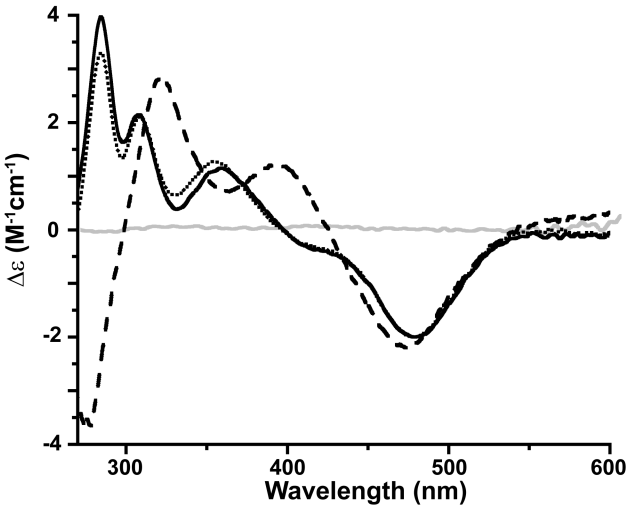

Figure 4.17. Comparative CD spectra for NiSODA Ru(arene) complexes. CD spectra from NiSODA (dashed line), NiSODA-Ru(η^6-C_6Me_6)(H_2O)](NO_3)$_2$ (solid line), and NiSODA-Ru(η^6-p-cymene)(H_2O)](NO_3)$_2$ (dots) in NEM buffer (50 mM, pH 7.5). The apopeptide solution alone is shown in grey.

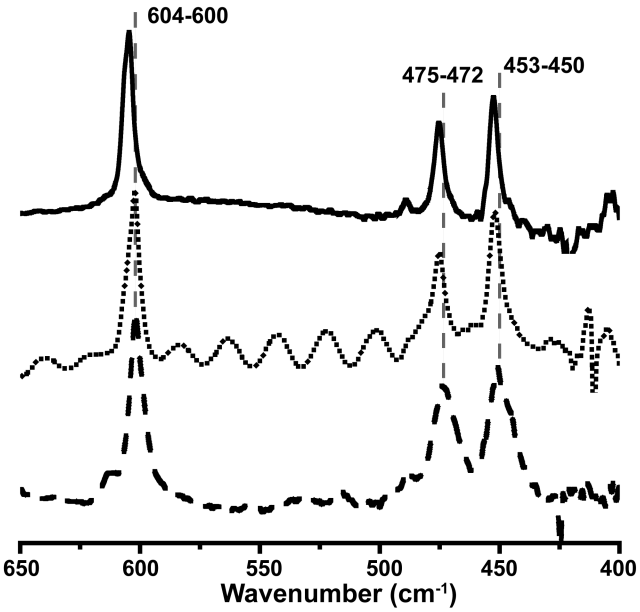

Figure 4.18. Comparative FTIR spectra for NiSODA Ru(arene) complexes. FTIR spectra from NiSODA (dashed line), [NiSODA-Ru(η^6-*p*-cymene)(H_2O)](NO_3)$_2$ (dotted line), and [NiSODA-Ru(η^6-C_6Me_6)(H_2O)](NO_3)$_2$ (solid line). All the samples were prepared as KBr pellets. Gray dashed lines highlight the shifts in peak positions to higher wavenumbers for the Ni-Ru complexes.

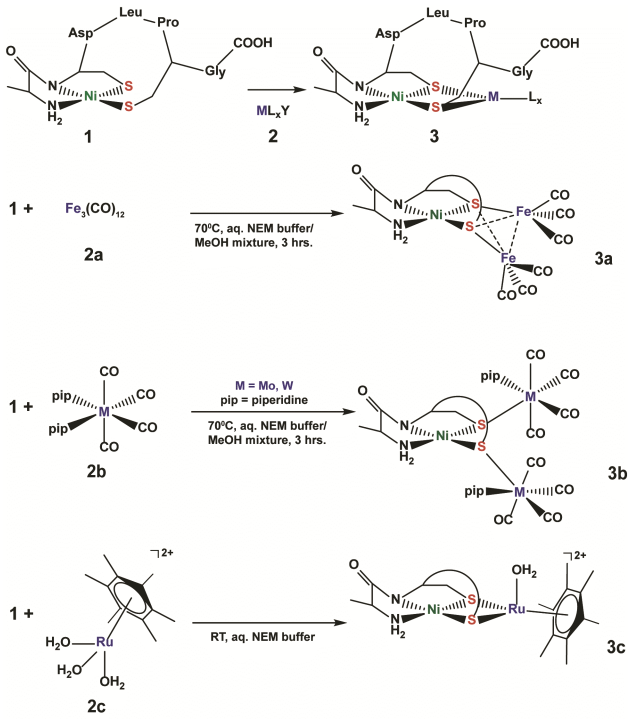

Scheme 4.1. **General synthetic strategy for heterometallic sulfur bridged metallopeptides.** The general methodology for the synthesis of heterometallic Ni-M (M=Ru, Fe_2, W, and Mo) complexes in SODA; L_x generally represents π-accepting ligands and Y represents readily exchangeable ligands.

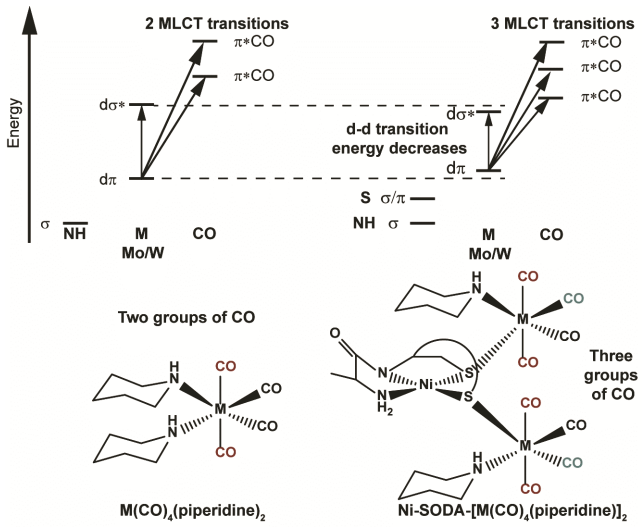

Scheme 4.2. Molecular symmetry induced changes in the optical spectra for NiSODA-$[M(CO)_4(piperidine)]_2$ (M=Mo, W). Partial molecular orbital energy diagram depicting the effect of the substitution of a single piperidine ligand from the precursor Mo or W complex by an alkyl thiolate. The structures below correspond to the diagram above.

Table 4.1 Sulfur Core Electron Binding Energies for NiSODA and NiSODA-$[Mo(CO)_4(piperidine)]_2$ derived from XPS data

Compound	Energy	
	S $2p_{3/2}$ reduced[1]	*S $2p_{3/2}$ oxidized*
NiSODA	163.0	168.0
NiSODA-$[Mo(CO)_4(piperidine)]_2$	164.0	169.3
Difference	1.0	1.3

4.5. References:

1. Cammack, R., Frey, M. & Robson, R. *Hydrogen as Fuel*. (CRC: 2002).

2. Fontecilla-Camps, J. C., Volbeda, A. & Frey, M. Hydrogen biocatalysis: a tale of two metals. *Trends Biotechnol.* **14**, 417–420 (1996).

3. Volbeda, A. *et al.* Crystal structure of the nickel-iron hydrogenase from Desulfovibrio gigas. *Nature* **373**, 580–587 (1995).

4. Ohki, Y. & Tatsumi, K. Thiolate-Bridged Iron–Nickel Models for the Active Site of [NiFe] Hydrogenase. *Eur. J. Inorg. Chem.* **2011**, 973–985 (2011).

5. Canaguier, S., Artero, V. & Fontecave, M. Modelling NiFe hydrogenases: nickel-based electrocatalysts for hydrogen production. *Dalton Trans.* 315 (2008).doi:10.1039/b713567j

6. Ogo, S. *et al.* A Dinuclear Ni({μ}-H)Ru Complex Derived from H_2. *Science* **316**, 585–587 (2007).

7. Chalbot, M.-C., Mills, A. M., Spek, A. L., Long, G. J. & Bouwman, E. Structure and Electronic Properties of [Ni(dsdm){$Fe(CO)_3$}$_2$], an Unusual, Triangular Nickel Diiron Compound. *Eur. J. Inorg. Chem.* **2003**, 453–457 (2003).

8. Hsieh, C.-H., Chupik, R. B., Brothers, S. M., Hall, M. B. & Darensbourg, M. Y. cis-Dithiolatonickel as metalloligand to dinitrosyl iron units: the di-metallic structure of Ni(μ-SR)[$Fe(NO)_2$] and an unexpected, abbreviated metalloadamantyl cluster, Ni_2(μ-SR)$_4$[$Fe(NO)_2$]$_3$. *Dalton Trans.* **40**, 6047 (2011).

9. Zhu, W. *et al.* Modulation of the electronic structure and the Ni–Fe distance in heterobimetallic models for the active site in [NiFe] hydrogenase. *Proc. Natl. Acad. Sci. USA* **102**, 18280–18285 (2005).

10. Li, Z., Ohki, Y. & Tatsumi, K. Dithiolato-Bridged Dinuclear Iron-Nickel Complexes [$Fe(CO)_2(CN)_2$(μ-$SCH_2CH_2CH_2S$)Ni(S_2CNR_2)]$^-$ Modeling the Active Site of [NiFe] Hydrogenase. *J. Am. Chem. Soc.* **127**, 8950–8951 (2005).

11. Carroll, M. E., Barton, B. E., Gray, D. L., Mack, A. E. & Rauchfuss, T. B. Active-Site Models for the Nickel–Iron Hydrogenases: Effects of Ligands on Reactivity and Catalytic Properties. *Inorg. Chem.* **50**, 9554–9563 (2011).

12. Liebgott, P.-P. *et al.* Original Design of an Oxygen-Tolerant [NiFe] Hydrogenase: Major Effect of a Valine-to-Cysteine Mutation near the Active Site. *J. Am. Chem. Soc.* **133**, 986–997 (2011).

13. McIntosh, C. L., Germer, F., Schulz, R., Appel, J. & Jones, A. K. The [NiFe]-Hydrogenase of the Cyanobacterium Synechocystis sp. PCC 6803 Works Bidirectionally with a Bias to H2 Production. *J. Am. Chem. Soc.* **133**, 11308–11319 (2011).

14. Goris, T. *et al.* A unique iron-sulfur cluster is crucial for oxygen tolerance of a [NiFe]-hydrogenase. *Nat. Chem. Biol.* **7**, 310–318 (2011).

15. Iranzo, O., Chakraborty, S., Hemmingsen, L. & Pecoraro, V. L. Controlling and Fine Tuning the Physical Properties of Two Identical Metal Coordination Sites in De Novo Designed Three Stranded Coiled Coil Peptides. *J. Am. Chem. Soc.* **133**, 239–251 (2011).

16. Korendovych, I. V. *et al.* De Novo Design and Molecular Assembly of a Transmembrane Diporphyrin-Binding Protein Complex. *J. Am. Chem. Soc.* **132**, 15516–15518 (2010).

17. Shiga, D. *et al.* Creation of a Type 1 Blue Copper Site within a de Novo Coiled-Coil Protein Scaffold. *J. Am. Chem. Soc.* **132**, 18191–18198 (2010).

18. Lu, Y., Yeung, N., Sieracki, N. & Marshall, N. M. Design of functional metalloproteins. *Nature* **460**, 855–862 (2009).

19. Nanda, V. & Koder, R. L. Designing artificial enzymes by intuition and computation. *Nat. Chem.* **2**, 15–24 (2010).

20. Koder, R. L. *et al.* Design and engineering of an O2 transport protein. *Nature* **458**, 305–309 (2009).

21. Reddi, A. R., Guzman, T. R., Breece, R. M., Tierney, D. L. & Gibney, B. R. Deducing the Energetic Cost of Protein Folding in Zinc Finger Proteins Using Designed Metallopeptides. *J. Am. Chem. Soc.* **129**, 12815–12827 (2007).

22. Kennedy, M. L. & Gibney, B. R. Proton Coupling to $[4Fe\text{-}4S]^{2+/+}$ and $[4Fe\text{-}4Se]^{2+/+}$ Oxidation and Reduction in a Designed Protein. *J. Am. Chem. Soc.* **124**, 6826–6827 (2002).

23. Xie, F., Sutherland, D. E. K., Stillman, M. J. & Ogawa, M. Y. Cu(I) binding properties of a designed metalloprotein. *J. Inorg. Biochem.* **104**, 261–267 (2010).

24. Zastrow, M. L., Peacock, A. F. A., Stuckey, J. A. & Pecoraro, V. L. Hydrolytic catalysis and structural stabilization in a designed metalloprotein. *Nat. Chem.* **4**, 118–123 (2012).

25. Laplaza, C. E. & Holm, R. H. Helix−Loop−Helix Peptides as Scaffolds for the Construction of Bridged Metal Assemblies in Proteins: The Spectroscopic A-Cluster Structure in Carbon Monoxide Dehydrogenase. *J. Am. Chem. Soc.* **123**, 10255–10264 (2001).

26. Musgrave, K. B., Laplaza, C. E., Holm, R. H., Hedman, B. & Hodgson, K. O. Structural Characterization of Metallopeptides Designed as Scaffolds for the Stabilization of Nickel(II)-Fe4S4 Bridged Assemblies by X-ray Absorption Spectroscopy. *J. Am. Chem. Soc.* **124**, 3083–3092 (2002).

27. de Hatten, X., Bothe, E., Merz, K., Huc, I. & Metzler-Nolte, N. A Ferrocene–Peptide Conjugate as a Hydrogenase Model System. *Eur. J. Inorg. Chem.* **2008**, 4530–4537 (2008).

28. Fedorova, A., Chaudhari, A. & Ogawa, M. Y. Photoinduced Electron-Transfer along α-Helical and Coiled-Coil Metallopeptides. *J. Am. Chem. Soc.* **125**, 357–362 (2003).

29. Green, K. N., Jeffery, S. P., Reibenspies, J. H. & Darensbourg, M. Y. A Nickel Tripeptide as a Metallodithiolate Ligand Anchor for Resin-Bound Organometallics. *J. Am. Chem. Soc.* **128**, 6493–6498 (2006).

30. Jones, A. K., Lichtenstein, B. R., Dutta, A., Gordon, G. & Dutton, P. L. Synthetic Hydrogenases: Incorporation of an Iron Carbonyl Thiolate into a Designed Peptide. *J. Am. Chem. Soc.* **129**, 14844–14845 (2007).

31. Roy, S., Shinde, S., Hamilton, G. A., Hartnett, H. E. & Jones, A. K. Artificial [FeFe]-Hydrogenase: On Resin Modification of an Amino Acid to Anchor a Hexacarbonyldiiron Cluster in a Peptide Framework. *Eur. J. Inorg. Chem.* **2011**, 1050–1055 (2011).

32. Apfel, U.-P. *et al.* Synthetic and Electrochemical Studies of [2Fe2S] Complexes Containing a 4-Amino-1,2-dithiolane-4-carboxylic Acid Moiety. *Eur. J. Inorg. Chem.* **2010**, 5079–5086 (2010).

33. Sano, Y., Onoda, A. & Hayashi, T. A hydrogenase model system based on the sequence of cytochrome c: photochemical hydrogen evolution in aqueous media. *Chem. Commun.* **47**, 8229 (2011).

34. Jain, A. *et al.* Incorporating Peptides in the Outer-Coordination Sphere of Bioinspired Electrocatalysts for Hydrogen Production. *Inorg. Chem.* **50**, 4073–4085 (2011).

35. Choudhury, S. B. *et al.* Examination of the Nickel Site Structure and Reaction Mechanism in Streptomyces seoulensis Superoxide Dismutase. *Biochem.* **38**, 3744–3752 (1999).

36. Wuerges, J. *et al.* Crystal structure of nickel-containing superoxide dismutase reveals another type of active site. *Proc. Natl. Acad. Sci. USA* **101**, 8569–8574 (2004).

37. Barondeau, D. P., Kassmann, C. J., Bruns, C. K., Tainer, J. A. & Getzoff, E. D. Nickel Superoxide Dismutase Structure and Mechanism. *Biochem.* **43**, 8038–8047 (2004).

38. Neupane, K. P., Gearty, K., Francis, A. & Shearer, J. Probing Variable Axial Ligation in Nickel Superoxide Dismutase Utilizing Metallopeptide-Based Models: Insight into the Superoxide Disproportionation Mechanism. *J. Am. Chem. Soc.* **129**, 14605–14618 (2007).

39. Stebler-Röthlisberger, M. & Ludi, A. Preparative chemistry with $[Ru(\eta^6\text{-arene})(H_2O)_3]^{2+}$: bis-arene and monobenzene complexes with O, N and S donors. *Polyhedron* **5**, 1217–1221 (1986).

40. Jahncke, M., Meister, G., Rheinwald, G., Stoeckli-Evans, H. & Süss-Fink, G. Dinuclear (Arene)ruthenium Hydrido Complexes: Synthesis, Structure, and Fluxionality of $(C_6Me_6)_2Ru_2H_3(BH_4)$. *Organometallics* **16**, 1137–1143 (1997).

41. Wang, Q. *et al.* The Synthesis and Electronic Structure of a Novel $[Ni'S_4'Fe_2(CO)_6]$ Radical Cluster: Implications for the Active Site of the [NiFe] Hydrogenases. *Chem. Eur. J.* **10**, 3384–3396 (2004).

42. Perra, A. *et al.* Electrocatalytic production of hydrogen by a synthetic model of [NiFe] hydrogenases. *Chem. Commun.* 1103–1105 (2006).

43. Works, C. F. Synthesis, Purification, and Characterization of a μ-(1,3-propanedithiolato)-hexacarbonyldiiron. Laboratory Experiment or Mini-Project for Inorganic Chemistry or Integrated Laboratory. *J. Chem. Educ.* **84**, 836 (2007).

44. Neupane, K. P. & Shearer, J. The Influence of Amine/Amide versus Bisamide Coordination in Nickel Superoxide Dismutase. *Inorg. Chem.* **45**, 10552–10566 (2006).

45. Rampersad, M. V. *et al.* Characterization of Steric and Electronic Properties of NiN_2S_2 Complexes as S-Donor Metallodithiolate Ligands. *J. Am. Chem. Soc.* **127**, 17323–17334 (2005).

46. Best, S. A. *et al.* X-ray photoelectron spectra of inorganic molecules. 18. Observations on sulfur 2p binding energies in transition metal complexes of sulfur-containing ligands. *Inorg. Chem.* **16**, 1976–1979 (1977).

47. Srinivasan, V., Stiefel, E. I., Elsberry, A. & Walton, R. A. X-ray photoelectron spectra of inorganic molecules. 21. Sulfur 2p chemical shifts associated with the binding of thiol and thioether groups of transition metal ions. *J. Am. Chem. Soc.* **101**, 2611–2614 (1979).

48. Ainscough, E. W., Brodie, A. M., Larsen, N. G. & Stevens, M. R. Sulphur ligand metal complexes. Part 10 [1]. Sulphur-nitrogen donor ligand complexes of the group 6 metal carbonyls. *Inorg. Chim. Acta* **50**, 215–220 (1981).

49. Asali, K. J., El-Khateeb, M. & Musa, M. M. Bimetallic Complexes with Bridging Dithiaalkane Ligands: Preparation and Kinetic Study. *J. Coord. Chem.* **55**, 1199–1207 (2002).

50. Asali, K. J., El-Khateeb, M. & Salhab, R. Bimetallic group 6 metal tetracarbonyls doubly bridged by bisphosphine and/or dithiaalkane ligands. *Transition Met. Chem.* **28**, 544–547 (2003).

51. El-khateeb, M., Asali, KJ & Musa, M. M. Dinuclear group VIB metal carbonyl complexes bridged by bis(diphenylphosphino)alkanes. *Transition Met. Chem.* **27**, 163–165 (2002).

52. Goff, S. E. J., Nolan, T. F., George, M. W. & Poliakoff, M. Chemistry of Reactive Organometallic Compounds at Low Temperatures and High Pressures: Reactions of $M(CO)_6$ (M = Cr, Mo, W), $(\eta^6\text{-}C_6H_3Me_3)M(CO)_3$ (M = Cr and Mo), and $W(CO)_5CS$ with H_2 and N_2 in Polyethylene Matrices. *Organometallics* **17**, 2730–2737 (1998).

53. Darensbourg, D. J., Burch, R. R. & Darensbourg, M. Y. Preparation of a stereospecifically carbon-13 monoxide-labeled $[(\mu\text{-}H)[Mo(CO)_5]_2]^-$ species and analysis of its carbonyl stretching vibrational modes. *Inorg. Chem.* **17**, 2677–2680 (1978).

54. Kincaid, J. R. & Nakamoto, K. Vibrational spectra and normal coordinate analysis of bis(glycino) complexes with Ni(II), Cu(II) and Co(II). *Spectrochim. Acta, Part A* **32**, 277–283 (1976).

55. Condrate, R. A. & Nakamoto, K. Infrared Spectra and Normal Coordinate Analysis of Metal Glycino Complexes. *J. Chem. Phys.* **42**, 2590–2598 (1965).

56. Jeffery, S. P., Singleton, M. L., Reibenspies, J. H. & Darensbourg, M. Y. Control of S-Based Aggregation: Designed Synthesis of NiM2 and Ni2M Trinuclear Complexes. *Inorg. Chem.* **46**, 179–185 (2007).

57. Weber, W. & Ford, P. C. Photosubstitution reactions of the ruthenium(II) arene complexes $Ru(\eta^6\text{-arene})L_3^{2+}$ (L = ammonia or water) in aqueous solution. *Inorg. Chem.* **25**, 1088–1092 (1986).

58. Böck, A., King, P. W., Blokesch, M. & Posewitz, M. C. Maturation of Hydrogenases. *Advances in Microbial Physiology* **51**, 1–71 (2006).

59. Doukov, T. I., Iverson, T. M., Seravalli, J., Ragsdale, S. W. & Drennan, C. L. A Ni-Fe-Cu Center in a Bifunctional Carbon Monoxide Dehydrogenase/ Acetyl-CoA Synthase. *Science* **298**, 567–572 (2002).

60. Darnault, C. *et al.* Ni-Zn-[Fe4-S4] and Ni-Ni-[Fe4-S4] clusters in closed and open α subunits of acetyl-CoA synthase/carbon monoxide dehydrogenase. *Nat. Struct. Mol. Biol.* **10**, 271–279 (2003).

61. Svetlitchnyi, V. *et al.* A functional Ni-Ni-[4Fe-4S] cluster in the monomeric acetyl-CoA synthase from Carboxydothermus hydrogenoformans. *Proc. Natl. Acad. Sci. USA* **101**, 446–451 (2004).

62. Rees, D. C. Great Metalloclusters in Enzymology. *Ann. Rev. Biochem.* **71**, 221–246 (2002).

63. Howard, J. B. & Rees, D. C. How many metals does it take to fix N_2? A mechanistic overview of biological nitrogen fixation. *Proc. Natl. Acad. Sci. USA* **103**, 17088–17093 (2006).

64. Zouni, A. *et al.* Crystal structure of photosystem II from Synechococcus elongatus at 3.8 Å resolution. *Nature* **409**, 739–743 (2001).

65. Umena, Y., Kawakami, K., Shen, J.-R. & Kamiya, N. Crystal structure of oxygen-evolving photosystem II at a resolution of 1.9 Å. *Nature* **473**, 55–60 (2011).

66. Gale, E. M., Cowart, D. M., Scott, R. A. & Harrop, T. C. Dipeptide-Based Models of Nickel Superoxide Dismutase: Solvent Effects Highlight a Critical Role to Ni–S Bonding and Active Site Stabilization. *Inorg. Chem.* **50**, 10460–10471 (2011).

67. Drennan, C. L., Doukov, T. I. & Ragsdale, S. W. The metalloclusters of carbon monoxide dehydrogenase/acetyl-CoA synthase: a story in pictures. *J. Biol. Inorg. Chem.* **9**, 511–515 (2004).

Chapter 5

Photophysical properties of sulfur bridged [NiRu(bpy)$_2$] dyads: comparison of small molecule and peptide coordinated complexes

*Arnab Dutta[†§], Gerdenis Kodis[†§], Thomas Groy[†], Souvik Roy[†§], Jennifer C. Schmitt[‡], Jason Shearer[‡], Anne K. Jones[†§]**

[†]Department of Chemistry and Biochemistry, [§]Center for Bio-Inspired Solar Fuel Production, [∞] School of Earth and Space Exploration; Arizona State University, Tempe, AZ 85287

[‡]Department of Chemistry, University of Nevada, Reno, Nevada 89557

5.0. Abstract

Ruthenium (II) bis(bipyridyl) complexes are widely used as photosensitizers in artificial photosynthetic applications, and many biological metallocenters rely on bridging sulfur ligands to conjoin disparate parts. In this chapter, I combine these two ideas by synthesizing sulfur bridged NiRu complexes consisting of a $Ni(N_2S_2)$ unit connected to a $Ru(bpy)_2$ photosensitizer. Three new complexes are described. Two of them utilize a small organic ligand in the $Ni(N_2S_2)$ complex and are distinguished only by different Ni:Ru ratios of 1:1 and 2:1. The third uses the metallopeptide NiSODA as starting material. All three complexes share similar spectroscopy. Features typical of $Ru(bpy)_2(L)_2$ complexes are observed as well as new transitions that can be attributed to the sulfur ligands. Steady state and time resolved spectroscopies are used to characterize the excited stated process leading to photoemission. Notably, the emission quantum yield of the peptide complex (4×10^{-3}) is nearly an order of magnitude better than the other complexes although the energies of the excited states are relatively similar. It is likely that this phenomenon is a result of the increased rigidity of the peptide; this suggests designed peptides may offer unique opportunities for developing novel photochemical systems.

5.1 Introduction:

Since the first report of their synthesis in 1955,[1] ruthenium (II) bis(bipyridl) complexes have been explored for a range of applications including use as therapeutic medicinal agents, oxidation catalysts, and for solar energy conversion.[2–7] In parallel, as shown in **Figure 5.1**, significant research has been undertaken to develop artificial photosensitized catalytic systems that absorb solar energy to produce a charge-separated state capable of performing catalysis.[8,9] Polypyridyl coordinated metal complexes are popular choices as photosensitizers in these systems due to their strong absorbance in the visible region and stable photo-excited states.[10,11]

Although photo-excited mononuclear polypyridyl metallocomplexes can catalyze some redox reactions, multielectron transformations typically require them to be combined with another metallic system. Two different types of heterometallic systems are possible: intermolecular and intramolecular.[12] The former consist of a mixture of photosensitizer and catalysts in solution. Electronic communication between the two components occurs either via discrete redox mediators in the solution or solvent. Various combinations of polypyridyl photosensitizers utilizing Ru, Os, Ir, and Pt together with catalysts such as Rh, Co, Fe, and Ni complexes as well as nanoparticles have been investigated,[13–20] but covalent connection of the two parts in an intramolecular system has facilitated more efficient photo-driven electron transfer and catalysis while suppressing non-productive relaxation of the Ru-polypyridyl ^{3}MLCT excited state.[12,21] Of

particular note, the covalent combination of a binuclear manganese complex intended as a mimic of the natural oxygen-evolving complex from photosynthesis together with a Ru-terpyridine photosensitizer created a system capable of photooxidation of water to O_2.[22]

Living organisms catalyze many difficult multi-electron redox transformations such as nitrogen or carbon dioxide reduction under relatively mild conditions, using earth abundant materials, and with high selectivity. Protein engineering or *de novo* design of bio-inspired catalysts may offer avenues to produce robust industrial catalysts with similar advantages. As both a tool for studying electron transfer in proteins and a means to create photo-catalytic systems, a number of studies have demonstrated functional intermolecular connections between Ru-polypyridyl complexes and natural or designed redox active metalloproteins.[23–28] Nonetheless, although many natural heteronuclear metalloclusters exist in biology, there are no reported examples of artificial heteronuclear clusters including both a protein or peptide ligand and an Ru-polypyridyl complex. As shown in **Figure 5.2**, many of the heteronuclear metalloclusters in biology responsible for catalyzing concerted multielectron redox reactions possess bridging sulfur ligands such as inorganic sulfide or peptidic cysteine or methionine.[29–32] Similarly, sulfur ligands can often serve as reactive sites in inorganic or organometallic compounds to facilitate formation of higher nuclearity complexes,[33–35] and the research groups of Meyer and Stiefel have pioneered the synthesis of *cis*-$Ru(bpy)_2(S')_2$ complexes in which S′ is a sulfur ligand such as a thiolate, thioether, or sulfide.[36,37]

In this work, we explore the impact on the photochemical properties of $Ru(bpy)_2$ of bridging via thiolate sulfur to a second nickel center. We have synthesized three new NiRu complexes. Each consists of a $Ni-N_2S_2$ fragment bridged via thiolate sulfur to the $Ru(bpy)_2$ unit. In the first two, the nickel is coordinated via a small organic ligand. In the third, we take advantage of previous work in which we showed that the cysteine ligands of the artificial metallopeptide Ni-SODA (ACDLPCG) can serve as reactive sites to bridge to heterometallic fragment to created a peptide coordinate $NiRu(bpy)_2$ complex.[38] The photophysical properties of all three complexes are characterized, and the impact of the peptide on the photochemistry is considered.

5.2. Experimental Section:

Inorganic syntheses were performed under a nitrogen atmosphere using a double-manifold Schlenk vacuum line. Unless otherwise specified, all the chemicals and solvents, of highest available grades, were obtained from Sigma-Aldrich (Milwaukee, WI) and were used as received. Aqueous solutions were prepared using purified water (resistivity 18.2 MΩ cm).

Physical Measurements

Steady-state absorbance measurements were executed on a Hewlett-Packard 8453 spectrophotometer using quartz cuvettes with a 1 cm pathlength. Circular dichroism (CD) spectroscopy was performed on Jasco-815 spectropolarimeter using a rectangular quartz cell with a pathlength of 0.1 cm. Steady state Fluorescence

spectra were measured in a 1 cm quartz cuvette (Hellma QC) using a QuantaMaster 40 spectrofluorometer (Photon Technology International) with a 2.0 mm slit width (0.5 mm slitwidth was used for the reference $Ru(bpy)_3(PF_6)_2$ sample). Corrected emission spectra were measured from 500 to 750 nm, followed by aqueous buffer or acetonitrile background subtraction. FTIR (Fourier transformed infrared) spectra of the samples were recorded as KBr pellets either utilizing a Thermo Nicolet Avatar-360 spectrometer or Bruker Vertex 70 FTIR spectrometer. A KBr pellet without any sample added was used as a reference. For the samples, each spectrum is an average of 512 scans at 1 cm^{-1} resolution. NMR spectra were recorded at 400 MHz (^1H) using Varian Liquid-State NMR instruments in CD_3CN solutions (99.8%, Cambridge Isotopes Laboratories Inc.) or in D_2O (99.9%, Cambridge Isotopes Laboratories Inc.) unless otherwise noted. MALDI-MS (matrix assisted laser desorption ionization mass spectrometry) characterization of peptides and metallopeptide samples was performed on a Voyager DE STR instrument. Isotope Pattern Calculator v4.0 developed by Junhua Yan was used for the calculation of the molecular mass with isotopic abundances.

***X-Ray Crystallography*:** Crystals were mounted on the end of a thin glass fiber using Apiezon type N grease and optically centered. Cell parameter measurements and single-crystal diffraction data collection were obtained at low temperature (123 K) with a Bruker Smart APEX diffractometer using graphite monochromated Mo Kα radiation (λ = 0.71073 Å) in the ω–φ scanning mode. Structures were solved by direct methods and refined by full-matrix least-squares on F^2. Disorder of the aliphatic ring portions of the Ni-bearing ligand is present in

both **2** and **3** (please see discussion in results). The following is the list of the programs used: data collection, Bruker Instrument Service v2010.9.0.0; cell refinement and data reduction, Bruker SAINT V7.68A; structure solution and refinement, SHELXS-97; molecular graphics, Bruker XShell v6.3.1; preparation of material for publication, Bruker APEX2 v2010.9-1.[39–42] Details of crystal data and parameters for data collection and refinement are listed in **Table 5.1**.

Time-Resolved Emission: Fluorescence decay kinetics were measured using the time-correlated single-photon counting (TCSPC) technique. The excitation source was a titanium sapphire (Ti:S) laser (Spectra-Physics, Millennia pumped Tsunami) with a 130 fs pulse duration operated at 82 MHz. The laser output was sent through a frequency doubler and pulse selector (Spectra Physics, Model 3980) to obtain 400 nm excitation pulses at a 4 MHz repetition rate. Fluorescence emission was collected at 90° and detected using a double-grating monochromator (Jobin-Yvon, Gemini-180) and a microchannel plate photomultiplier tube (Hamamatsu R3809U-50). The polarization of the emission was 54.7° relative to that of the excitation. Data acquisition was done using a single photon counting card (Becker-Hickl, SPC-830). The instrument response function (IRF) had a FWHM of ~45 ps, measured from the scattering of sample at the excitation wavelength. The data was globally fitted as sum of exponential decays including IRF deconvolution using locally written software (ASUFIT) developed in a MATLAB environment (Mathworks Inc.).

Time-Resolved Absorption: Femtosecond to nanosecond transient absorption measurements were acquired with a kHz pulsed laser source and a pump-probe

optical setup. Laser pulses of 100 fs at 800 nm were generated from an amplified, mode-locked titanium sapphire kHz laser system (Millennia/Tsunami/Spitfire, Spectra Physics). Part of the laser pulse energy was sent through an optical delay line and focused on a 2 mm sapphire plate to generate a white light continuum to serve as the probe beam. The remainder of the pulse energy was used to pump an optical parametric amplifier (Spectra Physics) to generate excitation pulses at different wavelengths, which were modulated using a mechanical chopper. The excitation intensity was adjusted using a continuously variable neutral density filter. The probe beam was sent through a monochromator (SP150, Action Res. Corp.) and recorded by a diode detector (Model 2032, New Focus Inc.) and box car (SR250, Stanford Research Systems). The IRF was *ca.* 200 fs.

Transient absorption data analysis was also carried out using ASUFIT. In brief, decay-associated spectra were obtained by fitting the transient absorption kinetic traces over a selected wavelength region simultaneously as described by Equation 1 (parallel kinetic model),

$$\Delta A(\lambda,t) = \sum_{i=1}^{n} A_i(\lambda)\exp(-t/\tau_i) \qquad (1)$$

where $\Delta A(\lambda,t)$ is the observed absorption change at a given wavelength at time delay t and n is the number of kinetic components used in the fitting. A plot of $A_i(\lambda)$ versus wavelength is called a decay-associated spectrum (DAS) and represents the amplitude spectrum of the i^{th} kinetic component, which has a lifetime of τ_i. The global analysis procedures described here have been extensively reviewed. Random errors associated with the reported lifetimes obtained from fluorescence and transient absorption measurements are typically ≤ 5%.

Peptide synthesis and purification

The seven amino acid peptide SODA (ACDLPCG) was synthesized, purified via HPLC, and analyzed by MALDI-MS and analytical HPLC as described in the peptide synthesis and purification section in ***Chapter 2***.

Metallocomplex and metallopeptide synthesis

The complexes N,N'-dimethyl-N,N'-bis(2-mercaptoethyl)-1, 3-propanediaminenickel (II) (Ni-N_2S_2)[43], *cis*-Ru(bpy)$_2$Cl$_2$[44], tris-(2,2'-bipyridine)ruthenium (II) hexafluorophosphate [Ru(bpy)$_3$(PF_6)$_2$] [45] and the nickel bound SODA (ACDLPCG) peptide (Ni-SODA) were prepared and characterized by UV-vis spectroscopy and mass spectrometry as described in published procedures.[46]

***cis*-diaquabis-(2,2'-bipyridine)ruthenium (II) nitrate [*cis*-Ru(bpy)$_2$(OH_2)$_2$(NO_3)$_2$] complex (1):** *cis*-Ru(bpy)$_2$(OH_2)$_2$(NO_3)$_2$ was prepared via a modification of the method reported by Fukuzumi *et al.*[47] *cis*-Ru(bpy)$_2$Cl$_2$ (97.0 mg, 0.2 mmol) and $AgNO_3$ (68.0 mg, 0.2 mmol) were stirred in the dark in a 1:1 water/acetone mixture (~20 mL) for two hours with occasional 5 minute sonication intervals. The resultant mixture was centrifuged to separate the AgCl precipitate. The red supernatant was evaporated under reduced pressure to 5mL followed by lyophilization to produce a red powder. Yield: 95.0 mg (83%). λ_{max} nm (ε / $M^{-1}cm^{-1}$) (in water): 484 (8,212), 341 (6,364), 290 (55,000), 243 (19,400), 255 (shoulder).

μ-thiolato-[N,N'-dimethyl-N,N'-bis(2-mercaptoethyl)-1,3-propanediaminenickel(II)][*cis*-acetonitrilebis-(2,2'-bipyridine)ruthenium(II)]

hexafluorophosphate [(Ni-N_2S_2) (μ-S)*cis*-Ru(bpy)$_2$(CH_3CN)(PF_6)$_2$] / NiRu 1:1 complex (2): The NiRu 1:1 complex **2** was prepared via modification of a procedure reported by Yoshimura *et al.*[48] **1** (115.0 mg, 0.2 mmole) and Ni-N_2S_2 (56.0 mg, 0.2 mmole) were dissolved separately in nitrogen-saturated water. The Ni complex solution was added dropwise to the solution of **1** and stirred at room temperature overnight in the dark. A saturated KPF_6 aqueous solution was added to the resulting red solution to precipitate **2**. The precipitate was washed with water and dried under a vacuum. Yield: 132.0 mg (64%). λ_{max} nm (ε $M^{-1}cm^{-1}$) (in acetonitrile): 535 (shoulder), 440 (7,625), 346 (shoulder), 290 (52,000), 243 (35,600), 255 (shoulder). MALDI-MS: $[M\text{-}PF_6^- + 2O]^+$: 867.72 (experimental), 867.45 (calculated). (The molecular ion loses one PF_6^- counter ion and binds 2O atoms during ionization to produce an overall charge of +1)

μ,μ″-dithiolato-bis[N,N'-dimethyl-N,N'-bis(2-mercaptoethyl)-1,3-propanediaminenickel(II)][*cis*-acetonitrilebis-(2,2'-bipyridine)ruthenium(II)] hexafluorophosphate [(Ni-N_2S_2)$_2$ (μ,μ″-S)(*cis*-Ru(bpy)$_2$(PF_6)$_2$] / NiRu 2:1 complex (3): The NiRu 2:1 complex **3** was synthesized in a process similar to that used for **2**. The only difference was the stoichiometry of the reaction. Two equivalents of Ni-N_2S_2 were reacted with one equivalent of **1**. Yield: 124.0 mg (49%). λ_{max} nm (ε $M^{-1}cm^{-1}$) (in acetonitrile): 535(4,700), 444 (7,215), 346 (shoulder), 290 (52,000), 246 (46,000), 255 (shoulder). MALDI-MS: $[M\text{-}PF_6^- \text{-} Ni^{2+} + 2Na^+]^+$: 1100.31(experimental), 1100.08 (calculated). The molecular ion loses one of each PF_6^- and Ni^{2+} ion while adding two Na^+ ions. The net charge is +1.

Brownish red colored single crystals of both complexes **2** and **3**, suitable for X-ray diffraction analysis, were grown by the slow diffusion of di-ethyl ether into their respective concentrated acetonitrile solutions.

μ-thiolato-[Ni(II)-SODA][*cis*-aquobis-(2,2'-bipyridine)ruthenium(II)] nitrate [(Ni-SODA) (μ-S)*cis*-Ru(bpy)$_2$(H_2O)(NO_3)$_2$] complex (4): 1 mL of 1.3 mM (1.3 μmole) NiSODA (50 mM NEM (N-ethyl morpholine) buffer (pH=7.5)) was added slowly to 430 μL of a 3 mM (1.3 μmole) aqueous solution of **1**. The resultant solution was stirred in the dark overnight. The mixture was purified via analytical HPLC. (Flow gradient 0-100% acetonitrile in water in 100 minutes, Flow rate = 0.5 ml/min) R_t = 32.0 min (analytical). λ_{max} nm (ε $M^{-1}cm^{-1}$) (in water): 600 (shoulder), 490 (6,975), 444 (shoulder), 346 (7,560), 290 (50,000), 243 (36,700), 255 (shoulder). MALDI-MS: $[M\text{-solvent-}H^+\text{-}2NO_3^-]^+$: 1146.55 (experimental), 1146.45 (calculated). The solvent molecule, one proton, and the two NO_3^- counter anions are excluded from the molecular ion to produce an overall charge of +1.

5.3. Results

X-ray crystal structures: The sulfur-bridged heterobimetallic NiRu complexes μ-thiolato-[N,N'-dimethyl-N,N'-bis(2-mercaptoethyl)-1,3-propanediaminenickel (II)][*cis*-acetonitrilebis-(2,2'-bipyridine)ruthenium(II)] hexafluorophosphate (**2**) and μ,μ″-dithiolato-bis[N,N'-dimethyl-N,N'-bis(2-mercaptoethyl)-1,3-propanediaminenickel(II)][*cis*-acetonitrilebis-(2,2'-bipyridine)ruthenium(II)]

hexafluorophosphate (**3**) were synthesized via reactions between [*cis*-$Ru(bpy)_2(OH_2)_2(NO_3)_2$] (**1**) and N,N'-dimethyl-N,N'-bis(2-mercaptoethyl)-1, 3-propanediaminenickel (II) (Ni-N_2S_2). The stoichiometry of the starting materials was used to control the identity of the product; reaction of a 1:1 ratio of Ru and Ni precursors led to formation of **2**, and utilization of a 1:2 ratio of Ru to Ni favored formation of **3**. Both complexes could be precipitated by the addition of KPF_6 to yield reddish brown compounds. Single crystals of complexes **2** and **3** suitable for X-ray diffraction analysis were obtained by slow diffusion of diethyl ether into a saturated 1:1 acetonitrile/ methanol solution of the complex.

Figure 5.3 shows the crystal structure of **2,** and **Table 5.2** lists selected bond lengths and bond angles. The Ru of **2** is situated in an octahedral first coordination sphere consisting of four nitrogens from two distinct bpy ligands, an acetonitrile nitrogen (solvent), and a single sulfur atom that serves as the only bridge to the Ni-N_2S_2 moiety. The Ru-N(acetonitrile) and Ru-S bond distances are 2.041 Å and 2.417 Å, respectively. The latter is comparable to the Ru-S distance (2.405 Å) found in an analogous S-bridged tetranuclear Ru_2Ni_2 complex reported by Yoshimura *et al.*[48] At an aggregate level, the average Ru-N(bpy) bond distance is 2.0575 Å, a value similar to those reported for other *cis*-$Ru(bpy)_2(dithiolate)_2$ complexes.[37,48–50] However, considering the individual Ru-N(bpy) bonds, the Ru-N(bpy) bond *trans* to the thiolate is longer (2.066 Å) than the bond *trans* to the acetonitrile (2.037 Å). The stronger σ-donating propensity of the thiolate ligand compared to acetonitrile is likely responsible. The N-Ru-N bond angles for the N

atoms originating from the same bpy ligand are 78.26º and 78.97º. These values are typical for bpy and reflect the preferred bite angle of the ligand.

The geometry of the Ni is largely unchanged from that of the mononuclear starting material; the metallocenter remains in a square planar coordination environment with unchanged Ni-S and Ni-N distances. However, it is worth noting that the motions of the N_2S_2 ligand are severely restricted in the crystal. The crystal packing induces symmetry in the structure and forces a *syn*-orientation for the two methyl groups connected to the N atoms of the N_2S_2 ligand. The electron density found for the ligand was modeled with two different partially occupied conformers with different *syn*-orientations of the N-methyl groups. Each of these conformations creates a different chair conformation for the six-membered NiN_2(propylene) ring. The Ni and the two N atoms retain their original locations in these two different conformers, but the propylene ring carbons, the N methyl groups, and the C atoms next to the N in the ethylene chain of the N_2S_2 ligand shift their positions, denoted as α and β, respectively, in **Figure 5.4**.

Complex **3** XRD data reveals the presence of two molecules in the asymmetric unit. Severe disorder in the propylene ring of the N_2S_2 ligand chain in one of those molecules prevents the precise modeling of the electronic density, which results in the partially resolved structure of the asymmetric unit with only one well defined molecule. Several models with various combinations of chair conformers similar to **2** were also attempted for the disordered ligand portion of **3** but unfortunately no significant improvement in fit was obtained. The structure of the well defined molecule is shown in **Figure 5.5**. The metal connectivity of the

trimetallic complex **3** is similar to that of the bimetallic **2,** but the acetonitrile ligand is replaced by a second Ni(N_2S_2) unit. The first coordination sphere of the Ru consists of four bpy nitrogens and two thiolates, each from a different Ni unit.

Although both thiolates of **1** might be expected to be reactive centers and form bridges to heterometallic fragments, the crystal structures of **2** and **3** clearly demonstrate formation of complexes in which only a single S of a Ni-N_2S_2 unit bridges to the Ru center. There is only a single reported binuclear NiRu complex in which the metals are bridged through two thiolates.[48] Structural investigation of that complex showed that the S-Ru-S angle was noticeably acute (76.02º) and the Ni atom markedly distorted from the square plane.

In essence, formation of two *cis*- positioned Ru-S bonds in a binuclear Ni-Ru complex imposes significant geometric constraints because it requires establishment of a four membered $RuNiS_2$ metallacycle. The Ru-S-Ni bond angle of **2** is 121.29°, and severe strain on all the bond angles would be necessary to form the 90° angle required for a dithiolate structure. The presence of both methyl and propylene groups on the N_2S_2 ligand further decrease the likelihood of forming dithiolate bridged structures by restricting distortion of the Ni from the square plane of the ligand.

To explore the effect of exchanging the N_2S_2 nickel ligand for a peptide, an analogous reaction between **1** and NiSODA at a 1:1 ration of each was undertaken. The resulting compound, complex **4**, was then purified via HPLC (**Figure 5.6**). Unfortunately, crystals of this metallopeptide could not be obtained, likely due to

the inherent disorder and flexibility of the peptide itself. However, spectroscopic data presented herein suggests that **4** has a topology analogous to that of **2.**

^{1}H NMR spectroscopy: The number of distinct ^{1}H NMR signals from the aromatic protons of the bipyridine ligand of the $Ru(bpy)_x$ (x=2 or 3) moiety can be used to probe the local geometry around the Ru center in solution (**Scheme 5.1**).[51] In short, the symmetry properties of the complex determine the number of chemically inequivalent bpy proton resonances. **Figure 5.7** shows the ^{1}H NMR spectra of complexes **1-4** in the region of chemical shift from 6 to 12 ppm in which the bpy proton signals occur. The spectrum from **1** features eight distinct resonances for the sixteen bpy protons. As shown in **Scheme 5.1**, a C_2 axis bisecting the H_2O-Ru-OH_2 angle of **1** renders the bpy ligands equivalent but each of the rings on the same ligand distinguishable from the other by virtue of their position relative to the water molecules. Thus symmetry constraints also predict eight distinct chemical environments for the bpy protons of **1**. In contrast, as shown in **Figure 5.7**, the spectrum of **2** features 16 distinct bpy proton resonances since the complex has lower symmetry. The presence of an acetonitrile and a sulfur ligand *cis* to one another as shown in the crystal structure renders the bpy ligands as well as the rings within them inequivalent. This means that each proton is in a unique chemical environment. Thus the solution ^{1}H NMR spectrum of **2** is consistent with the solid state structure determined crystallographically. As shown in **Figure 5.7**, the spectrum of **3**, featuring 8 resonances, is remarkably similar to that of **1**. This is in keeping with the symmetry predicted by the X-ray structure.

Although it was not possible to obtain single crystals of **4**, the NMR spectrum includes sixteen resonances in the aromatic region. Thus we conclude that the symmetry properties of **4** are identical to those of **2**, and the metallopeptide is likely a NiRu complex. MALDI-MS analysis of the metallopeptide also yielded a peak for a NiRu parent ion of the expected composition ($[M\text{-solvent-}H^+\text{-}2NO_3^-]^+$).

One major difference between the bpy proton NMR signals of complex **2** and **4** was the extent of down-field shift. Those of **4** were shifted further down-field (~11.7 δ ppm) than **2** (~9.8 δ ppm). The presence of the peptide framework in **4** is likely playing a role as it may alter the electronic environment and solvent accessibility around the metallocenters.

Optical spectroscopy: Figure 5.8 shows steady state UV-vis absorption spectra from complexes **1**-**4** recorded in acetonitrile (**2**, **3**) or water (**1**, **4**) (concentrations of the solutions were in the range of 1×10^{-5} M to 2×10^{-5} M; quantitative data is summarized in **Table 5.3**). All the spectra exhibit bands associated with both metal to ligand charge transfer (MLCT) and ligand based transitions that are typical of ruthenium polypyridyl complexes.[21,36,37,52] The UV-vis spectrum of complex **1** in water consists of bands centered at 484, 341, 290, and 243 nm along with a shoulder at 255 nm. There are two possible explanations in the literature for the bands at 484 and 341 nm. The first explanations is that they can both be assigned as $Ru(d_\pi) \rightarrow \pi^*_{bpy}$ MLCT transitions. Because the Ru(II) center is a low spin d^6 system in the $Ru(bpy)_2$ framework and a C_2 axis in the Ru(bpy) unit splits the bipyridine π* orbitals into symmetric (χ) and anti-symmetric (ψ) orbitals,

there is a possibility of two MLCT based transitions [$d_\pi \rightarrow \pi^*(\chi)$ and $d_\pi \rightarrow \pi^*(\psi)$]: the 341 and 484 nm bands.[53–56] However, some authors have offered a second interpretation of these bands, suggesting that the 340 nm band is a metal centered (MC) transition.[21,57] The two additional UV-region bands at 290 and 243 nm can be attributed to ligand based $\pi \rightarrow \pi^*(\chi)$ and $\pi \rightarrow \pi^*(\psi)$ transitions respectively. A high energy MLCT band may account for the shoulder at 255 nm.[21,52,57]

The spectra of **2** and **3**, although similar to one another, have obvious differences from that of **1** in both the visible and UV regions. The characteristic $d_\pi \rightarrow \pi^*(\chi)$ MLCT band at 484 nm for **1** was blue-shifted to 440 nm for **2** and **3** (**Figure 5.8, Table 5.3**). This blue shift likely results from the substitution of the water ligands in **1** by the weaker π-donor ligands, thiolates or thiolate and acetonitrile, in **2** and **3**. A new lower energy band also appears for the thiolate ligated complexes around 535 nm. This band may arise from interaction between the Ru_d and S ligand orbitals as reported earlier for studies of various thiolate and sulfide bound $Ru(bpy)_2$ complexes.[36,37,58] In support of this assignment, we note that **3** has two Ru-S bonds compared to the one present in **2**, and the intensity of the 535 nm absorption for **3** is approximately double that of **2**. In the UV region, the 290 nm band remained almost unaltered with modifications in the ligand environment of the $Ru(bpy)_2$ fragment, but the 245 nm band changed markedly. Like the 535 nm band, the 245 nm band increases in intensity with increasing number of Ru-coordinated thiolates. Root *et al*. reported that Ru-thiolate

complexes can undergo $S_{\sigma}\rightarrow Ru_{d\sigma^*}$ ligand to metal charge transfer (LMCT) based transitions; such a transition can explain the feature observed at 245 nm.[36]

The spectrum of **4** could be described as a combination that of **1** together with that of **2** or **3**. The MLCT band of the peptide coordinated complex, **4**, like that of **1**, appears at 490 nm. This transition is likely red-shifted relative to the other Ni-Ru complexes because of the presence of a water as opposed to an acetonitrile ligand. New shoulders at 444 and 600 nm appear in the spectrum of **4**. By analogy to complexes **2** and **3**, these features can be attributed to the blue-shifted $d_{\pi}\rightarrow\pi^*(\chi)$ MLCT and the transition associated with Ru_d and S ligand orbitals, respectively. The presence of transitions attributable to both water and thiolate ligands in the coordination sphere of the Ru in the spectrum of **4** provide evidence complementary to the NMR data that an asymmetric Ru(II) center is present in this complex in solution.

Luminescence spectroscopy: Steady state luminescence spectra of complexes **1-4** were recorded at 298 K in deoxygenated CH_3CN solution (complex **2**, **3**) or aqueous solution (complex **1**, **4**). Samples were excited at 455 nm and emission was monitored over the range 550-750 nm. **1** exhibits an emission band centered around 616 nm which was red shifted to 622-625 nm for the sulfur bridged heterometallic complexes (**2-4**) (**Figure 5.9**, **Table 5.3**). The emission intensity was weaker for complexes **2** and **3** (in CH_3CN) than the peptide bound complex **4** in aqueous solution. To quantify these differences, the quantum yield for emission

was determined relative to an acetonitrile solution of $Ru(bpy)_3(PF_6)_2$ (Φ_{em} = 0.062) using equation (2):[59–61]

$$\Phi_{em,s} = \Phi_{em,r} (A_r/A_s)(I_s/I_r)(n_s/n_r)^2 \quad (2)$$

in which the absorbances, emission intensities and refractive indices of sample and reference are denoted as A_s, A_r, I_s, I_r, n_s and n_r, respectively. Samples were prepared such that the absorbance at 455 nm for complexes **1-4** as well as the reference complex $Ru(bpy)_3(PF_6)_2$ was 0.5. For complexes **1** and **4**, the refractive index of water (n_{water} = 1.333) was used for n_s, and for complexes **2** and **3** $n_s=n_{acetonitrile}$ = 1.346. The peptide based complex **4** has a ~10 fold higher quantum yield than complexes **2** and **3**, and the presence of the relatively rigid peptide framework may play a role (**Figure 5.9**, **Table 5.3**). To investigate the photophysical characteristics in more detail, time resolved emission measurements of the complexes were performed.

Time resolved emission spectroscopy: Time correlated single photon counting (TC-SPC) was used to probe the excited state emission properties at 620 nm following excitation at 400 nm. Complexes **2** and **3** were measured in CH_3CN whereas **1** and **4** were observed in H_2O. Nonetheless, in all cases, the emission is associated with decay of the triplet metal to ligand charge transfer (^{3}MLCT) state. As shown in **Figure 5.10**, the relaxation of **1** can be fit with a single exponential with a 43 ps lifetime (98%). The emission kinetics of complexes **2-4** also include a similar short-lived component (46-48 ps), but analysis shows the existence of additional longer lived (580 ps-7 ns) components contributing 20-30% of the total

emission. Amplitude averaged luminescence decay lifetimes can be calculated as 943, 782, and 143 ps for complexes **2**, **3**, and **4**, respectively. To further resolve the excited state properties of these complexes, ultrafast transient absorption spectroscopy was undertaken.

Ultrafast transient absorption spectroscopy: To gain a better insight into the excited state properties of these complexes, transient absorption spectra for complexes **1**-**4** were recorded following ultrafast excitation at 400 (Ru to bpy charge transfer) and 580 nm (Ru to S charge transfer). Since data were similar at both wavelengths, only results from 400 nm excitation will be discussed here (**Figure 5.11**). We first consider the data from complex **1**. Two features are immediately obvious in the spectra: a ground state bleaching at 500 nm and an induced absorption at 650 nm. The 500 nm bleaching corresponds to the MLCT based ground state absorption shown in **Figure 5.8**. Both the bleaching and the induced absorption have highest intensity at the earliest points in the experiments and decay in later traces (2, 31 and 75 ps traces). In comparison, the transient absorption spectra complexes **2-4** include similar induced absorption bands with maxima in the range 600-650 nm (**Figure 5.11**). However, spectra from complexes **2** and **3** do not contain any prominent bleaching in the 450-500 nm region. This is consistent with the fact that their corresponding ground state MLCT absorption bands are blue-shifted by ~ 50 nm relative to **1** (**Figure 5.8**). Only the peptide-bound complex **4** shows weak bleaching around 480 nm

attributable to the red-edge of its ground state absorption (**Figure 5.8, Figure 5.11**).

For each complex, transient absorption kinetics was measured at a number of fixed wavelengths, and representative data for each compound at a particular wavelength is shown in **Figure 5.12**. The entire collection of kinetic traces for each complex was globally fit to determine decay lifetimes and amplitudes (**Table 5.4**). Data for **1** could be fit with only three exponential components whereas complexes **2-4** required four components. For all complexes, faster time constants are the major contributor to the multi-exponential decays. In general, fast time constants (<15 ps) have been attributed to processes such as internal conversion (IC), ultrafast intersystem crossing (ISC) due to heavy atom effects, and vibrational cooling.[62–64] Liu *et al.* suggested that for $Ru(bpy)_2(solvent)_2$ complexes, the photo-excited ^{3}MLCT state relaxes to the ground state on a timescale of approximately 50 ps. By analogy, we hypothesize that for complexes **1-4** the photo-excited ^{1}MLCT state converts rapidly (<300 fs) to a ^{3}MLCT state that cools/relaxes within 1-15 ps and recombines to a metal centered ^{3}MC state (40-7000 ps) which in turn relaxes quickly (<40 ps) to the ground state.[62]

5.4. Discussion and conclusions:

In this project, we have exploited the reactivity of the thiolate sulfurs of a Ni-N_2S_2 moiety to create heterometallic NiRu complexes bridged to a $Ru(bpy)_2$ unit via the sulfur. By varying the stoichiometry of the Ni and Ru precursors during

the synthesis, complexes with Ni:Ru ratios of 1:1 (Complex **2**) and 2:1 (Complex **3**) were generated. To investigate the influence of a peptidic ligand on the properties of this type of metallocomplex, an analogous 1:1 complex was prepared using the metallopeptide Ni-SODA as starting material. Both steady state and time resolved spectroscopies have been utilized to characterize the photochemistry of these complexes.

Steady state UV-vis absorption spectra for these compounds show all of the transitions typically associated with $Ru(bpy)_2(L)_2$ units. In addition, a new feature is present on the red edge of the Ru→ bpy MLCT band. This band likely arises from introduction of sulfur character into the frontier molecular orbitals, and provides evidence that the thiolate ligands influence the spectroscopy of the Ru center. The steady state emission spectra for complexes **1-4** are remarkably similar to one another in terms of energy; only a slight red shift of the emission maximum was observed for the NiRu complexes relative to the Ru precursor. However, the emission quantum yields of complexes **2** and **3** are approximately an order of magnitude lower than that of **4**. Time resolved luminescence spectroscopy was undertaken characterize this difference. In all cases, rapid (<100s of ps) quenching of the photoexcited state occurred, and the dominant process for all complexes was on the 43-48 ps timescale. These findings are similar to the excited state properties of $Ru(bpy)_2(CH_3CN)_2$, and suggest that the energies of the photoexcited states have not been dramatically impacted by incorporation of the sulfur ligands.[62] As shown in **Scheme 5.2**, radiative emission of the Ru-polypyridyl complexes occurs from the excited ^{3}MLCT state.[11,21] There

are typically three processes that can lead to relaxation from the excited ^{3}MLCT state back to the ground state: radiative decay, non-radiative decay, and conversion to a ^{3}MC state followed by non-radiative decay. The weak field ligands present in all of the complexes in this study tends to favor relaxation via the ^{3}MC state, and the rate of conversion between the ^{3}MLCT and ^{3}MC states is known to be significantly influenced by the structural dynamics of the Ru-polypyridyl moiety.[65–67] The quantum yield is the ratio between the radiative processes (k_r) and the sum of all relaxation processes ($k_r+k_{nr}+k_a$). Although all three complexes in this study relax via similar mechanisms and with similar kinetics, the quantum yield of emission for **4** is an order of magnitude higher than the others. Thus we conclude that some feature of **4** decreases the probability of relaxation via non-radiative decay processes without influencing the energies of the relevant states. The most obvious difference between **4** and complexes **2** and **3** is the presence of the peptide, and we hypothesize that rigidity of the peptide relative to the smaller organic ligand of complexes **2** and **3** is the determining factor in the higher quantum yield of **4**. In short, increased ligand rigidity may lead to less accessible vibrational modes in the excited state and weaker coupling between the ^{3}MLCT state and the ^{3}MC state. The net effect would be higher occupancy of the ^{3}MLCT state and increased quantum yield.

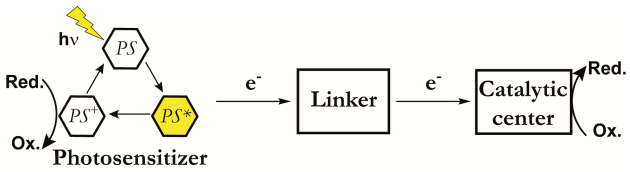

Figure 5.1. General scheme of photosensitized catalysis.

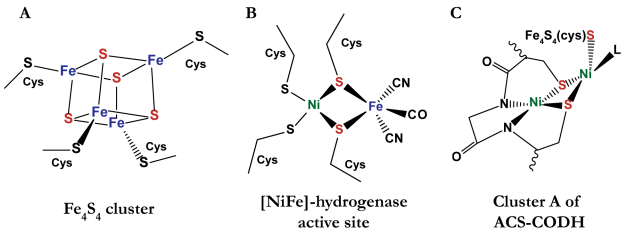

Figure 5.2. Examples of sulfur ligated metalloclusters in nature. Polymetallic clusters formed through sulfur bridging ligands found in biology: (A) Fe_4S_4 cluster, (B) [NiFe]-hydrogenase active site, and (C) Cluster A of ACS-CODH.

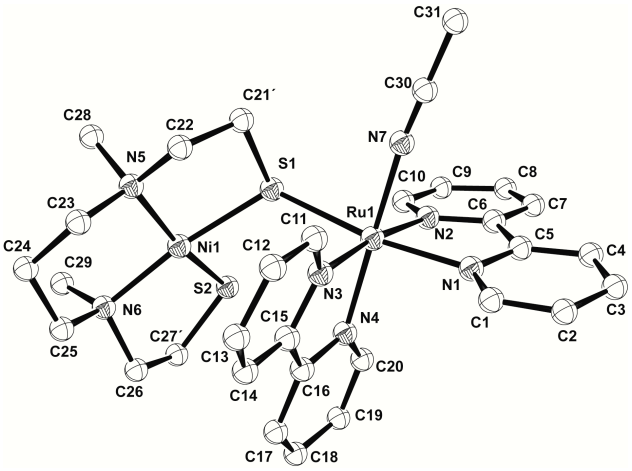

Figure 5.3. X-ray crystal structure of μ-thiolato-[N,N'-dimethyl-N,N'-bis(2-mercaptoethyl)-1,3-propanediaminenickel (II)][*cis*-acetonitrilebis-(2,2'-bipyridine)ruthenium(II)] hexafluorophosphate. Molecular structure of **2** with thermal ellipsoids drawn at 50% probability level. Hydrogen atoms have been omitted for clarity.

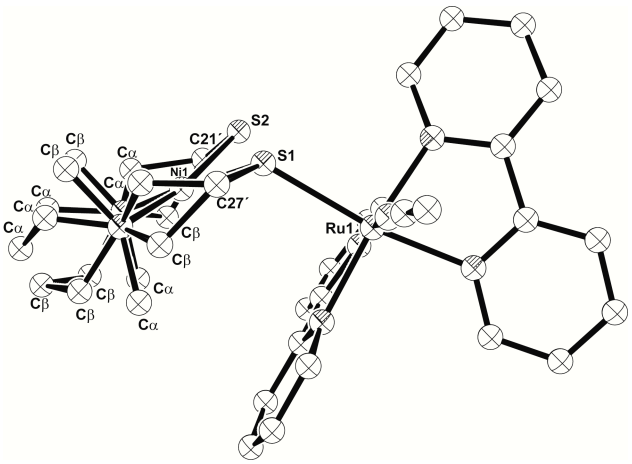

Figure 5.4. Two different conformers found for the molecular structure of μ-thiolato-[N,N'-dimethyl-N,N'-bis(2-mercaptoethyl)-1,3-propanediaminenickel (II)][*cis*-acetonitrilebis-(2,2'-bipyridine)ruthenium(II)] hexafluorophosphate . The structures are drawn with thermal ellipsoids at 50% probability level. Carbon atoms belonging to the different conformers are denoted by α and β, respectively. Hydrogen atoms have been omitted for clarity.

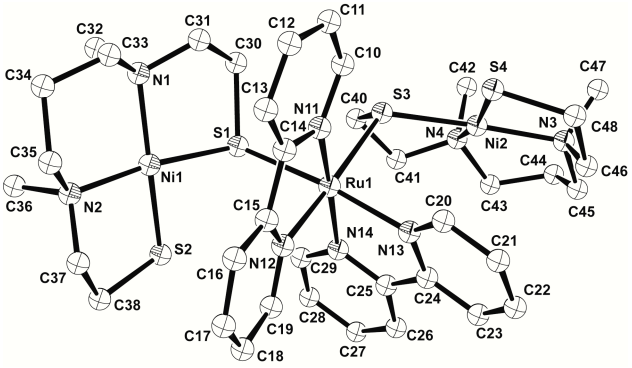

Figure 5.5. Molecular structure of μ,μ″-dithiolato-bis[N,N'-dimethyl-N,N'-bis(2-mercaptoethyl)-1,3-propanediaminenickel(II)][*cis*-acetonitrilebis-(2,2'-bipyridine)ruthenium(II)] hexafluorophosphate. Fully resolved molecular structure from the asymmetric unit of **3** with thermal ellipsoids drawn at 50% probability level. Hydrogen atoms have been omitted for clarity.

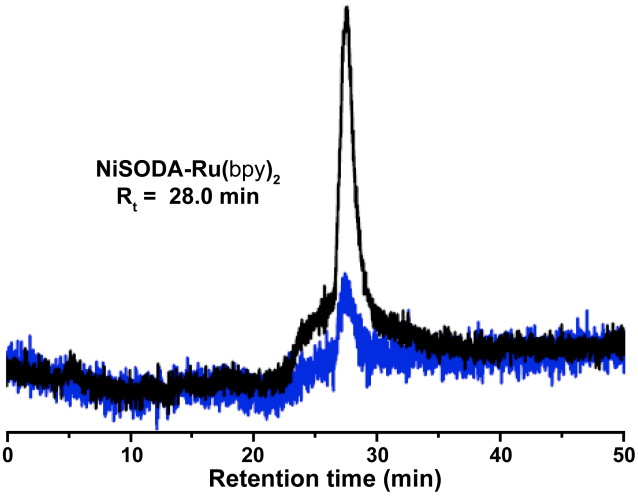

Figure 5.6. Analytical HPLC chromatogram for NiSODA-Ru(bpy)$_2$ complex. Probe wavelength during HPLC: 275 nm: black and 330 nm: blue. Experimental conditions: 0-50% neat acetonitrile in water in 50 minutes with a 1% gradient and flow rate = 0.5 mL/min.

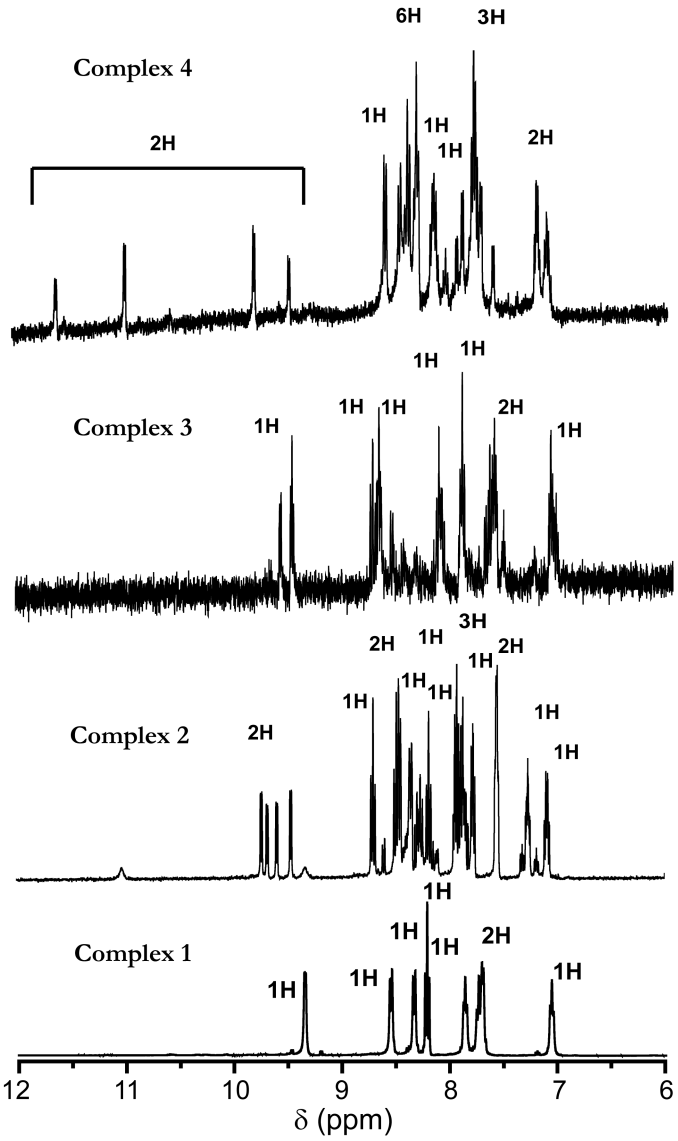

Figure 5.7. Comparative ^{1}H NMR spectra. Aromatic (bipyridine) region ^{1}H NMR spectra for complexes **1** (in D_2O), **2** (in CD_3CN), **3** (in CD_3CN), and **4** (in D_2O) at room temperature.

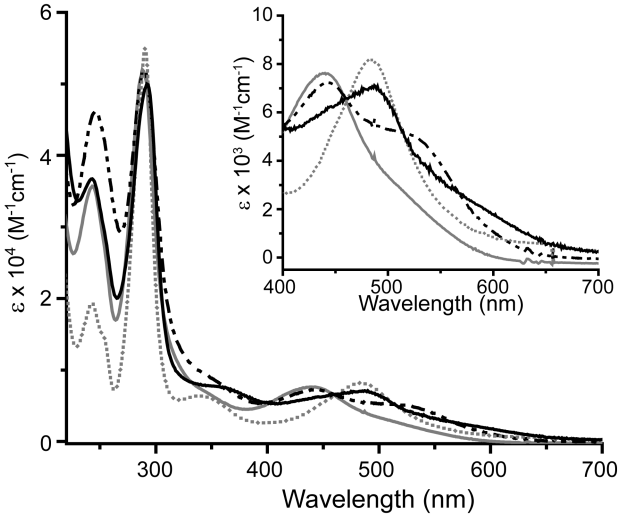

Figure 5.8. Comparative optical absorbance spectra. UV-vis absorption spectra for complexes **1** (in H_2O) (grey dotted line), **2** (in CH_3CN) (grey solid line), **3** (in CH_3CN) (black dash-dotted line), and **4** (in aqueous buffered solution, pH 7.5) (black solid line) recorded at room temperature. The inset shows the absorbances in the visible region.

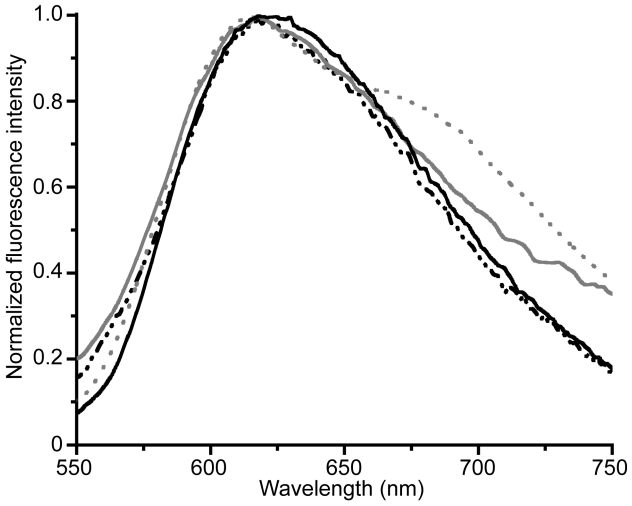

Figure 5.9. Comparative emission spectra. Steady state emission spectra for complexes **1** (grey dotted line), **2** (grey solid line), **3** (black dash-dotted line), and **4** (black solid line). Other experimental conditions are as defined in Figure 5.7.

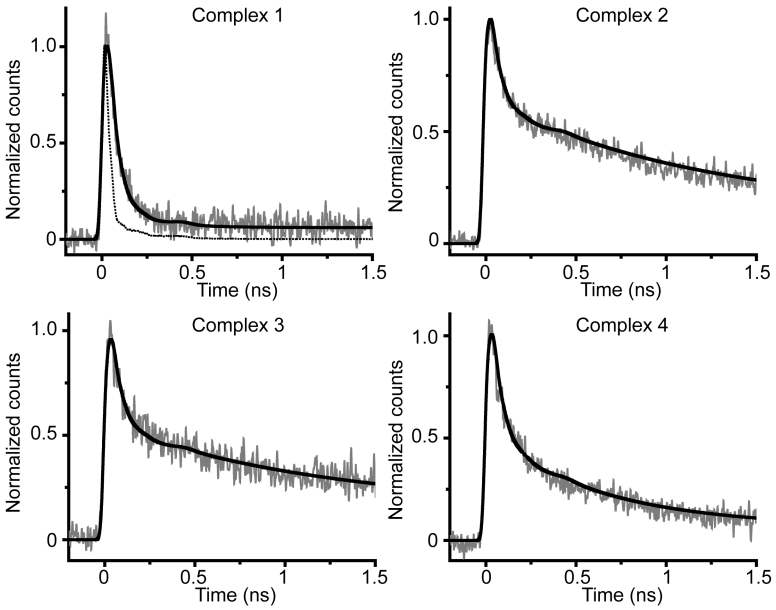

Figure 5.10. Comparative time resolved emission spectra. Time resolved emission kinetics at 620 nm with excitation at 400 nm for the complexes as indicated. All the raw data and fitted data are shown in grey and black solid lines, respectively. The IRF is shown as a dotted line in the first panel. Data from each complex was fit using the following parameters: **1**: τ=42.6 ps (96%); **2**: τ_1=48 ps (75%), τ_2=980 ps (14%), τ_3=7.09 ns (11%); **3**: τ_1=46 ps (72%), τ_2=930 ps (16%), τ_3=5.06 ns (12%); **4**: τ_1=47 ps (82%), τ_2=580 ps (18%). Other experimental conditions are as defined in Figure 5.7.

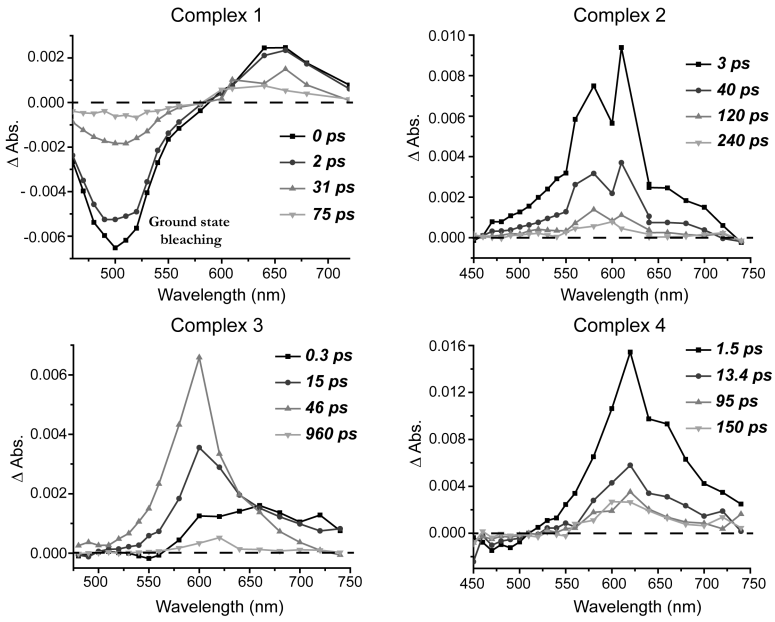

Figure 5.11. **Comparative transient absorption spectra.** Transient absorption spectra following excitation at 400 nm at various decay times for complexes **1-4** as indicated. Other experimental conditions are as defined in Figure 5.7.

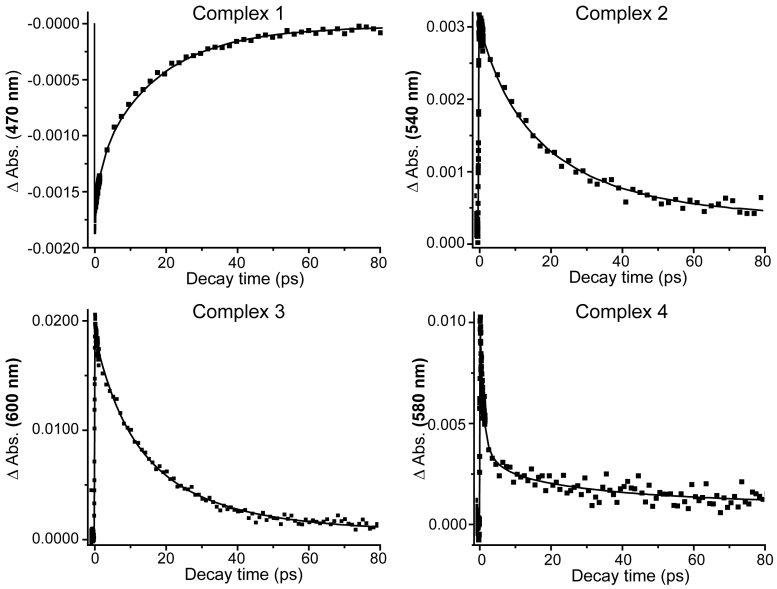

Figure 5.12. Comparative transient absorption kinetics. Transient absorption kinetics following excitation at 400 nm for complexes **1-4** as indicated. The solid lines show fits using the following parameters: **1**: τ_1=4.26 ps (24%), τ_2=34 ps (73%), τ_3=200 ps (3%); **2**: τ_1=0.74 ps (2%), τ_2=13 ps (25%); τ_3=48 ps (70%), τ_4=940 ps (4%); **3**: τ_1=0.28 ps (22%), τ_2=15 ps (30%), τ_3=46 ps (45%), τ_4=960 ps (3%); **4**: τ_1=0.72 ps (43%), τ_2=5 ps (34%), τ_3=46 ps (11%), τ_4=540 ps (12%). Other experimental conditions are as defined in Figure 5.7.

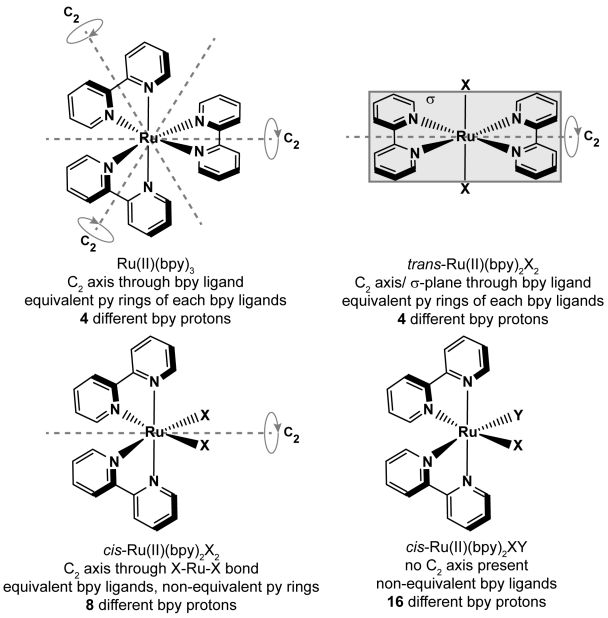

Scheme 5.1. Molecular symmetery in various $Ru(bpy)_x$ complexes (x=2 or 3).

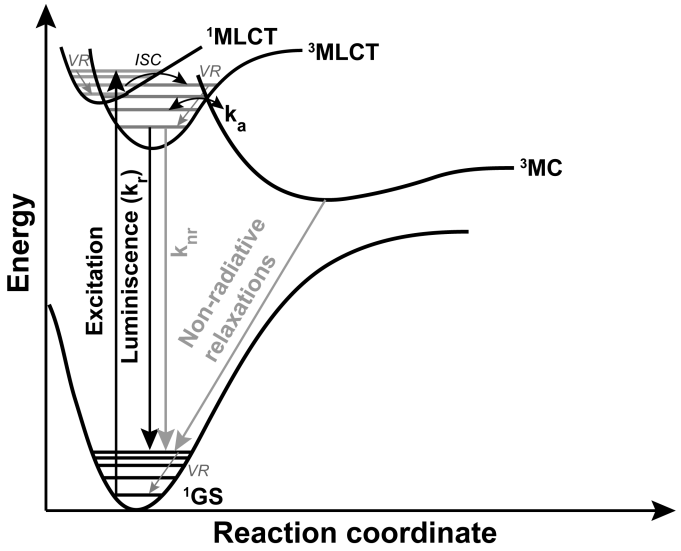

Scheme 5.2. Energy diagram of hypothetically accessible photo-physical states for $Ru(bpy)_2$ moiety in *cis*-diaquabis-(2,2'-bipyridine)ruthenium (II) nitrate and other sulfur bridged NiRu complexes.

Table 5.1. Crystallographic experimental data for NiRu 1:1 complex 2.

Parameter	2
Empirical formula	$C_{34}H_{43}F_{12}N_8ONiP_2RuS_2$
Formula weight	1093.60
Temperature (K)	123(2)
Wavelength (Å)	0.71073
Z	2
Crystal system	Triclinic
Space group (HM new)	P -1
***a* (Å)**	13.358(3)
***b* (Å)**	13.7586(17)
***c* (Å)**	14.3063(18)
α (°)	116.550(2)
β (°)	110.663(3)
γ (°)	94.183(2)
Volume (Å^3)	2115.5(6)
μ (mm^{-1})	1.070
Density (g cm^{-3})	1.717
Goodness-of-fit	1.017
R_1, wR_2 [$I > 2\sigma(I)$]	0.0405, 0.0918
R_1, wR_2 (all data)	0.0519, 0.0971

Table 5.2. Selected bond lengths (Å) and bond angles (°) for **2**.

Bond lengths			
Ru(1)-N(1)	2.066(3)	**Ru(1)-S(1)**	2.4167(10)
Ru(1)-N(2)	2.079(3)	**Ni(1)-S(1)**	2.1954(10)
Ru(1)-N(3)	2.048(3)	**Ni(1)-S(2)**	2.1644(11)
Ru(1)-N(4)	2.037(3)	**Ni(1)-N(5)**	2.005(3)
Ru(1)-N(7)	2.041(3)	**Ni(1)-N(6)**	1.993(3)
Bond angles			
N(1)-Ru(1)-N(2)	78.26(12)	**N(4)-Ru(1)-N(7)**	174.88(12)
N(3)-Ru(1)-N(4)	78.97(13)	**N(5)-Ni(1)-S(1)**	89.84(9)
N(2)-Ru(1)-N(3)	172.54(12)	**N(6)- Ni(1)-S(2)**	88.81(10)
N(1)-Ru(1)-N(7)	83.91(12)	**S(1)- Ni(1)-S(2)**	85.46(4)
N(2)-Ru(1)-N(7)	87.94(12)	**Ni(1)-S(1)-Ru(1)**	121.29(4)
N(3)-Ru(1)-N(7)	96.61(12)	**Ru(1)-N(7)-C(30)**	173.7(3)

Table 5.3. Steady-state absorption and emission spectral parameters for complexes **1-4**

Complex	Electronic absorption [λ (nm), ε (M^{-1} cm^{-1})]	Emission spectra [λ_{em} (nm)] λ_{ex} 455 nm	Quantum yield (Φ_{em}) Relative to $Ru(bpy)_3(PF_6)_2$ in CH_3CN (Φ_{em}=0.062)
1	484 (8212), 341 (6364), 290 (55000), 243 (19400), 255 (shoulder)	616	4×10^{-4}
2	535(shoulder), 440 (7625), 346 (shoulder), 290 (52000), 243 (35600), 255 (shoulder)	622	3×10^{-4}
3	535(4700), 444 (7215), 346 (shoulder), 290 (52000), 246 (46000), 255 (shoulder)	622	1×10^{-4}
4	600 (shoulder), 490 (6975), 444 (shoulder), 346 (7560), 290 (50000), 243 (36700), 255 (shoulder)	625	4×10^{-3}

Table 5.4. Time resolved absorption and emission data for complexes **1**-**4**.

Complex	Lifetimes (τ) (% contribution); emission data[a]	τ_{av}[b]	Lifetimes (τ) (% contribution), absorption data (400 nm)[c]	Lifetimes (τ) (% contribution), absorption data (580 nm)[d]
1	***42.6 ps (98%)***	***43 ps***	4.26 ps (24%) ***34 ps (73%)*** 200 ps (3%)	–
2	***48 ps (75%)*** 980 ps (14%) 7.09 ns (11%)	***943 ps***	0.74 ps (2%) 13 ps (25%) ***48 ps (70%)*** 940 ps (3%)	***1.3 ps (41%)*** 32 ps (30%) 115 ps (29%)
3	***46 ps (72%)*** 930 ps (16%) 5.06 ns (12%)	***782 ps***	0.28 ps (22%) 15 ps (30%) ***46 ps (45%)*** 960 ps (3%)	1.3 ps (22%) ***32 ps (58%)*** 115 ps (20%)
4	***47 ps (82%)*** 580 ps (18%)	***143 ps***	***0.72 ps (43%)*** 5 ps (34%) 46 ps (11%) 540 ps (12%)	0.6 ps (15%) 21 ps (32%) ***156 ps (53%)***

[a] Lifetimes obtained from multi-exponential fitting of time resolved emission data (λ_{ex} 400 nm, λ_{em} 620 nm). [b] Amplitude averaged time constant for time-resolved emission data. [c] Lifetimes obtained from the multi-exponential fitting of transient absorption data with λ_{ex} 400 nm. Probe wavelengths were as follows: **1**: 470 nm, **2**: 540 nm, **3**: 600 nm, **4**: 580 nm. [d] Lifetimes obtained from the multi-exponential fitting of transient absorption data with λ_{ex} 580 nm. Probe wavelengths were as follows: **2**: 620 nm, **3**: 620 nm, **4**: 670 nm.

5.5. References:

1. Miller, R. R., Brandt, W. W., Puke, M. & Puke, O. S. F. Metal-Amine Coördination Compounds. V. The Ruthenium-2,2'-Bipyridine System1,2,3. *J. Am. Chem. Soc.* **77**, 3178–3180 (1955).

2. Vos, J. G. & Kelly, J. M. Ruthenium polypyridyl chemistry; from basic research to applications and back again. *Dalton Trans.* 4869–4883 (2006).doi:10.1039/b606490f

3. Moucheron, C. From cisplatin to photoreactive Ru complexes: targeting DNA for biomedical applications. *New J. Chem.* **33**, 235–245 (2009).

4. Concepcion, J. J. *et al.* Making Oxygen with Ruthenium Complexes. *Acc. Chem. Res.* **42**, 1954–1965 (2009).

5. Gust, D., Moore, T. A. & Moore, A. L. Mimicking Photosynthetic Solar Energy Transduction. *Acc. Chem. Res.* **34**, 40–48 (2001).

6. Gust, D., Moore, A. L. & Moore, T. A. *Electron Transfer in Chemistry: Catalysis of electron transfer, heterogenous systems, gas-phase systems*. **3**, (Wiley-VCH: Weinheim, 2001).

7. Gust, D., Moore, T. A. & Moore, A. L. Solar Fuels via Artificial Photosynthesis. *Acc. Chem. Res.* **42**, 1890–1898 (2009).

8. Wasielewski, M. R. Photoinduced Electron-transfer in Supramolecular Systems for Artificial Photosynthesis. *Chem. Rev.* **92**, 435–461 (1992).

9. Collings, A. F. & Critchley, C. *Artificial Photosynthesis: From Basic Biology to Industrial Application*. (John Wiley & Sons: 2007).

10. Reynal, A. & Palomares, E. Ruthenium Polypyridyl Sensitisers in Dye Solar Cells Based on Mesoporous TiO_2. *Eur. J. Inorg. Chem.* **2011**, 4509–4526 (2011).

11. Campagna, S., Puntoriero, F., Nastasi, F., Bergamini, G. & Balzani, V. Photochemistry and Photophysics of Coordination Compounds: Ruthenium. *Photochemistry and Photophysics of Coordination Compounds I* **280**, 117–214 (2007).

12. Inagaki, A. & Akita, M. Visible-light promoted bimetallic catalysis. *Coord. Chem. Rev.* **254**, 1220–1239 (2010).

13. Ozawa, H., Haga, M. & Sakai, K. A Photo-Hydrogen-Evolving Molecular Device Driving Visible-Light-Induced EDTA-Reduction of Water into Molecular Hydrogen. *J. Am. Chem. Soc.* **128**, 4926–4927 (2006).

14. Rau, S. *et al.* A Supramolecular Photocatalyst for the Production of Hydrogen and the Selective Hydrogenation of Tolane. *Angew. Chem. Int. Ed.* **45**, 6215–6218 (2006).

15. Elvington, M., Brown, J., Arachchige, S. M. & Brewer, K. J. Photocatalytic hydrogen production from water employing a Ru, Rh, Ru molecular device for photoinitiated electron collection. *J. Am. Chem. Soc.* **129**, 10644–10645.(2007).

16. Fihri, A., Artero, V., Pereira, A. & Fontecave, M. Efficient H_2-producing photocatalytic systems based on cyclometalated iridium- and tricarbonylrhenium-diimine photosensitizers and cobaloxime catalysts. *Dalton Trans.* 5567 (2008).doi:10.1039/b812605b

17. Fihri, A. *et al.* Cobaloxime-Based Photocatalytic Devices for Hydrogen Production. *Angew. Chem. Int. Ed.* **47**, 564–567 (2008).

18. Craig, C. A., Spreer, L. O., Otvos, J. W. & Calvin, M. Photochemical reduction of carbon dioxide using nickel tetraazamacrocycles. *J. Phys. Chem.* **94**, 7957–7960 (1990).

19. Hori, H., Johnson, F. P. A., Koike, K., Ishitani, O. & Ibusuki, T. Efficient photocatalytic CO_2 reduction using $[Re(bpy)(CO)_3\{P(OEt)_3\}]^+$. *J. Photochem. Photobiol. A-Chem.* **96**, 171–174 (1996).

20. Koike, K. *et al.* Key process of the photocatalytic reduction of CO_2 using $[Re(4,4'\text{-X-2-bipyridine})(CO)_3PR_3]^+$ (X = CH_3, H, CF_3; PR_3 = phosphorus ligands): Dark reaction of the one-electron-reduced complexes with CO_2. *Organometallics* **16**, 5724–5729 (1997).

21. Juris, A. *et al.* Ru(II) polypyridine complexes: photophysics, photochemistry, eletrochemistry, and chemiluminescence. *Coord. Chem. Rev.* **84**, 85–277 (1988).

22. Magnuson, A. *et al.* Biomimetic and Microbial Approaches to Solar Fuel Generation. *Acc. Chem. Res.* **42**, 1899–1909 (2009).

23. Langen, R. *et al.* Electron tunneling in proteins: coupling through a beta strand. *Science* **268**, 1733–1735 (1995).

24. Mines, G. A. *et al.* Rates of heme oxidation and reduction in Ru(His33)cytochrome c at very high driving forces. *J. Am. Chem. Soc.* **118**, 1961–1965 (1996).

25. Dempsey, J. L., Winkler, J. R. & Gray, H. B. Proton-Coupled Electron Flow in Protein Redox Machines. *Chem. Rev.* **110**, 7024–7039 (2010).

26. Roth, L. E., Nguyen, J. C. & Tezcan, F. A. ATP- and Iron−Protein-Independent Activation of Nitrogenase Catalysis by Light. *J. Am. Chem. Soc.* **132**, 13672–13674 (2010).

27. Sano, Y., Onoda, A. & Hayashi, T. A hydrogenase model system based on the sequence of cytochrome c: photochemical hydrogen evolution in aqueous media. *Chem. Commun.* **47**, 8229–8231 (2011).

28. Sano, Y., Onoda, A. & Hayashi, T. Photocatalytic hydrogen evolution by a diiron hydrogenase model based on a peptide fragment of cytochrome c(556) with an attached diiron carbonyl cluster and an attached ruthenium photosensitizer. *J. Inorg. Biochem.* **108**, 159–162 (2012).

29. Volbeda, A. *et al.* Crystal structure of the nickel-iron hydrogenase from Desulfovibrio gigas. *Nature* **373**, 580–587 (1995).

30. Volbeda, A. *et al.* Structure of the [NiFe] Hydrogenase Active Site: Evidence for Biologically Uncommon Fe Ligands. *J. Am. Chem. Soc.* **118**, 12989–12996 (1996).

31. Peters, J. W., Lanzilotta, W. N., Lemon, B. J. & Seefeldt, L. C. X-ray crystal structure of the Fe-only hydrogenase (Cpl) from Clostridium pasteurianum to 1.8 angstrom resolution. *Science* **282**, 1853–1858 (1998).

32. Doukov, T. I., Iverson, T. M., Seravalli, J., Ragsdale, S. W. & Drennan, C. L. A Ni-Fe-Cu center in a bifunctional carbon monoxide dehydrogenase/acetyl-CoA synthase. *Science* **298**, 567–572 (2002).

33. Gloaguen, F. & Rauchfuss, T. B. Small molecule mimics of hydrogenases: hydrides and redox. *Chem. Soc. Rev.* **38**, 100 (2009).

34. Ohki, Y. & Tatsumi, K. Thiolate-Bridged Iron-Nickel Models for the Active Site of [NiFe] Hydrogenase. *Eur. J. Inorg. Chem.* 973–985 (2011).doi:10.1002/ejic.201001087

35. Artero, V. & Fontecave, M. Light-driven bioinspired water splitting: Recent developments in photoelectrode materials. *C. R. Chim.* **14**, 799–810 (2011).

36. Root, M. J., Sullivan, B. P., Meyer, T. J. & Deutsch, E. Thioether, thiolato, and 1,1-dithioato complexes of bis(2,2'-bipyridine)ruthenium(II) and bis(2,2'-bipyridine)osmium(II). *Coord. Chem. Rev.* **24**, 2731–2739 (1985).

37. Greaney, M. A., Coyle, C. L., Harmer, M. A., Jordan, A. & Stiefel, E. I. Synthesis and characterization of mononuclear and dinuclear bis(2,2'-bipyridine)ruthenium(II) complexes containing sulfur-donor ligands. *Inorg. Chem.* **28**, 912–920 (1989).

38. Dutta, A., Hamilton, G., A., Hartnett, H., E. & Jones, A. K.*Inorg. Chem.* (2012).

39. Bruker, XShell ver. 6.3.1, Bruker AXS Inc., Madison, Wisconsin, USA

40. Bruker, SAINT-Plus. Bruker AXS Inc., Madison, Wisconsin, USA (2009).

41. Bruker, APEX2, SADABS. Bruker AXS Inc., Madison, Wisconsin, USA. (2010).

42. Sheldrick, G. M. A short history of SHELX. *Acta Crystallogr., Sect. A: Found. Crystallogr.* **64**, 112–122 (2008).

43. Colpas, G. J., Kumar, M., Day, R. O. & Maroney, M. J. Structural investigations of nickel complexes with nitrogen and sulfur donor ligands. *Inorg. Chem.* **29**, 4779–4788 (1990).

44. Sullivan, B. P., Salmon, D. J. & Meyer, T. J. Mixed phosphine 2,2'-bipyridine complexes of ruthenium. *Inorg. Chem.* **17**, 3334–3341 (1978).

45. Browne, W. R. *et al.* Probing inter-ligand excited state interaction in homo and heteroleptic ruthenium(II) polypyridyl complexes using selective deuteriation. *Inorg. Chim. Acta* **360**, 1183–1190 (2007).

46. Neupane, K. P., Gearty, K., Francis, A. & Shearer, J. Probing Variable Axial Ligation in Nickel Superoxide Dismutase Utilizing Metallopeptide-Based Models: Insight into the Superoxide Disproportionation Mechanism. *J. Am. Chem. Soc.* **129**, 14605–14618 (2007).

47. Fukuzumi, S., Kobayashi, T. & Suenobu, T. Formic Acid Acting as an Efficient Oxygen Scavenger in Four-Electron Reduction of Oxygen Catalyzed by a Heterodinuclear Iridium−Ruthenium Complex in Water. *J. Am. Chem. Soc.* **132**, 11866–11867 (2010).

48. Yoshimura, T., Shinohara, A., Hirotsu, M., Ueno, K. & Konno, T. Sulfur-bridged dinuclear and tetranuclear complexes consisting of *cis*-$[Ru(bpy)_2]^{2+}$ and *cis*-$[Ni(aet)_2]$ units. *Bull. Chem. Soc. Jpn.* **79**, 1745–1747 (2006).

49. Matsuura, N., Igashira-Kamiyama, A., Kawamoto, T. & Konno, T. Meso and Racemic Isomers of a New S-Bridged Diruthenium(II) Complex with Pendant Aminoalkyl Groups. *Chem. Lett.* **34**, 1252–1253 (2005).

50. Matsuura, N., Kawarnoto, T. & Konno, T. Conversion of 2-aminoethanethiolate (aet) to 2-benzoylaminoethanethiolate (L) in a S-bridged diruthenium (II) complex composed of two cis-$[Ru(bpy)_2]$ units. Crystal structures of ΔΔ/ΛΛ-$[\{Ru(bpy)_2\}(2)-(\mu\text{-Haet})_2]^{4+}$ and ΔΔ/ΛΛ-$[\{Ru(bpy)_2\}_2(\mu\text{-L})_2]^{2+}$. *Bull. Chem. Soc. Jpn.* **79**, 297–299 (2006).

51. Walsh, J. L. & Durham, B. Trans isomers of ruthenium(II) complexes containing two bipyridine ligands. *Inorg. Chem.* **21**, 329–332 (1982).

52. Bryant, G., Fergusson, J. & Powell, H. Charge-transfer and intraligand electronic spectra of bipyridyl complexes of iron, ruthenium, and osmium. I. Bivalent complexes. *Aust. J. Chem.* **24**, 257–273 (1971).

53. Ceulemans, A. & Vanquickenborne, L. G. Charge-transfer spectra of iron(II)- and ruthenium(II)-tris(2,2'-bipyridyl) complexes. *J. Am. Chem. Soc.* **103**, 2238–2241 (1981).

54. Mayoh, B. & Day, P. The excited states of bipyridyl and phenanthroline complexes of Fe(III), Ru(II) and Ru(III): A molecular orbital study. *Theor. Chem. Acc.* **49**, 259–275 (1978).

55. Hipps, K. W. & Crosby, G. A. Charge-transfer excited states of ruthenium(II) complexes. III. Electron-ion coupling model for dπ* configurations. *J. Am. Chem. Soc.* **97**, 7042–7048 (1975).

56. Orgel, L. E. 715. Double bonding in chelated metal complexes. *J. Chem. Soc.* 3683 (1961).doi:10.1039/jr9610003683

57. Kalyanasundaram, K. Photophysics, photochemistry and solar energy conversion with tris(bipyridyl)ruthenium(II) and its analogues. *Coord. Chem. Rev.* **46**, 159–244 (1982).

58. Natsuaki, K., Nakano, M., Matsubayashi, G. & Arakawa, R. Preparation and spectroscopic properties of bis(2,2′-bipyridine)-ruthenium(II) complexes and related complexes with sulfur-rich dithiolato ligands and electrical conductivities of their oxidized species. *Inorg. Chim. Acta* **299**, 112–117 (2000).

59. Caspar, J. V. & Meyer, T. J. Photochemistry of tris(2,2'-bipyridine)ruthenium(2+) ion ($Ru(bpy)_3^{2+}$). Solvent effects. *J. Am. Chem. Soc.* **105**, 5583–5590 (1983).

60. Chen, P., Duesing, R., Graff, D. K. & Meyer, T. J. Intramolecular electron transfer in the inverted region. *J. Phys. Chem.* **95**, 5850–5858 (1991).

61. Crosby, G. A. & Demas, J. N. Measurement of photoluminescence quantum yields. Review. *J. Phys. Chem.* **75**, 991–1024 (1971).

62. Liu, Y. *et al.* Ultrafast Ligand Exchange: Detection of a Pentacoordinate Ru(II) Intermediate and Product Formation. *J. Am. Chem. Soc.* **131**, 26–27 (2008).

63. Rachford, A. A. & Rack, J. J. Picosecond Isomerization in Photochromic Ruthenium−Dimethyl Sulfoxide Complexes. *J. Am. Chem. Soc.* **128**, 14318–14324 (2006).

64. McCusker, J. K. Femtosecond Absorption Spectroscopy of Transition Metal Charge-Transfer Complexes. *Acc. Chem. Res.* **36**, 876–887 (2003).

65. Abrahamsson, M. *et al.* Steric influence on the excited-state lifetimes of ruthenium complexes with bipyridyl-alkanylene-pyridyl Ligands. *Inorg. Chem.* **47**, 3540–3548 (2008).

66. Osterman, T., Abrahamsson, M., Becker, H.-C., Hammarstrom, L. & Persson, P. Influence of Triplet State Multidimensionality on Excited State Lifetimes of Bis-tridentate Ru-II Complexes: A Computational Study. *J. Phys. Chem. A* **116**, 1041–1050 (2012).

67. Dinda, J., Liatard, S., Chauvin, J., Jouvenot, D. & Loiseau, F. Electronic and geometrical manipulation of the excited state of bis-terdentate homo- and heteroleptic ruthenium complexes. *Dalton Trans.* **40**, 3683–3688 (2011).

REFERENCES

Abrahamsson, Maria, Maria J. Lundqvist, Henriette Wolpher, Olof Johansson, Lars Eriksson, Jonas Bergquist, Torben Rasmussen, et al. 2008. "Steric influence on the excited-state lifetimes of ruthenium complexes with bipyridyl-alkanylene-pyridyl Ligands." *Inorg. Chem.* 47 (9): 3540–3548. doi:10.1021/ic7019457.

Ainscough, Eric W., Andrew M. Brodie, Nigel G. Larsen, and Mark R. Stevens. 1981. "Sulphur Ligand Metal Complexes. Part 10 [1]. Sulphur-nitrogen Donor Ligand Complexes of the Group 6 Metal Carbonyls." *Inorg. Chim. Acta* 50 (0): 215–220. doi:10.1016/S0020-1693(00)83746-9.

Altenbuchner, Josef, Martin Siemann-Herzberg, and Christoph Syldatk. 2001. "Hydantoinases and Related Enzymes as Biocatalysts for the Synthesis of Unnatural Chiral Amino Acids." *Curr. Opin. Biotechnol.* 12 (6): 559–563. doi:10.1016/S0958-1669(01)00263-4.

Angelosante, Jennifer, Lauren Schopp, Breia Lewis, Amber Vitalo, Dustin Titus, Rebecca Swanson, April Stanley, et al. 2011. "Synthesis and Characterization of an Unsymmetrical cobalt(III) Active Site Analogue of Nitrile Hydratase." *J. Biol. Inorg. Chem.* 16 (6): 937–947. doi:10.1007/s00775-011-0794-7.

Ankudinov, A. L., B. Ravel, J. J. Rehr, and S. D. Conradson. 1998. "Real-space Multiple-scattering Calculation and Interpretation of X-ray-absorption Near-edge Structure." *Phys. Rev. B* 58 (12): 7565–7576. doi:10.1103/PhysRevB.58.7565.

Apfel, Ulf-Peter, Christian R. Kowol, Enrico Morera, Helmar Görls, Gino Lucente, Bernhard K. Keppler, and Wolfgang Weigand. 2010. "Synthetic and Electrochemical Studies of [2Fe2S] Complexes Containing a 4-Amino-1,2-dithiolane-4-carboxylic Acid Moiety." *Eur. J. Inorg. Chem.* 2010 (32): 5079–5086. doi:10.1002/ejic.201000619.

Arakawa, Takatoshi, Yoshiaki Kawano, Shingo Kataoka, Yoko Katayama, Nobuo Kamiya, Masafumi Yohda, and Masafumi Odaka. 2007. "Structure of Thiocyanate Hydrolase: A New Nitrile Hydratase Family Protein with a Novel Five-coordinate Cobalt(III) Center." *J. Mol. Biol.* 366 (5): 1497–1509. doi:10.1016/j.jmb.2006.12.011.

Arakawa, Takatoshi, Yoshiaki Kawano, Yoko Katayama, Hiroshi Nakayama, Naoshi Dohmae, Masafumi Yohda, and Masafumi Odaka. 2009. "Structural Basis for Catalytic Activation of Thiocyanate Hydrolase Involving Metal-

Ligated Cysteine Modification." *J. Am. Chem. Soc.* 131 (41): 14838–14843. doi:10.1021/ja903979s.

Artero, Vincent, and Marc Fontecave. 2011. "Light-driven bioinspired water splitting: Recent developments in photoelectrode materials." *C. R. Chimie* 14 (9): 799–810. doi:10.1016/j.crci.2011.06.004.

Asali, Khalil J., Mohammad El-Khateeb, and Musa M. Musa. 2002. "Bimetallic Complexes with Bridging Dithiaalkane Ligands: Preparation and Kinetic Study." *J. Coord. Chem.* 55 (10): 1199–1207. doi:10.1080/0095897021000025534.

Asali, Khalil J., Mohammad El-Khateeb, and R. Salhab. 2003. "Bimetallic Group 6 Metal Tetracarbonyls Doubly Bridged by Bisphosphine And/or Dithiaalkane Ligands." *Transition Met. Chem.* 28 (5): 544–547.

Banerjee, Sharma, and Banerjee. 2002. "The Nitrile-degrading Enzymes: Current Status and Future Prospects." *Appl. Microbiol. Biotechnol.* 60 (1): 33–44. doi:10.1007/s00253-002-1062-0.

Barondeau, David P., Carey J. Kassmann, Cami K. Bruns, John A. Tainer, and Elizabeth D. Getzoff. 2004. "Nickel Superoxide Dismutase Structure and Mechanism." *Biochemistry* 43 (25): 8038–8047. doi:10.1021/bi0496081.

Bertini, Ivano, Harry B. Gray, E. I. Stiefel, and Valentine, J. S. 2007. *Biological Inorganic Chemistry: Structure and Reactivity*. University Science Books.

Best, Stephen A., Patrick. Brant, Robert D. Feltham, Thomas B. Rauchfuss, D. Max. Roundhill, and Richard A. Walton. 1977. "X-ray Photoelectron Spectra of Inorganic Molecules. 18. Observations on Sulfur 2p Binding Energies in Transition Metal Complexes of Sulfur-containing Ligands." *Inorg. Chem.* 16 (8): 1976–1979. doi:10.1021/ic50174a030.

Blaser, Hans Ulrich, and Hans-Jürgen Federsel, eds. 2010. *Asymmetric Catalysis on Industrial Scale: Challenges, Approaches and Solutions*. 2nd ed. Wiley-VCH.

Böck, August, Paul W. King, Melanie Blokesch, and Matthew C. Posewitz. 2006. "Maturation of Hydrogenases." In *Advances in Microbial Physiology*, ed. R.K. Poole, 51:1–71. Elsevier.

Bourles, Emilie, Rodolphe Alves de Sousa, Erwan Galardon, Michel Giorgi, and Isabelle Artaud. 2005. "Direct Synthesis of a Thiolato-S and Sulfinato-S Co^{III} Complex Related to the Active Site of Nitrile Hydratase: A Pathway to the

Post-Translational Oxidation of the Protein." *Angew. Chem. Int. Ed.* 44 (38): 6162–6165. doi:10.1002/anie.200500814.

Browne, Wesley R., Paolo Passaniti, Maria Teresa Gandolfi, Roberto Ballardini, William Henry, Adrian Guckian, Noel O'Boyle, John J. McGarvey, and Johannes G. Vos. 2007. "Probing Inter-ligand Excited State Interaction in Homo and Heteroleptic ruthenium(II) Polypyridyl Complexes Using Selective Deuteriation." *Inorg. Chim. Acta* 360 (3): 1183–1190. doi:10.1016/j.ica.2006.08.049.

Bruker, APEX2, SADABS. Bruker AXS Inc., Madison, Wisconsin, USA. 2010. . Bruker AXS Inc., Madison, Wisconsin, USA.

Bruker, SAINT-Plus. Bruker AXS Inc., Madison, Wisconsin, USA. 2009. . Bruker AXS Inc., Madison, Wisconsin, USA.

Bruker, XShell ver. 6.3.1, Bruker AXS Inc., Madison, Wisconsin, USA. . Bruker AXS Inc., Madison, Wisconsin, USA.

Bryant, GM, JE Fergusson, and HKJ Powell. 1971. "Charge-transfer and Intraligand Electronic Spectra of Bipyridyl Complexes of Iron, Ruthenium, and Osmium. I. Bivalent Complexes." *Aust. J. Chem.* 24 (2): 257–273.

Cammack, Richard, Michel Frey, and Robert Robson. 2002. *Hydrogen as Fuel*. 1st ed. CRC.

Campagna, Sebastiano, Fausto Puntoriero, Francesco Nastasi, Giacomo Bergamini, and Vincenzo Balzani. 2007. "Photochemistry and Photophysics of Coordination Compounds: Ruthenium." In *Photochemistry and Photophysics of Coordination Compounds I*, ed. Vincenzo Balzani and Sebastiano Campagna, 280:117–214. Topics in Current Chemistry. Springer Berlin/Heidelberg.

Canaguier, Sigolène, Vincent Artero, and Marc Fontecave. 2008. "Modelling NiFe Hydrogenases: Nickel-based Electrocatalysts for Hydrogen Production." *Dalton Trans.* (3): 315. doi:10.1039/b713567j.

Carroll, Maria E., Bryan E. Barton, Danielle L. Gray, Amanda E. Mack, and Thomas B. Rauchfuss. 2011. "Active-Site Models for the Nickel–Iron Hydrogenases: Effects of Ligands on Reactivity and Catalytic Properties." *Inorg. Chem.* 50 (19): 9554–9563. doi:10.1021/ic2012759.

Caspar, Jonathan V., and Thomas J. Meyer. 1983. "Photochemistry of Tris(2,2'-bipyridine)ruthenium(2+) Ion ($Ru(bpy)_3^{2+}$). Solvent Effects." *J. Am. Chem. Soc.* 105 (17): 5583–5590. doi:10.1021/ja00355a009.

Ceulemans, A., and L. G. Vanquickenborne. 1981. “Charge-transfer Spectra of iron(II)- and ruthenium(II)-tris(2,2’-bipyridyl) Complexes.” *J. Am. Chem. Soc.* 103 (9): 2238–2241. doi:10.1021/ja00399a017.

Chalbot, Marie-Cécile, Allison M. Mills, Anthony L. Spek, Gary J. Long, and Elisabeth Bouwman. 2003. “Structure and Electronic Properties of [Ni(dsdm){$Fe(CO)_3$}$_2$], an Unusual, Triangular Nickel Diiron Compound.” *Eur. J. Inorg. Chem.* 2003 (3): 453–457. doi:10.1002/ejic.200390064.

Chen, Pingyun, Rich Duesing, Darla K. Graff, and Thomas J. Meyer. 1991. “Intramolecular Electron Transfer in the Inverted Region.” *J. Phys. Chem.* 95 (15): 5850–5858. doi:10.1021/j100168a027.

Chen, X. H., M. H. Chu, and D. P. Giedroc. 2000. “Spectroscopic characterization of Co(II)-, Ni(II)-, and Cd(II)-substituted wild-type and non-native retroviral-type zinc finger peptides.” *J. Biol. Inorg. Chem.* 5 (1): 93–101.

Chohan, Balwant S., and Michael J. Maroney. 2006. “Selective Oxidations of a Dithiolate Complex Produce a Mixed Sulfonate/Thiolate Complex.” *Inorg. Chem.* 45 (5): 1906–1908. doi:10.1021/ic051982h.

Choudhury, Suranjan B., Jin-Won Lee, Gerard Davidson, Yang-In Yim, Kurethara Bose, Manju L. Sharma, Sa-Ouk Kang, Diane E. Cabelli, and Michael J. Maroney. 1999. “Examination of the Nickel Site Structure and Reaction Mechanism in Streptomyces Seoulensis Superoxide Dismutase.” *Biochemistry* 38 (12): 3744–3752. doi:10.1021/bi982537j.

Claiborne, Al, Joanne I. Yeh, T. Conn Mallett, James Luba, Edward J. Crane, Véronique Charrier, and Derek Parsonage. 1999. “Protein-Sulfenic Acids: Diverse Roles for an Unlikely Player in Enzyme Catalysis and Redox Regulation.” *Biochemistry* 38 (47): 15407–15416. doi:10.1021/bi992025k.

Collings, Anthony F., and Christa Critchley. 2007. *Artificial Photosynthesis: From Basic Biology to Industrial Application*. John Wiley & Sons.

Colpas, Gerard J., Manoj Kumar, Roberta O. Day, and Michael J. Maroney. 1990. “Structural Investigations of Nickel Complexes with Nitrogen and Sulfur Donor Ligands.” *Inorg. Chem.* 29 (23): 4779–4788. doi:10.1021/ic00348a037.

Concepcion, Javier J., Jonah W. Jurss, M. Kyle Brennaman, Paul G. Hoertz, Antonio Otavio T. Patrocinio, Neyde Yukie Murakami Iha, Joseph L. Templeton, and Thomas J. Meyer. 2009. “Making Oxygen with Ruthenium Complexes.” *Acc. Chem. Res.* 42 (12): 1954–1965. doi:10.1021/ar9001526.

Condrate, Robert A, and Kazuo Nakamoto. 1965. “Infrared Spectra and Normal Coordinate Analysis of Metal Glycino Complexes.” *J. Chem. Phys*. 42 (7): 2590–2598. doi:10.1063/1.1696337.

Cornils, Boy, and Wolfgang A. Herrmann, eds. 2002. *Applied Homogeneous Catalysis with Organometallic Compounds: A Comprehensive Handbook in Three Volumes*. 2nd, Ed. Wiley-VCH.

Craig, Carl A., Larry O. Spreer, John W. Otvos, and Melvin. Calvin. 1990. “Photochemical Reduction of Carbon Dioxide Using Nickel Tetraazamacrocycles.” *J. Phys. Chem.* 94 (20): 7957–7960. doi:10.1021/j100383a038.

Crosby, Glenn A., and James N. Demas. 1971. “Measurement of Photoluminescence Quantum Yields. Review.” *J. Phys. Chem.* 75 (8): 991–1024. doi:10.1021/j100678a001.

Crow, James, Mitchell. 2007. “The Perfect Host.” *Chemistry World* 4 (7): 50–53.

Darensbourg, Donald J., Robert R. Burch, and Marcetta Y. Darensbourg. 1978. “Preparation of a Stereospecifically Carbon-13 Monoxide-labeled [(μ-H)[$Mo(CO)_5]_2]^-$ Species and Analysis of Its Carbonyl Stretching Vibrational Modes.” *Inorg. Chem.* 17 (9): 2677–2680. doi:10.1021/ic50187a061.

Darnault, Claudine, Anne Volbeda, Eun Jin Kim, Pierre Legrand, Xavier Vernède, Paul A. Lindahl, and Juan C. Fontecilla-Camps. 2003. “Ni-Zn-[Fe4-S4] and Ni-Ni-[Fe4-S4] Clusters in Closed and Open α Subunits of acetyl-CoA Synthase/carbon Monoxide Dehydrogenase.” *Nat. Struct. Mol. Biol.* 10 (4): 271–279. doi:10.1038/nsb912.

Dempsey, Jillian L., Jay R. Winkler, and Harry B. Gray. 2010. “Proton-Coupled Electron Flow in Protein Redox Machines.” *Chem. Rev.* 110 (12): 7024–7039. doi:10.1021/cr100182b.

Deuss, Peter J., René den Heeten, Wouter Laan, and Paul C. J. Kamer. 2011. “Bioinspired Catalyst Design and Artificial Metalloenzymes.” *Chem. Eur. J.* 17 (17): 4680–4698. doi:10.1002/chem.201003646.

Dey, Abhishek, Stephen P. Jeffrey, Marcetta Darensbourg, Keith O. Hodgson, Britt Hedman, and Edward I. Solomon. 2007. “Sulfur K-Edge XAS and DFT Studies on Ni^{II} Complexes with Oxidized Thiolate Ligands: Implications for the Roles of Oxidized Thiolates in the Active Sites of Fe and Co Nitrile Hydratase.” *Inorg. Chem.* 46 (12): 4989–4996. doi:10.1021/ic070244l.

Dickinson, Bryan C, and Christopher J Chang. 2011. “Chemistry and Biology of Reactive Oxygen Species in Signaling or Stress Responses.” *Nat. Chem. Biol.* 7 (8): 504–511. doi:10.1038/nchembio.607.

Dinda, Joydev, Sebastien Liatard, Jerome Chauvin, Damien Jouvenot, and Frederique Loiseau. 2011. “Electronic and geometrical manipulation of the excited state of bis-terdentate homo- and heteroleptic ruthenium complexes.” *Dalton Trans.* 40 (14): 3683–3688. doi:10.1039/c0dt01197e.

Douchiche, Olfa, Azeddine Driouich, and Claudine Morvan. 2010. “Spatial Regulation of Cell-wall Structure in Response to Heavy Metal Stress: Cadmium-induced Alteration of the Methyl-esterification Pattern of Homogalacturonans.” *Ann. Bot.* 105 (3): 481–491. doi:10.1093/aob/mcp306.

Doukov, T. I., T. M. Iverson, J. Seravalli, S. W. Ragsdale, and C. L. Drennan. 2002. “A Ni-Fe-Cu center in a bifunctional carbon monoxide dehydrogenase/acetyl-CoA synthase.” *Science* 298 (5593): 567–572. doi:10.1126/science.1075843.

Drennan, Catherine L., Tzanko I. Doukov, and Stephen W. Ragsdale. 2004. “The Metalloclusters of Carbon Monoxide dehydrogenase/acetyl-CoA Synthase: a Story in Pictures.” *J. Biol. Inorg. Chem.* 9 (5): 511–515. doi:10.1007/s00775-004-0563-y.

Drum, David E., and Bert L. Vallee. 1970. “Optical Properties of Catalytically Active Cobalt and Cadmium Liver Alcohol Dehydrogenases.” *Biochem. Biophys. Res. Commun.* 41 (1): 33–39. doi:10.1016/0006-291X(70)90464-X.

Dutta, Arnab, M. Flores, Souvik Roy, Jennifer Schmitt C., Greg Hamilton, A, Hillairy Hartnett E., J. Shearer, and Anne K. Jones. “Unpublished Data.”

Dutta, Arnab, Greg Hamilton, A, Hillairy Hartnett, and Anne K. Jones. 2012b. “Construction of Heterometallic Clusters in a Small Peptide Scaffold, as [NiFe]-hydrogenase Models: Development of a Synthetic Methodology.” *Inorganic Chemistry* (Article ASAP). doi:10.1021/ic2026818.

El-khateeb, M., Asali K.J., and Musa M. M. 2002. “Dinuclear Group VIB Metal Carbonyl Complexes Bridged by Bis(diphenylphosphino)alkanes.” *Transition Met. Chem.* 27 (2): 163–165.

Ellman, George L. 1958. “A Colorimetric Method for Determining Low Concentrations of Mercaptans.” *Arch. Biochem. Biophys.* 74 (2): 443–450. doi:10.1016/0003-9861(58)90014-6.

Elvington, Mark, Jared Brown, Shamindri M. Arachchige, and Karen J. Brewer. 2007. “Photocatalytic hydrogen production from water employing a Ru, Rh, Ru molecular device for photoinitiated electron collection.” *J. Am. Chem. Soc.* 129 (35): 10644–10645. doi:10.1021/ja073123t.

Endo I., Odaka M., and Yohda M. 1999. “An Enzyme Controlled by Light: The Molecular Mechanism of Photoreactivity in Nitrile Hydratase.” *Trends Biotechnol.* 17 (6): 244–248. doi:10.1016/S0167-7799(99)01303-7.

Evans, D. F. 1959. “400. The Determination of the Paramagnetic Susceptibility of Substances in Solution by Nuclear Magnetic Resonance.” *J. Chem. Soc.*: 2003–2005. doi:10.1039/JR9590002003.

Farmer, Patrick J., Touradj Solouki, Daniel K. Mills, Takako Soma, David H. Russell, Joseph H. Reibenspies, and Marcetta Y. Darensbourg. 1992. “Isotopic Labeling Investigation of the Oxygenation of Nickel-bound Thiolates by Molecular Oxygen.” *J. Am. Chem. Soc.* 114 (12): 4601–4605. doi:10.1021/ja00038a023.

Farmer, Patrick J., Jean-Noel Verpeaux, Christian Amatore, Marcetta Y. Darensbourg, and Ghezai Musie. 1994. “Reduction-Promoted Sulfur-Oxygen Bond Cleavage in a Nickel Sulfenate as a Model for the Activation of [NiFe] Hydrogenase.” *J. Am. Chem. Soc.* 116 (20): 9355–9356. doi:10.1021/ja00099a073.

Fedorova, Anna, Anita Chaudhari, and Michael Y. Ogawa. 2003. “Photoinduced Electron-Transfer Along α-Helical and Coiled-Coil Metallopeptides.” *J. Am. Chem. Soc.* 125 (2): 357–362. doi:10.1021/ja026140l.

Fihri, Aziz, Vincent Artero, Alexandre Pereira, and Marc Fontecave. 2008. “Efficient H2-producing Photocatalytic Systems Based on Cyclometalated Iridium- and Tricarbonylrhenium-diimine Photosensitizers and Cobaloxime Catalysts.” *Dalton Trans.* (41): 5567. doi:10.1039/b812605b.

Fihri, Aziz, Vincent Artero, Mathieu Razavet, Carole Baffert, Winfried Leibl, and Marc Fontecave. 2008. “Cobaloxime-Based Photocatalytic Devices for Hydrogen Production.” *Angew. Chem. Int. Ed.* 47 (3): 564–567. doi:10.1002/anie.200702953.

Flores, M., R. Isaacson, E. Abresch, R. Calvo, W. Lubitz, and G. Feher. 2007. “Protein-Cofactor Interactions in Bacterial Reaction Centers from Rhodobacter Sphaeroides R-26: II. Geometry of the Hydrogen Bonds to the Primary Quinone $Q_A^{\cdot -}$ by ^1H and ^2H ENDOR Spectroscopy.” *Biophys. J.* 92 (2): 671–682. doi:10.1529/biophysj.106.092460.

Fontecave, Marc, and Vincent Artero. 2011. “Bioinspired Catalysis at the Crossroads Between Biology and Chemistry: A Remarkable Example of an Electrocatalytic Material Mimicking Hydrogenases.” *C. R. Chimie* 14 (4): 362–371. doi:10.1016/j.crci.2010.01.013.

Fontecilla-Camps, Juan C., Anne Volbeda, and Michel Frey. 1996. “Hydrogen Biocatalysis: a Tale of Two Metals.” *Trends Biotechnol.* 14 (11): 417–420. doi:10.1016/0167-7799(96)30021-8.

Fukuzumi, Shunichi, Takeshi Kobayashi, and Tomoyoshi Suenobu. 2010. “Formic Acid Acting as an Efficient Oxygen Scavenger in Four-Electron Reduction of Oxygen Catalyzed by a Heterodinuclear Iridium−Ruthenium Complex in Water.” *J. Am. Chem. Soc.* 132 (34): 11866–11867. doi:10.1021/ja104486h.

Galardon, Erwan, Michel Giorgi, and Isabelle Artaud. 2004. “Oxygenation of Thiolates to S-bonded Sulfinate in an iron(III) Complex Related to Nitrile Hydratase.” *Chemical Commun.* (3): 286–287. doi:10.1039/B312318A.

Gale, Eric M., Darin M. Cowart, Robert A. Scott, and Todd C. Harrop. 2011. “Dipeptide-Based Models of Nickel Superoxide Dismutase: Solvent Effects Highlight a Critical Role to Ni–S Bonding and Active Site Stabilization.” *Inorg. Chem.* 50 (20): 10460–10471. doi:10.1021/ic2016462.

Galvez, Cesar, David G. Ho, Armin Azod, and Matthias Selke. 2001. “Reaction of a Coordinated Cysteinato Ligand with Singlet Oxygen: Photooxidation of (Cysteinato-N,S)bis(ethylenediamine)cobalt(III).” *J. Am. Chem. Soc.* 123 (14): 3381–3382. doi:10.1021/ja003993+.

Geiger, William E. 2011. “Reflections on Future Directions in Organometallic Electrochemistry.” *Organometallics* 30 (1): 28–31. doi:10.1021/om1010758.

Gibney, B. R., and P. L. Dutton. 2001. “De novo design and synthesis of heme proteins.” *Adv. Inorg. Chem. Vol 51* 51: 409–455.

Gloaguen, Frédéric, and Thomas B. Rauchfuss. 2009. “Small Molecule Mimics of Hydrogenases: Hydrides and Redox.” *Chem. Soc. Rev.* 38 (1): 100. doi:10.1039/b801796b.

Goff, Simon E. J., Trevor F. Nolan, Michael W. George, and Martyn Poliakoff. 1998. “Chemistry of Reactive Organometallic Compounds at Low Temperatures and High Pressures: Reactions of $M(CO)_6$ (M = Cr, Mo, W), (η^6-$C_6H_3Me_3$)$M(CO)_3$ (M = Cr and Mo), and $W(CO)_5CS$ with H_2 and N_2 in Polyethylene Matrices.” *Organometallics* 17 (13): 2730–2737. doi:10.1021/om970474f.

Goodman, Catherine M., Sungwook Choi, Scott Shandler, and William F. DeGrado. 2007. “Foldamers as versatile frameworks for the design and evolution of function.” *Nat. Chem. Biol.* 3 (5): 252–262. doi:10.1038/nchembio876.

Goris, Tobias, Annemarie F. Wait, Miguel Saggu, Johannes Fritsch, Nina Heidary, Matthias Stein, Ingo Zebger, et al. 2011. “A Unique Iron-sulfur Cluster is Crucial for Oxygen Tolerance of a [NiFe]-hydrogenase.” *Nat. Chem. Biol.* 7 (5): 310–318. doi:10.1038/nchembio.555.

Grant, Douglas H. 1995. “Paramagnetic Susceptibility by NMR: The ‘Solvent Correction’ Reexamined.” *J. Chem. Educ.* 72 (1): 39. doi:10.1021/ed072p39.

Grapperhaus, Craig A., Marcetta Y. Darensbourg, Lloyd W. Sumner, and David H. Russell. 1996. “Template Effect for O_2 Addition Across cis-Sulfur Sites in Nickel Dithiolates.” *J. Am. Chem. Soc.* 118 (7): 1791–1792. doi:10.1021/ja953489i.

Gray, Harry B. 2003. “Biological Inorganic Chemistry at the Beginning of the 21st Century.” *Proc. Natl. Acad. Sci. USA* 100 (7): 3563–3568. doi:10.1073/pnas.0730378100.

Greaney, M. A., C. L. Coyle, M. A. Harmer, A. Jordan, and E. I. Stiefel. 1989. “Synthesis and Characterization of Mononuclear and Dinuclear bis(2,2’-bipyridine)ruthenium(II) Complexes Containing Sulfur-donor Ligands.” *Inorg. Chem.* 28 (5): 912–920. doi:10.1021/ic00304a023.

Green, Kayla N., Stephen P. Jeffery, Joseph H. Reibenspies, and Marcetta Y. Darensbourg. 2006. “A Nickel Tripeptide as a Metallodithiolate Ligand Anchor for Resin-Bound Organometallics.” *J. Am. Chem. Soc* 128 (19): 6493–6498. doi:10.1021/ja060876r.

Greenfield, Norma J., and Serge N. Timasheff. 1975. “Enzyme Ligand Complexes: Spectroscopic Studie.” *Crit. Rev. Biochem. Mol. Biol.* 3 (1): 71–110. doi:10.3109/10409237509102553.

Gruttadauria, Michelangelo, and Francesco Giacalone, eds. 2011. *Catalytic Methods in Asymmetric Synthesis: Advanced Materials, Techniques, and Applications*.

Guengerich, F. Peter. 2012. “Thematic Minireview Series: Metals in Biology 2012.” *J. Biol. Chem.* 287 (17): 13508–13509. doi:10.1074/jbc.R112.355933.

Gust, Devens, Ana L. Moore, and Thomas A. Moore. 2001. *Electron Transfer in Chemistry: Catalysis of Electron Transfer, Heterogenous Systems, Gas-phase Systems*. Vol. 3. Weinheim: Wiley-VCH.

Gust, Devens, Thomas A. Moore, and Ana L. Moore. 2001. "Mimicking Photosynthetic Solar Energy Transduction." *Acc. Chem. Res.* 34 (1): 40–48. doi:10.1021/ar9801301.

Gust, Devens, Thomas A. Moore, and Ana L. Moore. 2009. "Solar Fuels via Artificial Photosynthesis." *Acc. Chem. Res.* 42 (12): 1890–1898. doi:10.1021/ar900209b.

Hagen, Jens. 2006. *Industrial Catalysis: A Practical Approach*. John Wiley & Sons.

Hambourger, Michael, Miguel Gervaldo, Drazenka Svedruzic, Paul W. King, Devens Gust, Maria Ghirardi, Ana L. Moore, and Thomas A. Moore. 2008. "[FeFe]-Hydrogenase-Catalyzed H2 Production in a Photoelectrochemical Biofuel Cell." *J. Am. Chem. Soc.* 130 (6): 2015–2022. doi:10.1021/ja077691k.

de Hatten, Xavier, Eberhardt Bothe, Klaus Merz, Ivan Huc, and Nils Metzler-Nolte. 2008. "A Ferrocene–Peptide Conjugate as a Hydrogenase Model System." *Eur. J. Inorg. Chem.* 2008 (29): 4530–4537. doi:10.1002/ejic.200800566.

Hillard, Elizabeth A., and Gérard Jaouen. 2011. "Bioorganometallics: Future Trends in Drug Discovery, Analytical Chemistry, and Catalysis." *Organometallics* 30 (1): 20–27. doi:10.1021/om100964h.

Hintermair, Ulrich, Giancarlo Franciò, and Walter Leitner. 2011. "Continuous Flow Organometallic Catalysis: New Wind in Old Sails." *Chemical Commun.* 47 (13): 3691–3701. doi:10.1039/C0CC04958A.

Hipps, K. W., and G. A. Crosby. 1975. "Charge-transfer Excited States of ruthenium(II) Complexes. III. Electron-ion Coupling Model for dπ* Configurations." *J. Am. Chem. Soc.* 97 (24): 7042–7048. doi:10.1021/ja00857a015.

Hori, H., F. P. A. Johnson, K. Koike, O. Ishitani, and T. Ibusuki. 1996. "Efficient photocatalytic CO_2 reduction using $[Re(bpy)(CO)_3\{P(OEt)_3\}]^+$." *J. Photochem. Photobiol.* 96 (1-3): 171–174. doi:10.1016/1010-6030(95)04298-9.

Howard, James B., and Douglas C. Rees. 2006. “How Many Metals Does It Take to Fix N_2? A Mechanistic Overview of Biological Nitrogen Fixation.” *Proc. Natl. Acad. Sci. USA* 103 (46): 17088–17093. doi:10.1073/pnas.0603978103.

Hsieh, Chung-Hung, Rachel B. Chupik, Scott M. Brothers, Michael B. Hall, and Marcetta Y. Darensbourg. 2011. “cis-Dithiolatonickel as Metalloligand to Dinitrosyl Iron Units: The Di-metallic Structure of $Ni(\mu\text{-}SR)[Fe(NO)_2]$ and an Unexpected, Abbreviated Metalloadamantyl Cluster, $Ni_2(\mu\text{-}SR)_4[Fe(NO)_2]_3$.” *Dalton Trans.* 40 (22): 6047. doi:10.1039/c1dt10438a.

Huang, Cheng-Yang, Yun-Peng Chao, and Yuh-Shyong Yang. 2003. “Purification of Industrial Hydantoinase in One Chromatographic Step Without Affinity Tag.” *Protein Expression Purif.* 30 (1): 134–139. doi:10.1016/S1046-5928(03)00092-5.

Huang, Weijun, Jia Jia, John Cummings, Mark Nelson, Gunter Schneider, and Ylva Lindqvist. 1997. “Crystal Structure of Nitrile Hydratase Reveals a Novel Iron Centre in a Novel Fold.” *Structure* 5 (5): 691–699. doi:10.1016/S0969-2126(97)00223-2.

Igor Pro. Lake Oswego, OR: WaveMetrics, Inc. 2011.

Inagaki, Akiko, and Munetaka Akita. 2010. “Visible-light Promoted Bimetallic Catalysis.” *Coord. Chem. Rev.* 54 (11–12): 1220–1239. doi:10.1016/j.ccr.2009.11.003.

Iranzo, Olga, Saumen Chakraborty, Lars Hemmingsen, and Vincent L. Pecoraro. 2011. “Controlling and Fine Tuning the Physical Properties of Two Identical Metal Coordination Sites in De Novo Designed Three Stranded Coiled Coil Peptides.” *J. Am. Chem. Soc.* 133 (2): 239–251. doi:10.1021/ja104433n.

Jacobson, M. Z., W. G. Colella, and D. M. Golden. 2005. “Cleaning the Air and Improving Health with Hydrogen Fuel-Cell Vehicles.” *Science* 308 (5730). New Series: 1901–1905.

Jahncke, Manfred, Götz Meister, Gerd Rheinwald, Helen Stoeckli-Evans, and Georg Süss-Fink. 1997. “Dinuclear (Arene)ruthenium Hydrido Complexes: Synthesis, Structure, and Fluxionality of $(C_6Me_6)_2Ru_2H_3(BH_4)$.” *Organometallics* 16 (6): 1137–1143. doi:10.1021/om960840f.

Jain, Avijita, Sheri Lense, John C. Linehan, Simone Raugei, Herman Cho, Daniel L. DuBois, and Wendy J. Shaw. 2011. “Incorporating Peptides in the Outer-Coordination Sphere of Bioinspired Electrocatalysts for Hydrogen Production.” *Inorg Chem.* 50 (9): 4073–4085. doi:10.1021/ic1025872.

Jeffery, Stephen P., Michael L. Singleton, Joseph H. Reibenspies, and Marcetta Y. Darensbourg. 2007. "Control of S-Based Aggregation: Designed Synthesis of NiM2 and Ni2M Trinuclear Complexes." *Inorg Chem*. 46 (1): 179–185. doi:10.1021/ic061475f.

Jones, Anne K., Bruce R. Lichtenstein, Arnab Dutta, Gwyneth Gordon, and P. Leslie Dutton. 2007. "Synthetic Hydrogenases: Incorporation of an Iron Carbonyl Thiolate into a Designed Peptide." *J. Am. Chem. Soc.* 129 (48): 14844–14845. doi:10.1021/ja075116a.

Juris, A., V. Balzani, F. Barigelletti, S. Campagna, P. Belser, and A. von Zelewsky. 1988. "Ru(II) Polypyridine Complexes: Photophysics, Photochemistry, Eletrochemistry, and Chemiluminescence." *Coord. Chem. Rev.* 84: 85–277. doi:10.1016/0010-8545(88)80032-8.

Kaasjager, Vincent E., Elisabeth Bouwman, S. Gorter, Jan Reedijk, Craig A. Grapperhaus, Joseph H. Reibenspies, Jason J. Smee, Marcetta Y. Darensbourg, Agnes Derecskei-Kovacs, and Lisa M. Thomson. 2002. "Unique Reactivity of a Tetradentate N_2S_2 Complex of Nickel: Intermediates in the Production of Sulfur Oxygenates." *Inorg. Chem.* 41 (7): 1837–1844. doi:10.1021/ic010784x.

Kalyanasundaram, K. 1982. "Photophysics, Photochemistry and Solar Energy Conversion with tris(bipyridyl)ruthenium(II) and Its Analogues." *Coord. Chem. Rev.* 46 (0) (October): 159–244. doi:10.1016/0010-8545(82)85003-0.

Karlsson, B.Göran, Roland Aasa, Bo G. Malmström, and Lennart G. Lundberg. 1989. "Rack-induced Bonding in Blue Copper Proteins: Spectroscopic Properties and Reduction Potential of the Azurin Mutant Met-121 → Leu." *FEBS Letters* 253 (1–2): 99–102. doi:10.1016/0014-5793(89)80938-X.

Katayama, Yoko, Kanako Hashimoto, Hiroshi Nakayama, Hiroyuki Mino, Masaki Nojiri, Taka-aki Ono, Hiroshi Nyunoya, Masafumi Yohda, Koji Takio, and Masafumi Odaka. 2005. "Thiocyanate Hydrolase Is a Cobalt-Containing Metalloenzyme with a Cysteine-Sulfinic Acid Ligand." *J. Am. Chem. Soc.* 128 (3): 728–729. doi:10.1021/ja057010q.

Kennedy, M. L., and B. R. Gibney. 2001. "Metalloprotein and redox protein design." *Curr. Opin. Struct. Biol.* 11 (4) (August): 485–490. doi:10.1016/S0959-440X(00)00237-2.

Kennedy, Michelle L., and Brian R. Gibney. 2002. "Proton Coupling to [4Fe-4S]$^{2+/+}$ and [4Fe-4Se]$^{2+/+}$ Oxidation and Reduction in a Designed Protein." *J. Am. Chem. Soc.* 124 (24): 6826–6827. doi:10.1021/ja0171613.

Kincaid, James R., and Kazuo Nakamoto. 1976. “Vibrational Spectra and Normal Coordinate Analysis of Bis(glycino) Complexes with Ni(II), Cu(II) and Co(II).” *Spectrochim. Acta Part A* 32 (2): 277–283. doi:10.1016/0584-8539(76)80078-5.

Kirk, Ole, Torben Vedel Borchert, and Claus Crone Fuglsang. 2002. “Industrial Enzyme Applications.” *Curr. Opin. Biotechnol.* 13 (4): 345–351. doi:10.1016/S0958-1669(02)00328-2.

Kobayashi, Michihiko, Toru Nagasawa, and Hideaki Yamada. 1992. “Enzymatic Synthesis of Acrylamide: a Success Story Not yet Over.” *Trends Biotechnol.* 10 (0): 402–408. doi:10.1016/0167-7799(92)90283-2.

Kobayashi, Michihiko, and Sakayu Shimizu. 1998. “Metalloenzyme Nitrile Hydratase: Structure, Regulation, and Application to Biotechnology.” *Nat. Biotechnol.* 16 (8): 733–736. doi:10.1038/nbt0898-733.

Koder, Ronald L., J. L. Ross Anderson, Lee A. Solomon, Konda S. Reddy, Christopher C. Moser, and P. Leslie Dutton. 2009. “Design and Engineering of an O_2 Transport Protein.” *Nature* 458 (7236): 305–309. doi:10.1038/nature07841.

Koike, K., H. Hori, M. Ishizuka, J. R. Westwell, K. Takeuchi, T. Ibusuki, K. Enjouji, H. Konno, K. Sakamoto, and O. Ishitani. 1997. “Key process of the photocatalytic reduction of CO_2 using $[Re(4,4\text{ '-X-2-bipyridine})(CO)_3PR_3]^+$ ($X = CH_3$, H, CF_3; PR_3 = phosphorus ligands): Dark reaction of the one-electron-reduced complexes with CO_2.” *Organometallics* 16 (26): 5724–5729. doi:10.1021/om970608p.

Komeda, Hidenobu, Michihiko Kobayashi, and Sakayu Shimizu. 1997. “A Novel Transporter Involved in Cobalt Uptake.” *Proc. Natl. Acad. Sci. USA* 94 (1): 36–41.

Korendovych, Ivan V., Alessandro Senes, Yong Ho Kim, James D. Lear, H. Christopher Fry, Michael J. Therien, J. Kent Blasie, F. Ann Walker, and William F. DeGrado. 2010. “De Novo Design and Molecular Assembly of a Transmembrane Diporphyrin-Binding Protein Complex.” *J. Am. Chem. Soc.* 132 (44): 15516–15518. doi:10.1021/ja107487b.

Kovacs, Julie A. 2004. “Synthetic Analogues of Cysteinate-Ligated Non-Heme Iron and Non-Corrinoid Cobalt Enzymes.” *Chem. Rev.* 104 (2): 825–848. doi:10.1021/cr020619e.

Kung, Irene, Dirk Schweitzer, Jason Shearer, Wendy D. Taylor, Henry L. Jackson, Scott Lovell, and Julie A. Kovacs. 2000. “How Do Oxidized Thiolate Ligands

Affect the Electronic and Reactivity Properties of a Nitrile Hydratase Model Compound?" *J. Am. Chem. Soc.* 122 (34): 8299–8300. doi:10.1021/ja0017561.

Langen, R., I. J. Chang, J. P. Germanas, J. H. Richards, Winkler, and H. B. Gray. 1995. "Electron Tunneling in Proteins: Coupling Through a Beta Strand." *Science* 268 (5218): 1733–1735. doi:10.1126/science.7792598.

Laplaza, Catalina E., and R. H. Holm. 2001. "Helix−Loop−Helix Peptides as Scaffolds for the Construction of Bridged Metal Assemblies in Proteins: The Spectroscopic A-Cluster Structure in Carbon Monoxide Dehydrogenase." *J. Am. Chem. Soc.* 123 (42): 10255–10264. doi:10.1021/ja010851m.

Lee, Chien-Ming, Chien-Hong Chen, Hao-Wen Chen, Jo-Lu Hsu, Gene-Hsiang Lee, and Wen-Feng Liaw. 2005. "Nitrosylated Iron−Thiolate−Sulfinate Complexes with $\{Fe(NO)\}_{6/7}$ Electronic Cores: Relevance to the Transformation Between the Active and Inactive NO-Bound Forms of Iron-Containing Nitrile Hydratases." *Inorg. Chem.* 44 (19): 6670–6679. doi:10.1021/ic050108l.

Lee, Chien-Ming, Chung-Hung Hsieh, Amitava Dutta, Gene-Hsiang Lee, and Wen-Feng Liaw. 2003. "Oxygen Binding to Sulfur in Nitrosylated Iron−Thiolate Complexes: Relevance to the Fe-Containing Nitrile Hydratases." *J. Am. Chem. Soc.* 125 (38): 11492–11493. doi:10.1021/ja035292t.

Lever, A. B. 1986. *Inorganic Electronic Spectroscopy*. Elsevier.

Li, Z., Y. Ohki, and K. Tatsumi. 2005. "Dithiolato-Bridged Dinuclear Iron-Nickel Complexes $[Fe(CO)_2(CN)_2(\mu\text{-}SCH_2CH_2CH_2S)Ni(S_2CNR_2)]^-$ Modeling the Active Site of [NiFe] Hydrogenase." *J. Am. Chem. Soc.* 127 (25): 8950–8951.

Liebgott, Pierre-Pol, Antonio L. de Lacey, Bénédicte Burlat, Laurent Cournac, Pierre Richaud, Myriam Brugna, Victor M. Fernandez, et al. 2011. "Original Design of an Oxygen-Tolerant [NiFe] Hydrogenase: Major Effect of a Valine-to-Cysteine Mutation Near the Active Site." *J. Am. Chem. Soc.* 133 (4): 986–997. doi:10.1021/ja108787s.

Lippard, Stephen J., and Jeremy Mark Berg. 1994. *Principles of Bioinorganic Chemistry*. University Science Books.

Liu, Yao, David B. Turner, Tanya N. Singh, Alfredo M. Angeles-Boza, Abdellatif Chouai, Kim R. Dunbar, and Claudia Turro. 2008. "Ultrafast Ligand Exchange: Detection of a Pentacoordinate Ru(II) Intermediate and Product Formation." *J. Am. Chem. Soc.* 131 (1): 26–27. doi:10.1021/ja806860w.

Lu, Yi, Natasha Yeung, Nathan Sieracki, and Nicholas M. Marshall. 2009. "Design of Functional Metalloproteins." *Nature* 460 (7257): 855–862. doi:10.1038/nature08304.

Magnuson, Ann, Magnus Anderlund, Olof Johansson, Peter Lindblad, Reiner Lomoth, Tomas Polivka, Sascha Ott, et al. 2009. "Biomimetic and Microbial Approaches to Solar Fuel Generation." *Acc. Chem. Res.* 42 (12): 1899–1909. doi:10.1021/ar900127h.

Masitas, César A., Manoj Kumar, Mark S. Mashuta, Pawel M. Kozlowski, and Craig A. Grapperhaus. 2010. "Controlled Sulfur Oxygenation of the Ruthenium Dithiolate (4,7-Bis-(2′-methyl-2′-mercaptopropyl)-1-thia-4,7-diazacyclononane)$RuPPh_3$ Under Limiting O_2 Conditions Yields Thiolato/Sulfinato, Sulfenato/Sulfinato, and Bis-Sulfinato Derivatives." *Inorg. Chem.* 49 (23): 10875–10881. doi:10.1021/ic101221z.

Matsuura, N., T. Kawarnoto, and T. Konno. 2006. "Conversion of 2-aminoethanethiolate (aet) to 2-benzoylaminoethanethiolate (L) in a S-bridged diruthenium (II) complex composed of two cis-$[Ru(bpy)_2]$ units. Crystal structures of ΔΔ/ΛΛ-$[\{Ru(bpy)_2\}_2(\mu\text{-Haet})_2]^{4+}$ and ΔΔ/ΛΛ-$[\{Ru(bpy)_2\}_2(\mu\text{-L})_2]^{2+}$." *Bull. Chem. Soc. Jpn.* 79 (2): 297–299. doi:10.1246/bcsj.749.297.

Matsuura, Noriyuki, Asako Igashira-Kamiyama, Tatsuya Kawamoto, and Takumi Konno. 2005. "Meso and Racemic Isomers of a New S-Bridged Diruthenium(II) Complex with Pendant Aminoalkyl Groups." *Chem. Lett.* 34 (9): 1252–1253.

May, Sheldon W., and Jong-Yuan Kuo. 1978. "Preparation and Properties of cobalt(II) Rubredoxin." *Biochemistry* 17 (16): 3333–3338. doi:10.1021/bi00609a025.

Mayoh, Bryan, and Peter Day. 1978. "The Excited States of Bipyridyl and Phenanthroline Complexes of Fe(III), Ru(II) and Ru(III): A Molecular Orbital Study." *Theor. Chem. Acc*. 49 (3): 259–275. doi:10.1007/BF00550036.

McCusker, James K. 2003. "Femtosecond Absorption Spectroscopy of Transition Metal Charge-Transfer Complexes." *Acc. Chem. Res.* 36 (12): 876–887. doi:10.1021/ar030111d.

McIntosh, Chelsea L., Frauke Germer, Rüdiger Schulz, Jens Appel, and Anne K. Jones. 2011. "The [NiFe]-Hydrogenase of the Cyanobacterium Synechocystis Sp. PCC 6803 Works Bidirectionally with a Bias to H_2 Production." *J. Am. Chem. Soc.* 133 (29) (July 27): 11308–11319. doi:10.1021/ja203376y.

Miller, Ronald R., Warren W. Brandt, Marina Puke, and O.S.F. Puke. 1955. "Metal-Amine Coördination Compounds. V. The Ruthenium-2,2'-Bipyridine System1,2,3." *J. Am. Chem. Soc.* 77 (12): 3178–3180. doi:10.1021/ja01617a003.

Mines, G. A., M. J. Bjerrum, M. G. Hill, D. R. Casimiro, I. J. Chang, J. R. Winkler, and H. B. Gray. 1996. "Rates of heme oxidation and reduction in Ru(His33)cytochrome c at very high driving forces." *J. Am. Chem. Soc.* 118 (8): 1961–1965. doi:10.1021/ja9519243.

Mirza, Shaukat A., Michelle A. Pressler, Manoj Kumar, Roberta O. Day, and Michael J. Maroney. 1993. "Oxidation of Nickel Thiolate Ligands by Dioxygen." *Inorg. Chem.* 32 (6): 977–987. doi:10.1021/ic00058a038.

Miyanaga, Akimasa, Shinya Fushinobu, Kiyoshi Ito, and Takayoshi Wakagi. 2001. "Crystal Structure of Cobalt-Containing Nitrile Hydratase." *Biochem. Biophys. Res. Commun.* 288 (5): 1169–1174. doi:10.1006/bbrc.2001.5897.

Moore, David T., Bryan W. Berger, and William F. DeGrado. 2008. "Protein-Protein Interactions in the Membrane: Sequence, Structural, and Biological Motifs." *Structure* 16 (7): 991–1001. doi:10.1016/j.str.2008.05.007.

Morel, F. M. M., and N. M. Price. 2003. "The Biogeochemical Cycles of Trace Metals in the Oceans." *Science* 300 (5621): 944–947. doi:10.1126/science.1083545.

Moucheron, Cecile. 2009. "From cisplatin to photoreactive Ru complexes: targeting DNA for biomedical applications." *New J. Chem.* 33 (2): 235–245. doi:10.1039/b817016a.

Murakami, Taku, Masaki Nojiri, Hiroshi Nakayama, Naoshi Dohmae, Koji Takio, Masafumi Odaka, Isao Endo, Teruyuki Nagamune, and Masafumi Yohda. 2000. "Post-translational Modification Is Essential for Catalytic Activity of Nitrile Hydratase." *Protein Sci.* 9 (5): 1024–1030. doi:10.1110/ps.9.5.1024.

Musgrave, Kristin B., Catalina E. Laplaza, R. H. Holm, Britt Hedman, and Keith O. Hodgson. 2002. "Structural Characterization of Metallopeptides Designed as Scaffolds for the Stabilization of Nickel(II)-Fe4S4 Bridged Assemblies by X-ray Absorption Spectroscopy." *J. Am. Chem. Soc.* 124 (12): 3083–3092. doi:10.1021/ja011861q.

Nagashima, Shigehiro, Masayoshi Nakasako, Naoshi Dohmae, Masanari Tsujimura, Koji Takio, Masafumi Odaka, Masafumi Yohda, Nobuo Kamiya, and Isao Endo. 1998. "Novel Non-heme Iron Center of Nitrile Hydratase with

a Claw Setting of Oxygen Atoms." *Nat. Struct. Mol. Biol.* 5 (5): 347–351. doi:10.1038/nsb0598-347.

Nakamoto, Kazuo. 1986. *Infrared and Raman Spectra of Inorganic and Coordination Compounds*. 4th ed. Milawukee, Wisconsin: John Wiley & Sons.

Nakasako, Masayoshi, Masafumi Odaka, Masafumi Yohda, Naoshi Dohmae, Koji Takio, Nobuo Kamiya, and Isao Endo. 1999. "Tertiary and Quaternary Structures of Photoreactive Fe-Type Nitrile Hydratase from Rhodococcus Sp. N-771: Roles of Hydration Water Molecules in Stabilizing the Structures and the Structural Origin of the Substrate Specificity of the Enzyme." *Biochemistry* 38 (31): 9887–9898. doi:10.1021/bi982753s.

Nakashini, Koji, Nina Berova,, and Robert Woody W. 1994. *Circular Dichroism: Principles and Applications*. VCH publishers.

Nanda, Vikas, and Ronald L. Koder. 2010. "Designing Artificial Enzymes by Intuition and Computation." *Nat. Chem.* 2 (1): 15–24. doi:10.1038/nchem.473.

Natsuaki, Kazuhiro, Motohiro Nakano, Gen-etsu Matsubayashi, and Ryuichi Arakawa. 2000. "Preparation and Spectroscopic Properties of bis(2,2′-bipyridine)-ruthenium(II) Complexes and Related Complexes with Sulfur-rich Dithiolato Ligands and Electrical Conductivities of Their Oxidized Species." *Inorg. Chim. Acta* 299 (1): 112–117. doi:10.1016/S0020-1693(99)00475-2.

Neupane, Kosh P., Kristie Gearty, Ashish Francis, and Jason Shearer. 2007. "Probing Variable Axial Ligation in Nickel Superoxide Dismutase Utilizing Metallopeptide-Based Models: Insight into the Superoxide Disproportionation Mechanism." *J. Am. Chem. Soc.* 129 (47): 14605–14618. doi:10.1021/ja0731625.

Neupane, Kosh P., and Jason Shearer. 2006. "The Influence of Amine/Amide Versus Bisamide Coordination in Nickel Superoxide Dismutase." *Inorg. Chem.* 45 (26): 10552–10566. doi:10.1021/ic061156o.

Noveron, Juan C., Marilyn M. Olmstead, and Pradip K. Mascharak. 1999. "Co(III) Complexes with Carboxamido N and Thiolato S Donor Centers: Models for the Active Site of Co-Containing Nitrile Hydratases." *J. Am. Chem. Soc.* 121 (14): 3553–3554. doi:10.1021/ja9833523.

Noveron, Juan C., Marilyn M. Olmstead, and Pradip K. Mascharak. 2001. "A Synthetic Analogue of the Active Site of Fe-Containing Nitrile Hydratase with Carboxamido N and Thiolato S as Donors: Synthesis, Structure, and

Reactivities." *J. Am. Chem. Soc.* 123 (14): 3247–3259. doi:10.1021/ja001253v.

Ogo, Seiji, Ryota Kabe, Keiji Uehara, Bunsho Kure, Takashi Nishimura, Saija C. Menon, Ryosuke Harada, et al. 2007. "A Dinuclear Ni(μ-H)Ru Complex Derived from H_2." *Science* 316 (5824): 585–587. doi:10.1126/science.1138751.

Ohki, Yasuhiro, and Kazuyuki Tatsumi. 2011. "Thiolate-Bridged Iron-Nickel Models for the Active Site of [NiFe] Hydrogenase." *Eur. J. Inorg. Chem.* (7) (March): 973–985. doi:10.1002/ejic.201001087.

Okamoto, Sachi, and Lindsay D. Eltis. 2011. "The biological occurrence and trafficking of cobalt." *Metallomics* 3 (10): 963–970. doi:10.1039/c1mt00056j.

Orgel, L. E. 1961. "715. Double Bonding in Chelated Metal Complexes." *J. Chem. Soc.*: 3683. doi:10.1039/jr9610003683.

Osterman, Tomas, Maria Abrahamsson, Hans-Christian Becker, Leif Hammarstrom, and Petter Persson. 2012. "Influence of Triplet State Multidimensionality on Excited State Lifetimes of Bis-tridentate Ru-II Complexes: A Computational Study." *J. Phys. Chem. A* 116 (3): 1041–1050. doi:10.1021/jp207044a.

Ozawa, Hironobu, Masa-aki Haga, and Ken Sakai. 2006. "A Photo-Hydrogen-Evolving Molecular Device Driving Visible-Light-Induced EDTA-Reduction of Water into Molecular Hydrogen." *J. Am. Chem. Soc.* 128 (15): 4926–4927. doi:10.1021/ja058087h.

Paulsen, Candice E., and Kate S. Carroll. 2009. "Orchestrating Redox Signaling Networks Through Regulatory Cysteine Switches." *ACS Chem. Biol.* 5 (1): 47–62. doi:10.1021/cb900258z.

Perra, Alessandro, E. Stephen Davies, Jason R. Hyde, Qiang Wang, Jonathan McMaster, and Martin Schroder. 2006. "Electrocatalytic Production of Hydrogen by a Synthetic Model of [NiFe] Hydrogenases." *Chem. Commun.* (10): 1103–1105.

Peters, J. W., W. N. Lanzilotta, B. J. Lemon, and L. C. Seefeldt. 1998. "X-ray crystal structure of the Fe-only hydrogenase (Cpl) from Clostridium pasteurianum to 1.8 angstrom resolution." *Science* 282 (5395): 1853–1858. doi:10.1126/science.282.5395.1853.

Petros, Amy K., Amit R. Reddi, Michelle L. Kennedy, Alison G. Hyslop, and Brian R. Gibney. 2006. "Femtomolar Zn(II) Affinity in a Peptide-Based

Ligand Designed To Model Thiolate-Rich Metalloprotein Active Sites." *Inorg. Chem.* 45 (25): 9941–9958. doi:10.1021/ic052190q.

Petros, Amy K., Sarah E. Shaner, Alison L. Costello, David L. Tierney, and Brian R. Gibney. 2004. "Comparison of Cysteine and Penicillamine Ligands in a Co(II) Maquette." *Inorg. Chem.* 43 (16): 4793–4795. doi:10.1021/ic0497679.

Pietrzyk, Piotr, Monika Srebro, Mariusz Radoń, Zbigniew Sojka, and Artur Michalak. 2011. "Spin Ground State and Magnetic Properties of Cobalt(II): Relativistic DFT Calculations Guided by EPR Measurements of Bis(2,4-acetylacetonate)cobalt(II)-Based Complexes." *J. Phys. Chem. A* 115 (11): 2316–2324. doi:10.1021/jp109524t.

Rachford, Aaron A., and Jeffrey J. Rack. 2006. "Picosecond Isomerization in Photochromic Ruthenium−Dimethyl Sulfoxide Complexes." *J. Am. Chem. Soc.* 128 (44): 14318–14324. doi:10.1021/ja0641305.

Rampersad, Marilyn V., Stephen P. Jeffery, Melissa L. Golden, Jonghyuk Lee, Joseph H. Reibenspies, Donald J. Darensbourg, and Marcetta Y. Darensbourg. 2005. "Characterization of Steric and Electronic Properties of NiN2S2 Complexes as S-Donor Metallodithiolate Ligands." *J. Am. Chem. Soc.* 127 (49): 17323–17334. doi:10.1021/ja055051g.

Rat, M., R. Alves de Sousa, J. Vaissermann, P. Leduc, D. Mansuy, and I. Artaud. 2001. "Clean Oxidation of Thiolates to Sulfinates in a Four-coordinate CoIII Complex with a Mixed Carboxamido N–thiolato S Donor Set: Relevance to Nitrile Hydratase." *J. Inorg. Biochem.* 84 (3–4): 207–213. doi:10.1016/S0162-0134(01)00181-7.

Rau, Sven, Bernhard Schäfer, Dieter Gleich, Ernst Anders, Manfred Rudolph, Manfred Friedrich, Helmar Görls, William Henry, and Johannes G. Vos. 2006. "A Supramolecular Photocatalyst for the Production of Hydrogen and the Selective Hydrogenation of Tolane." *Angew. Chem. Intl. Ed.* 45 (37): 6215–6218. doi:10.1002/anie.200600543.

Reddi, Amit R., Tabitha R. Guzman, Robert M. Breece, David L. Tierney, and Brian R. Gibney. 2007. "Deducing the Energetic Cost of Protein Folding in Zinc Finger Proteins Using Designed Metallopeptides." *J. Am. Chem. Soc.* 129 (42): 12815–12827. doi:10.1021/ja073902+.

Rees, Douglas C. 2002. "Great Metalloclusters in Enzymology." *Ann. Rev. Biochem.* 71 (1): 221–246. doi:10.1146/annurev.biochem.71.110601.135406.

Reynal, Anna, and Emilio Palomares. 2011. “Ruthenium Polypyridyl Sensitisers in Dye Solar Cells Based on Mesoporous TiO_2.” *Eur. J. Inorg. Chem.* 2011 (29): 4509–4526. doi:10.1002/ejic.201100516.

Rizzi, Alberto C., Carlos D. Brondino, Rafael Calvo, Ricardo Baggio, María T. Garland, and Raul E. Rapp. 2003. “Structure and Magnetic Properties of Layered High-Spin Co(II)(*l*-threonine)$_2$(H_2O)$_2$.” *Inorg. Chem.* 42 (14): 4409–4416. doi:10.1021/ic026111b.

Roelfes, Gerard. 2007. “DNA and RNA Induced Enantioselectivity in Chemical Synthesis.” *Mol. Biosyst.* 3 (2): 126–135. doi:10.1039/B614527B.

Root, Michael J., B. Patrick Sullivan, Thomas J. Meyer, and Edward Deutsch. 1985. “Thioether, Thiolato, and 1,1-dithioato Complexes of bis(2,2’-bipyridine)ruthenium(II) and bis(2,2’-bipyridine)osmium(II).” *Inorg. Chem.* 24 (18): 2731–2739. doi:10.1021/ic00212a006.

Rosati, Fiora, and Gerard Roelfes. 2010. “Artificial Metalloenzymes.” *ChemCatChem* 2 (8): 916–927. doi:10.1002/cctc.201000011.

Roth, Lauren E., Joey C. Nguyen, and F. Akif Tezcan. 2010. “ATP- and Iron−Protein-Independent Activation of Nitrogenase Catalysis by Light.” *J. Am. Chem. Soc.* 132 (39): 13672–13674. doi:10.1021/ja1071866.

Roy, Souvik, Sandip Shinde, G. Alexander Hamilton, Hilairy E. Hartnett, and Anne K. Jones. 2011. “Artificial [FeFe]-Hydrogenase: On Resin Modification of an Amino Acid to Anchor a Hexacarbonyldiiron Cluster in a Peptide Framework.” *Eur. J. Inorg. Chem.* 2011 (7): 1050–1055. doi:10.1002/ejic.201000979.

Sano, Yohei, Akira Onoda, and Takashi Hayashi. 2011. “A hydrogenase model system based on the sequence of cytochrome c: photochemical hydrogen evolution in aqueous media.” *Chem. Communi.* 47 (29): 8229–8231. doi:10.1039/c1cc11157d.

Sano, Yohei, Akira Onoda, and Takashi Hayashi. 2012. “Photocatalytic hydrogen evolution by a diiron hydrogenase model based on a peptide fragment of cytochrome c(556) with an attached diiron carbonyl cluster and an attached ruthenium photosensitizer.” *J. Inorg. Biochem.* 108: 159–162. doi:10.1016/j.jinorgbio.2011.07.010.

Schühle, Daniel T., Joop A. Peters, and Jürgen Schatz. 2011. “Metal Binding Calixarenes with Potential Biomimetic and Biomedical Applications.” *Coord. Chem. Rev.* 255 (23–24): 2727–2745. doi:10.1016/j.ccr.2011.04.005.

Schulze, Birgit, and Marcel G Wubbolts. 1999. “Biocatalysis for Industrial Production of Fine Chemicals.” *Curr. Opin. Biotechnol.* 10 (6): 609–615. doi:10.1016/S0958-1669(99)00042-7.

Shearer, J., and R. S. Scarrow. 2011. *EXAFS123*. University of Nevada, Reno.

Shearer, Jason, Paige E. Callan, and Justina Amie. 2010. “Use of Metallopeptide Based Mimics Demonstrates That the Metalloprotein Nitrile Hydratase Requires Two Oxidized Cysteinates for Catalytic Activity.” *Inorg. Chem.* 49 (19): 9064–9077. doi:10.1021/ic101765h.

Shearer, Jason, Ahmad Dehestani, and Franklin Abanda. 2008. “Probing Variable Amine/Amide Ligation in $Ni^{II}N_2S_2$ Complexes Using Sulfur K-Edge and Nickel L-Edge X-ray Absorption Spectroscopies: Implications for the Active Site of Nickel Superoxide Dismutase.” *Inorg. Chem.* 47 (7) (April 1): 2649–2660. doi:10.1021/ic7019878.

Shearer, Jason, Irene Y. Kung, Scott Lovell, Werner Kaminsky, and Julie A. Kovacs. 2000. “Why Is There an ‘Inert’ Metal Center in the Active Site of Nitrile Hydratase? Reactivity and Ligand Dissociation from a Five-Coordinate Co(III) Nitrile Hydratase Model.” *J. Am. Chem. Soc.* 123 (3): 463–468. doi:10.1021/ja002642s.

Shearer, Jason. 2012. *Personal Communication*.

Sheldrick, George M. 2008. “A Short History of SHELX.” *Acta Crystallogr., Sect. A* 64 (1): 112–122. doi:10.1107/S0108767307043930.

Shiga, Daigo, Daisuke Nakane, Tomohiko Inomata, Yasuhiro Funahashi, Hideki Masuda, Akihiro Kikuchi, Masayuki Oda, et al. 2010. “Creation of a Type 1 Blue Copper Site Within a De Novo Coiled-Coil Protein Scaffold.” *J. Am. Chem. Soc.* 132 (51): 18191–18198. doi:10.1021/ja106263y.

Sigel, Helmut, and Roland Sigel, eds. 2005. *Metal Ions in Biological Systems, Volume 43 - Biogeochemical Cycles of Elements*. 1st ed. CRC Press.

Solomon, Edward I. 2006. “Spectroscopic Methods in Bioinorganic Chemistry: Blue to Green to Red Copper Sites.” *Inorg. Chem.* 45 (20): 8012–8025. doi:10.1021/ic060450d.

Solomon, Edward I., and Ryan G. Hadt. 2011. “Recent advances in understanding blue copper proteins.” *Coord. Chem. Rev.* 255 (7-8): 774–789. doi:10.1016/j.ccr.2010.12.008.

Solomon, Edward I., and A. B. P. Lever. 2006. *Inorganic Electronic Structure and Spectroscopy*. Vol. I and II. 2 vols. Hoboken, New Jersey: Wiley Interscience.

Solomon, Edward I., Kevin W. Penfield, Andrew A. Gewirth, Michael D. Lowery, Susan E. Shadle, Jeffrey A. Guckert, and Louis B. LaCroix. 1996. "Electronic Structure of the Oxidized and Reduced Blue Copper Sites: Contributions to the Electron Transfer Pathway, Reduction Potential, and Geometry." *Inorg. Chim. Acta* 243 (1–2): 67–78. doi:10.1016/0020-1693(95)04893-6.

Song, Liya, Mingzhu Wang, Jiaji Shi, Zhiquan Xue, Mei-Xiang Wang, and Shijun Qian. 2007. "High Resolution X-ray Molecular Structure of the Nitrile Hydratase from Rhodococcus Erythropolis AJ270 Reveals Posttranslational Oxidation of Two Cysteines into Sulfinic Acids and a Novel Biocatalytic Nitrile Hydration Mechanism." *Biochem. Biophys. Res. Commun.* 362 (2): 319–324. doi:10.1016/j.bbrc.2007.07.184.

Srinivasan, V., E. I. Stiefel, A. Elsberry, and R. A. Walton. 1979. "X-ray Photoelectron Spectra of Inorganic Molecules. 21. Sulfur 2p Chemical Shifts Associated with the Binding of Thiol and Thioether Groups of Transition Metal Ions." *J. Am. Chem. Soc.* 101 (10): 2611–2614. doi:10.1021/ja00504a018.

Stebler-Röthlisberger, Monika, and Andreas Ludi. 1986. "Preparative Chemistry with $[Ru(\eta^6\text{-arene})(H_2O)_3]^{2+}$: Bis-arene and Monobenzene Complexes with O, N and S Donors." *Polyhedron* 5 (6): 1217–1221. doi:10.1016/S0277-5387(00)81395-9.

Stibrany, Robert T., Ronald Fikar, Mark Brader, Marc N. Potenza, Joseph A. Potenza, and Harvey J. Schugar. 2002. "Charge-Transfer Spectra of Structurally Characterized Mixed-Valence Thiolate-Bridged Cu(I)/Cu(II) Cluster Complexes." *Inorg. Chem.* 41 (20): 5203–5215. doi:10.1021/ic020156v.

Stoll, Stefan, and Arthur Schweiger. 2006. "EasySpin, a Comprehensive Software Package for Spectral Simulation and Analysis in EPR." *J. Magn. Reson.* 178 (1): 42–55. doi:10.1016/j.jmr.2005.08.013.

Sullivan, B. P., D. J. Salmon, and T. J. Meyer. 1978. "Mixed Phosphine 2,2'-bipyridine Complexes of Ruthenium." *Inorg. Chem.* 17 (12): 3334–3341. doi:10.1021/ic50190a006.

Svetlitchnyi, Vitali, Holger Dobbek, Wolfram Meyer-Klaucke, Thomas Meins, Bärbel Thiele, Piero Römer, Robert Huber, and Ortwin Meyer. 2004. "A Functional Ni-Ni-[4Fe-4S] Cluster in the Monomeric acetyl-CoA Synthase

from Carboxydothermus Hydrogenoformans." *Proc. Natl. Acad. Sci. USA* 101 (2): 446–451. doi:10.1073/pnas.0304262101.

Sykes, Ag. 1991. "Plastocyanin and the Blue Copper Proteins." *Struct. Bond.* 75: 175–224.

Tietze, Daniel, Hergen Breitzke, Diana Imhof, Erika Kothe, James Weston, and Gerd Buntkowsky. 2009. "New Insight into the Mode of Action of Nickel Superoxide Dismutase by Investigating Metallopeptide Substrate Models." *Chem. Eur. J.* 15 (2): 517–523. doi:10.1002/chem.200800870.

Umena, Yasufumi, Keisuke Kawakami, Jian-Ren Shen, and Nobuo Kamiya. 2011. "Crystal Structure of Oxygen-evolving Photosystem II at a Resolution of 1.9 Å." *Nature* 473 (7345): 55–60. doi:10.1038/nature09913.

VanZile, Michael L., Nathaniel J. Cosper, Robert A. Scott, and David P. Giedroc. 2000. "The Zinc Metalloregulatory Protein Synechococcus PCC7942 SmtB Binds a Single Zinc Ion Per Monomer with High Affinity in a Tetrahedral Coordination Geometry." *Biochemistry* 39 (38): 11818–11829. doi:10.1021/bi001140o.

Vasak, Milan, Jeremias H. R. Kaegi, Barton Holmquist, and Bert L. Vallee. 1981. "Spectral Studies of cobalt(II)- and nickel(II)-metallothionein." *Biochemistry* 20 (23): 6659–6664. doi:10.1021/bi00526a021.

Vincent, Kylie A., James A. Cracknell, Oliver Lenz, Ingo Zebger, Bärbel Friedrich, and Fraser A. Armstrong. 2005. "Electrocatalytic Hydrogen Oxidation by an Enzyme at High Carbon Monoxide or Oxygen Levels." *Proc. Natl. Acad. Sci. USA* 102 (47): 16951–16954. doi:10.1073/pnas.0504499102.

Volbeda, Anne, Marie-Helene Charon, Claudine Piras, E. Claude Hatchikian, Michel Frey, and Juan C. Fontecilla-Camps. 1995. "Crystal Structure of the Nickel-iron Hydrogenase from Desulfovibrio Gigas." *Nature* 373 (6515) (February 16): 580–587. doi:10.1038/373580a0.

Volbeda, Anne, Elsa Garcin, Claudine Piras, Antonio L. de Lacey, Victor M. Fernandez, E. Claude Hatchikian, Michel Frey, and Juan Carlos Fontecilla-Camps. 1996. "Structure of the [NiFe] Hydrogenase Active Site: Evidence for Biologically Uncommon Fe Ligands." *J. Am. Chem. Soc.* 118 (51) (January 1): 12989–12996. doi:10.1021/ja962270g.

Vos, Johannes G., and John M. Kelly. 2006. "Ruthenium polypyridyl chemistry; from basic research to applications and back again." *Dalton Trans.* (41): 4869–4883. doi:10.1039/b606490f.

Waldron, Kevin J., Julian C. Rutherford, Dianne Ford, and Nigel J. Robinson. 2009. “Metalloproteins and Metal Sensing.” *Nature* 460 (7257): 823–830. doi:10.1038/nature08300.

Walsh, Jerry L., and Bill. Durham. 1982. “Trans Isomers of ruthenium(II) Complexes Containing Two Bipyridine Ligands.” *Inorg. Chem.* 21 (1): 329–332. doi:10.1021/ic00131a060.

Wang, Qiang, J. Elaine Barclay, Alexander J. Blake, E. Stephen Davies, David J. Evans, Andrew C. Marr, Eric J. L. McInnes, Jonathan McMaster, Claire Wilson, and Martin Schröder. 2004. “The Synthesis and Electronic Structure of a Novel [Ni‘S_4’$Fe_2(CO)_6$] Radical Cluster: Implications for the Active Site of the [NiFe] Hydrogenases.” *Chem. Eur. J.* 10 (14): 3384–3396. doi:10.1002/chem.200305738.

Wasielewski, M. R. 1992. “Photoinduced Electron-transfer in Supramolecular Systems for Artificial Photosynthesis.” *Chem. Rev.* 92 (3) (May): 435–461. doi:10.1021/cr00011a005.

Weber, Walter, and Peter C. Ford. 1986. “Photosubstitution Reactions of the ruthenium(II) Arene Complexes Ru(η^6-arene)L_3^{2+} (L = Ammonia or Water) in Aqueous Solution.” *Inorg. Chem.* 25 (8): 1088–1092. doi:10.1021/ic00228a007.

Willner, I., Y.-M. Yan, B. Willner, and R. Tel-Vered. 2009. “Integrated Enzyme-Based Biofuel Cells–A Review.” *Fuel Cells* 9 (1): 7–24. doi:10.1002/fuce.200800115.

Works, Carmen F. 2007. “Synthesis, Purification, and Characterization of a M-(1,3-propanedithiolato)-hexacarbonyldiiron. Laboratory Experiment or Mini-Project for Inorganic Chemistry or Integrated Laboratory.” *J. Chem. Edu.* 84 (5): 836. doi:10.1021/ed084p836.

Wuerges, J. 2004. “Crystal Structure of Nickel-containing Superoxide Dismutase Reveals Another Type of Active Site.” *Proc. Natl. Acad. Sci. USA* 101 (23): 8569–8574. doi:10.1073/pnas.0308514101.

Xie, Fei, Duncan E.K. Sutherland, Martin J. Stillman, and Michael Y. Ogawa. 2010. “Cu(I) Binding Properties of a Designed Metalloprotein.” *J. Inorg. Biochem.*104 (3): 261–267. doi:10.1016/j.jinorgbio.2009.12.005.

Yamada, Hideaki, and Michihiko Kobayashi. 1996. “Nitrile Hydratase and Its Application to Industrial Production of Acrylamide.” *Biosci. Biotechnol. Biochem.* 60 (9): 1391–1400.

Yoshimura, Takashi, Atsushi Shinohara, Masakazu Hirotsu, Keiji Ueno, and Takumi Konno. 2006. "Sulfur-bridged dinuclear and tetranuclear complexes consisting of *cis*-$[Ru(bpy)_2]^{2+}$ and *cis*-$[Ni(aet)_2]$ units." *Bull. Chem. Soc. Jpn.* 79 (11): 1745–1747. doi:10.1246/bcsj.79.1745.

Zastrow, Melissa L., Anna F. A. Peacock, Jeanne A. Stuckey, and Vincent L. Pecoraro. 2012. "Hydrolytic Catalysis and Structural Stabilization in a Designed Metalloprotein." *Nat. Chem.* 4 (2): 118–123. doi:10.1038/nchem.1201.

Zhang, Ji, Xiang-Guang Meng, Xian-Cheng Zeng, and Xiao-Qi Yu. 2009. "Metallomicellar Supramolecular Systems and Their Applications in Catalytic Reactions." *Coord. Chem. Rev.* 253 (17–18): 2166–2177. doi:10.1016/j.ccr.2008.11.019.

Zheng, Ren-Chao, Yu-Guo Zheng, Yin-Chu Shen, and Michael C. Flickinger. 2009. "Acrylamide, Microbial Production by Nitrile Hydratase." In *Encyclopedia of Industrial Biotechnology*. John Wiley & Sons, Inc.

Zhou, Zhemin, Yoshiteru Hashimoto, Tianwei Cui, Yumi Washizawa, Hiroyuki Mino, and Michihiko Kobayashi. 2010. "Unique Biogenesis of High-Molecular Mass Multimeric Metalloenzyme Nitrile Hydratase: Intermediates and a Proposed Mechanism for Self-Subunit Swapping Maturation." *Biochemistry* 49 (44): 9638–9648. doi:10.1021/bi100651v.

Zhou, Zhemin, Yoshiteru Hashimoto, and Michihiko Kobayashi. 2005. "Nitrile Degradation by *Rhodococcus*: Useful Microbial Metabolism for Industrial Productions." *Actinomycetologica* 19 (1): 18–26.

Zhou, Zhemin, Yoshiteru Hashimoto, and Michihiko Kobayashi. 2009. "Self-Subunit Swapping Chaperone Needed for the Maturation of Multimeric Metalloenzyme Nitrile Hydratase by a Subunit Exchange Mechanism Also Carries Out the Oxidation of the Metal Ligand Cysteine Residues and Insertion of Cobalt." *J. Biol. Chem.* 284 (22): 14930–14938. doi:10.1074/jbc.M808464200.

Zhou, Zhemin, Yoshiteru Hashimoto, Kentaro Shiraki, and Michihiko Kobayashi. 2008. "Discovery of Posttranslational Maturation by Self-Subunit Swapping." *Proc. Natl. Acad. Sci. USA* 105 (39): 14849–14854. doi:10.1073/pnas.0803428105.

Zhu, Wenfeng, Andrew C. Marr, Qiang Wang, Frank Neese, Douglas J. E. Spencer, Alexander J. Blake, Paul A. Cooke, Claire Wilson, and Martin Schröder. 2005. "Modulation of the Electronic Structure and the Ni–Fe Distance in Heterobimetallic Models for the Active Site in [NiFe]-

hydrogenase." *Proc. Natl. Acad. Sci. USA* 102 (51): 18280–18285. doi:10.1073/pnas.0505779102.

Zouni, Athina, Horst-Tobias Witt, Jan Kern, Petra Fromme, Norbert Krauss, Wolfram Saenger, and Peter Orth. 2001. "Crystal Structure of Photosystem II from Synechococcus Elongatus at 3.8 Å Resolution." *Nature* 409 (6821): 739–743. doi:10.1038/35055589.

APPENDIX A

PERMISSION TO REPRODUCE CHAPTER 4 FROM INORGANIC CHEMISTRY

APPENDIX B

COAUTHOR APPROVAL

All co-authors have granted permission for use of the material in Chapters 2, 3, 4, and 5 for the purpose of this dissertation.